NATIONAL ADVISORY COMMITTEE FOR AERONAUTICS

TECHNICAL NOTE

No. 1596

AN INVESTIGATION OF THE SECTION CHARACTERISTICS OF PLAIN UNSEALED AILERONS ON AN NACA 66,1-115 AIRFOIL SECTION IN THE LANGLEY 8-FOOT HIGH-SPEED TUNNEL

By Arvo A. Luoma

Langley Aeronautical Laboratory
Langley Field, Va.

Washington
January 1949

NATIONAL ADVISORY COMMITTEE FOR AERONAUTICS

TECHNICAL NOTE NO. 1596

AN INVESTIGATION OF THE SECTION CHARACTERISTICS OF PLAIN UNSEALED AILERONS ON AN NACA 66,1-115 AIRFOIL SECTION IN THE LANGLEY 8-FOOT HIGH-SPEED TUNNEL

By Arvo A. Luoma

SUMMARY

Complete pressure-distribution measurements were made over a 24-inch-chord NACA 66,1-115 airfoil section equipped with unsealed 20-percent-chord plain ailerons of true-airfoil-contour profile and 30° beveled-trailing-edge profile. The model was tested with aerodynamically smooth surfaces. Section characteristics including airfoil normal-force, pitching-moment, aileron normal-force, and hinge-moment coefficients were determined from the pressure data for Mach numbers up to 0.75, and for various airfoil angles of attack and aileron deflections. The test Reynolds number at the highest speed was 7.5×10^{6}.

The aileron section effectiveness for both aileron profiles decreased appreciably with Mach number. The rate of change of airfoil section pitching-moment coefficient with respect to angle of attack at constant value of airfoil section normal-force coefficient increased with Mach number for both aileron profiles and thereby aggravated the wing-twist problem at high speeds. Changing the aileron profile from the true-contour profile to the 30° beveled-trailing-edge profile caused a decrease in aileron section effectiveness, irregular hinge-moment characteristics with over-balance at moderate deflections, a decrease in the section normal-force-coefficient-curve slopes, a decrease in aileron section loads, and a decrease in section critical Mach number of the airfoil at the larger negative deflections at constant airfoil section normal-force coefficient.

INTRODUCTION

The NACA has conducted extensive low-speed control-surface investigations over a period of years. Several investigations have been made at higher speeds to study the effects of compressibility on control-surface characteristics. Included in such high-speed investigations are the two-dimensional tests of references 1 to 3. A fuller knowledge of the effects of compressibility, however, is needed. In 1942 tests were made of the section characteristics of plain, unsealed ailerons on an NACA 66,1-115 airfoil section in the Langley 8-foot high-speed tunnel. The complete

analysis and publication of the results of these tests were deferred owing to the exigencies of other problems more closely connected with the war effort. The results are being published at this time to add to existing information on the effects of compressibility on wings with various types of control surfaces.

The specific purpose of the present tests was to determine the high-speed characteristics of an NACA 66,1-115 low-drag airfoil section equipped with 20-percent-chord plain ailerons. A true-contour aileron having ordinates the same as those of the rear part of the NACA 66,1-115 airfoil section was one of the ailerons tested. The results of reference 4 had shown, both theoretically and experimentally at low speeds, that the hinge moments of a control surface could be reduced by thickening and beveling the trailing edge. Additional tests were made, therefore, to determine the effects of compressibility on an NACA 66,1-115 airfoil section equipped with a beveled-trailing-edge aileron.

Section characteristics were determined from complete pressure distributions over the main portion of the airfoil and the aileron. The tests were made for Mach numbers up to 0.75 and included various wing angles of attack and aileron deflections.

SYMBOLS

The term "main portion of the airfoil" is used herein to mean that part of the airfoil excluding the aileron. The aerodynamic coefficients and other symbols used in this paper are as follows:

a speed of sound in undisturbed stream.

c section chord of airfoil with aileron neutral (fig. 1) (2.000 ft on model)

c_M chord of main portion of airfoil

c_a section chord of aileron measured along chord from hinge axis of aileron to trailing edge of aileron (0.400 ft on model)

c_h section hinge-moment coefficient of aileron about hinge axis determined from pressure-distribution data; component due to aileron chord force neglected $\left(\left(\frac{1}{c_a}\right)^2 \int_0^{c_a} (P_U - P_L) x \, dx\right)$

c_m section pitching-moment coefficient of airfoil about quarter-chord point of airfoil due to normal forces on main portion of airfoil and aileron; components due to chord forces on main portion of wing and aileron neglected

$$\left(\left(\frac{1}{c}\right)^2\left[\int_0^{c_M}\left(P_U - P_L\right)\left(x - \frac{c}{4}\right)dx + \int_0^{c_a}\left(P_U - P_L\right)x\,dx - c_{n_a}c_a\left(x_h - \frac{c}{4}\right)\cos\delta_a + c_{n_a}c_a y_h \sin\delta_a\right]\right)$$

c_n section normal-force coefficient of airfoil determined from pressure-distribution data; component due to aileron chord force neglected $\left(\frac{1}{c}\left(c_M c_{n_M} + c_a c_{n_a}\cos\delta_a\right)\right)$

c_{n_M} section normal-force coefficient of main portion of airfoil determined from pressure-distribution data $\left(\frac{1}{c_M}\int_0^{c_M}\left(P_L - P_U\right)dx\right)$

c_{n_a} section normal-force coefficient of aileron determined from pressure-distribution data $\left(\frac{1}{c_a}\int_{-r}^{c_a}\left(P_L - P_U\right)dx\right)$

M Mach number (V/a)

M_{cr} critical Mach number; that is, Mach number in undisturbed stream at which local velocity first reaches local velocity of sound at any point on airfoil surface

P pressure coefficient $\left(\frac{p_l - p}{q}\right)$

P_{cr} critical pressure coefficient; that is, pressure coefficient at any point on airfoil surface where local velocity is equal to local velocity of sound

p static pressure in undisturbed stream

p_l local static pressure at a point on airfoil section

q dynamic pressure in undisturbed stream $\left(\frac{1}{2}\rho V^2\right)$

R Reynolds number $(\rho Vc/\mu)$

r radius of round nose of aileron (0.0710 ft on model)

V velocity in undisturbed stream

x distance along chord from leading edge of airfoil or from hinge axis of aileron

x_h hinge-axis location along airfoil chord from leading edge of airfoil (1.600 ft on model)

y_h hinge-axis location normal to chord (0.0075 ft above chord on model)

α angle of attack

δ_a aileron deflection; positive when trailing edge is down

ρ mass density in undisturbed stream

μ coefficient of viscosity in undisturbed stream

Subscripts:

U upper surface

L lower surface

APPARATUS AND METHODS

Apparatus.- The tests were made in the Langley 8-foot high-speed tunnel, which is of the single-return, circular-cross-section, closed-throat type. The air-stream turbulence, as indicated by comparative airfoil measurements and by hot-wire measurements, is small but slightly higher than that of the Langley two-dimensional low-turbulence pressure

tunnel or that of free air. At the time of the tests, the maximum Mach number of the tunnel was approximately 0.75.

The model used in this investigation was a 24-inch-chord airfoil with a 20-percent-chord plain aileron, was of uniform cross section, and spanned the tunnel test section. The main portion of the airfoil passed through the walls of the tunnel with a small clearance gap and was attached to the balance frame of the tunnel in a manner typical of model installation in the Langley 8-foot high-speed tunnel for tests of this type (fig. 1). A gap of 1/16 inch was maintained between the ends of the aileron and the tunnel walls to permit deflection of the aileron. The main portion of the model was of two-steel-spar construction with $\frac{3}{4}$-inch steel ribs and $\frac{1}{4}$-inch cold-finished-steel skin built to conform to the ordinates of the NACA 66,1-115 airfoil section as given in table I.

Two aileron shapes were tested, and these shapes are designated as the true-contour aileron and the beveled-trailing-edge aileron. The general dimensions of the airfoil section are given in figure 2, and of the aileron sections, in figure 3. The profile of the true-contour aileron corresponded to the ordinates of the rear part of the NACA 66,1-115 airfoil section. The profile of the beveled-trailing-edge aileron was formed by a 30° trailing-edge angle and straight lines as shown in figure 3; thus a profile which was thicker than that of the true-contour aileron resulted. The ailerons were constructed of solid dural and were interchangeably attached to the same main portion of the model by six clamp-type hinges. The ailerons had no aerodynamic nose balance. No seal was used between the main portion of the airfoil and the aileron at any time during the tests. The gap between the aileron and the aileron cover plates on both upper and lower surfaces was 0.002c (fig. 2). The cover plates were made of $\frac{1}{8}$-inch steel.

Sufficient static-pressure orifices were installed on the main portion of the model and on the ailerons to determine the complete pressure distribution over the airfoil (fig. 2). The orifices were located in the region of the midspan of the model. The tests were made with a model having aerodynamically smooth surfaces.

Test procedure.- Airfoil normal-force, airfoil pitching-moment, aileron normal-force, and aileron hinge-moment data were determined from static-pressure-distribution measurements which were obtained by photographing a multiple-tube liquid manometer. The tests were made at various angles of attack and aileron deflections. Data were obtained for both aileron configurations at moderate deflections at Mach numbers of 0.25, 0.35, 0.457, 0.55, 0.60, 0.65, 0.70, 0.725, and approximately 0.75; data were obtained also at Mach numbers of 0.45, 0.50, and 0.675 for the true-contour aileron. Data for the larger aileron deflections were

obtained at maximum test Mach numbers which were lower than those for the moderate deflections. The test procedure consisted of setting the aileron at a given deflection and then making tests through the angle-of-attack range at each of the test Mach numbers. The Reynolds number range of the tests is shown in figure 4.

PRECISION

The discrepancies between the characteristics of a section at the midspan region of the airfoil as measured in the tunnel and the characteristics of the airfoil in free air are caused principally by the effects of tunnel-wall interference, air leakage through the clearance gap between the model and the tunnel walls, and tunnel air-stream turbulence.

An estimate of the tunnel-wall interference corrections which includes the effects of model constriction, wake blockage, and streamline curvature was made for the airfoil with the aileron undeflected by the methods of references 5 and 6, which are based on the assumption that the camber of the airfoil is small. For the value of the ratio of model airfoil chord to tunnel diameter (0.25) used in the present tests, the magnitude of the tunnel-wall-interference corrections is quite small. These corrections have not been applied to the data. At a Mach number of 0.70, the Mach number as presented is too low by 2 percent. At a Mach number of 0.70 and an airfoil section normal-force coefficient of 0.7, the airfoil section normal-force coefficient is too high by an increment of 0.05, the section pitching-moment coefficient is too high by 0.008, and the angle of attack is too low by 0.1°. At a Mach number of 0.70 and an airfoil section normal-force coefficient of 0.2, the airfoil section normal-force coefficient is too high by an increment of 0.015, the section pitching-moment coefficient is too high by 0.003, and the angle of attack is too low by 0.02°. At lower Mach numbers, the corrections are less than those given at a Mach number of 0.70.

The apparent choking Mach number of the model in the tunnel, based on the ratio of the projected thickness of the model to the tunnel diameter, was estimated to be 0.77 (reference 6). The data presented herein at a Mach number of 0.75, which was close to the estimated choking Mach number, should be considered to be of doubtful validity inasmuch as the air flow may have been influenced by the incipient choking restriction.

The air leakage through the clearance gap between the model and the tunnel walls had an insignificant effect since the pressure-distribution measurements were made near the midspan of the model and the span-chord ratio (4.0) was large. The numerical effects of air-stream turbulence are not known; however, the turbulence level of the Langley 8-foot high-speed tunnel is low.

RESULTS

The aerodynamic force and moment data presented herein were determined from the mechanical integration of diagrams of pressure coefficient P plotted against chord for pressures over the upper and lower surfaces of the main portion of the airfoil and of the aileron. These data may be considered to be section data. In the preparation of the figures, the various aerodynamic coefficients first were plotted against angle of attack at a given test Mach number and with aileron deflection as a parameter. From these basic plots, the variation of the coefficients with Mach number at a constant value of airfoil section normal-force coefficient and with aileron deflection as a parameter were determined. Most of the data included in this paper have been presented in this manner and thus show the variation of the coefficients with Mach number at a constant value of airfoil section normal-force coefficient.

Typical pressure-distribution plots at several Mach numbers for an angle of attack of 1° and an aileron deflection of 0° are given in figure 5 for the airfoil with the true-contour aileron. In figure 6 is shown the variation of section airfoil angle of attack and section pitching-moment coefficient with Mach number for the airfoil with the true-contour aileron at constant values of airfoil section normal-force coefficient. Plots of aileron section normal-force coefficient and section hinge-moment coefficient for the true-contour aileron against Mach number are to be found in figure 7. Aileron section loads may be determined from these data.

Representative pressure distributions for the airfoil with the beveled-trailing-edge aileron are given in figure 8. These date are for an angle of attack of 1° and an aileron deflection of 0°. Figure 9 shows the variation with Mach number of the section airfoil angle of attack and section pitching-moment coefficient of the airfoil with the beveled-trailing-edge aileron at constant values of airfoil section normal-force coefficient. Figure 10 presents the aileron section normal-force and section hinge-moment characteristics of the beveled-trailing-edge aileron.

The effects of the true-contour aileron and the beveled-trailing-edge aileron on the airfoil section-normal-force-coefficient-curve slopes $\left(\frac{\Delta c_n}{\Delta \alpha}\right)_{\delta_a=0^\circ}$ and $\left(\frac{\Delta c_n}{\Delta \delta_a}\right)_{\alpha=0^\circ}$ are compared in figure 11. The slopes shown are the average values for angles of attack from -1° to 1° and for aileron deflections from -1° to 1°. The variation of aileron section effectiveness $-\left(\frac{\Delta \alpha}{\Delta \delta_a}\right)_{c_n}$ with Mach number for the airfoil with the two ailerons at various values of airfoil section normal-force

coefficient is given in figure 12. The values of $-\left(\frac{\Delta\alpha}{\Delta\delta_a}\right)_{c_n}$ given are the average values for aileron deflections from -6° to 4° for the airfoil with the true-contour aileron and from -4° to 6° for the airfoil with the beveled-trailing-edge aileron.

The variation of the section critical Mach number of the airfoil with aileron deflection for the airfoil with the two ailerons is given in figure 13 for values of airfoil section normal-force coefficient from 0 to 0.6. The section critical Mach number was determined from the intersection of curves of minimum airfoil pressure coefficient plotted against Mach number with the curve of critical pressure coefficient plotted against Mach number. In a few cases, where the test Mach numbers were below the critical Mach number, the test data have been extrapolated a moderate amount to higher Mach numbers to obtain the critical Mach number values.

One of the problems of high-speed flight is the wing twist during rolling caused by the pitching moments developed by the lateral-control device. The rate of change of airfoil section pitching-moment coefficient with angle of attack $\left(\frac{\Delta c_m}{\Delta\alpha}\right)_{c_n}$ at a constant value of airfoil section normal-force coefficient is an index of the tendency of an aileron to twist a wing (as a result of the pitching moment developed by the aileron) in terms of the section effectiveness developed by the aileron, and therefore affords a proper comparison of the two ailerons as regards wing twisting. The ratio $\left(\frac{\Delta c_m}{\Delta\alpha}\right)_{c_n}$ was obtained by dividing values of $\left(\frac{\Delta c_m}{\Delta\delta_a}\right)_{c_n}$ by the corresponding values of aileron section effectiveness $\left(\frac{\Delta\alpha}{\Delta\delta_a}\right)_{c_n}$ given in figure 12 and applies for the same deflection range as the data of figure 12. The variation with Mach number of the ratio $\left(\frac{\Delta c_m}{\Delta\alpha}\right)_{c_n}$ is given in figure 14.

The section hinge-moment-coefficient derivatives $\left(\frac{\Delta c_h}{\Delta\delta_a}\right)_{\alpha=0^\circ}$ and $\left(\frac{\Delta c_h}{\Delta\alpha}\right)_{\delta_a=0^\circ}$ for the two configurations are presented in figure 15. These slopes are the average values for angles of attack from -1° to 1° and for aileron deflections from -1° to 1°. The action of the thickened trailing edge in relieving hinge moments is shown in figure 16 by representative pressure distributions over the aileron for deflections of -4° and 4° at an angle of attack of 1°.

The wing-drag coefficient C_D at an aileron deflection of 0° for the two aileron configurations is shown plotted against Mach number in figure 17 for various values of airfoil section normal-force coefficient. The drag coefficients were determined from force-test measurements of the drag of the complete wing and are based on the effective area of the complete wing in the tunnel. The drag coefficients shown are not two-dimensional data. The data are useful, however, in showing the changes in drag coefficient with changes in Mach number, and the relative effect of the two ailerons on the drag coefficient.

DISCUSSION

Aileron Section Effectiveness

The section effectiveness $-\left(\frac{\Delta\alpha}{\Delta\delta_a}\right)_{c_n}$ of the airfoil with either aileron at moderate deflections decreased markedly with an increase in Mach number (fig. 12). This decrease between the Mach numbers of 0.25 and 0.75 amounted to about one-half the low-speed values, at the lower values of airfoil section normal-force coefficient.

At a Mach number of 0.25, thickening the trailing edge had no effect on the aileron effectiveness at moderate deflections at low values of airfoil section normal-force coefficient and reduced this effectiveness at the higher values of airfoil section normal-force coefficient (fig. 12). Low-speed two-dimensional tests (references 4 and 7) have shown losses in aileron section effectiveness when the aileron trailing edge was beveled, and low-speed three-dimensional tests (references 8 and 9) have shown similar losses in rolling effectiveness for beveled ailerons. At test Mach numbers greater than 0.25, the present tests (fig. 12) showed appreciable losses in section aileron effectiveness when the aileron trailing edge was beveled.

The airfoil with the beveled-trailing-edge aileron showed a rather abrupt loss in effectiveness at deflections greater than 12° for airfoil section normal-force coefficients of 0.4 and less, as indicated by the data of figure 9. This abrupt loss in effectiveness was the result of stalling of the air flow at deflections greater than 12° as indicated by the pressure diagrams (not shown). At airfoil section normal-force coefficients greater than 0.4, the air flow was stalling at a deflection of 12° and at lower deflections. The stalling at the higher values of airfoil section normal-force coefficient occurred more gradually with increase in deflection than at the lower values of airfoil section normal-force coefficient, with a corresponding more uniform change in airfoil characteristics with change in deflection.

The characteristics of the airfoil with the true-contour aileron (fig. 6) at large deflections are more uniform with change in deflection

than those for the airfoil with the beveled-trailing-edge aileron. The pressure diagrams (not shown) indicated that at a deflection of 18° the air flow followed the contour of the true-contour aileron quite closely at the lower values of airfoil section normal-force coefficient and the lower Mach numbers. Separation occurred at the higher values of airfoil section normal-force coefficient and the higher Mach numbers. At a deflection of 12°, separation occurred at somewhat lower values of airfoil section normal-force coefficient and Mach number for the airfoil with the true-contour aileron than for the airfoil with the beveled-trailing-edge aileron.

As mentioned previously in the section entitled "Apparatus and Methods" the present tests were made with unsealed ailerons. Many tests have demonstrated that the characteristics of an airfoil with a sealed aileron are generally more satisfactory than those of an airfoil with an unsealed aileron. One of the unfavorable effects of an unsealed aileron gap is that the effectiveness of the aileron is less than when the gap is sealed. The low-speed data of references 8 and 9 indicate that an unsealed aileron gap reduces aileron effectiveness to a greater extent on an airfoil with a beveled-trailing-edge aileron than on an airfoil with a true-contour aileron.

Aileron Section Hinge Moments

The section hinge-moment characteristics of the beveled-trailing-edge aileron are irregular as shown by the data of figure 10. In the aileron deflection range from approximately -6° to 4°, the variation of section hinge-moment coefficient was irregular both with Mach number and aileron deflection. At larger aileron deflections the characteristics were more satisfactory.

Beveling the trailing edge reduced hinge moments by more than one-half at some of the test conditions at the larger deflections. The action of the thickened trailing edge in changing the air flow about the aileron and in relieving hinge moments is illustrated by the chordwise aileron pressure distributions shown in figure 16. At positive aileron deflections, the pressures on the aileron lower surface are usually more positive than those on the aileron upper surface. The bevel on the lower surface, where the pressures are more positive, speeds up the flow to a greater extent than the bevel on the upper surface; a hinge-moment component is thus introduced which acts in a way to relieve the main hinge moment. At negative deflections, the reverse action is generally true. From these tests the action of the bevel appeared to be greater at positive deflections.

Large increases in the section hinge-moment coefficient of the true-contour aileron at a deflection of 18° occurred for some of the combinations of Mach number and airfoil section normal-force coefficient. These increases in section hinge-moment coefficient were mainly due to development of appreciable separation of the flow off the upper surface

of the aileron, the separation occurring at lower Mach numbers as the airfoil section normal-force coefficient was increased (fig. 7).

The section hinge-moment slope $\left(\frac{\Delta c_h}{\Delta \delta_a}\right)_{\alpha=0^\circ}$ for the true-contour aileron at moderate deflections increased in magnitude between the Mach numbers of 0.25 and 0.68 by about three-fourths of the low-speed value (fig. 15). At higher Mach numbers up to the maximum test Mach number of 0.75, there was a reduction in magnitude of this hinge-moment parameter. The effect of beveling the aileron trailing edge to an angle of 30° was to cause an overbalance of the section parameter $\left(\frac{\Delta c_h}{\Delta \delta_a}\right)_{\alpha=0^\circ}$ at moderate deflections similar to that shown by other tests (references 8 to 10), and this over-balance was aggravated with Mach number (fig. 15). The section hinge-moment slope $\left(\frac{\Delta c_h}{\Delta \alpha}\right)_{\delta=0^\circ}$ for the true-contour aileron was essentially constant up to a Mach number of 0.68 and then rapidly increased in magnitude at higher Mach numbers up to the maximum test Mach number of 0.75. The section parameter $\left(\frac{\Delta c_h}{\Delta \alpha}\right)_{\delta=0^\circ}$ for the beveled-trailing-edge aileron was positive in algebraic sign and appreciably increased in magnitude with Mach number.

Low-speed tests (references 9 and 10) have shown that reducing the aileron gap or sealing the gap of a beveled aileron had small effect on the parameter $\left(\frac{\Delta c_h}{\Delta \alpha}\right)_{\delta}$, but reduced the overbalance of the parameter $\left(\frac{\Delta c_h}{\Delta \delta_a}\right)_{\alpha}$ at small aileron deflections.

Section Normal Force

Airfoil.- The section slope $\left(\frac{\Delta c_n}{\Delta \alpha}\right)_{\delta_a=0^\circ}$ for both configurations increased with Mach number up to a Mach number somewhat greater than the critical Mach number and then decreased with further increase in Mach number (figs. 11 and 13). The section slope $\left(\frac{\Delta c_n}{\Delta \delta_a}\right)_{\alpha=0^\circ}$ for both configurations was not affected very much by Mach number at subcritical speeds, and decreased at supercritical speeds (fig. 11).

The effect of beveling the trailing edge was to reduce the section slopes $\left(\frac{\Delta c_n}{\Delta \alpha}\right)_{\delta_a=0^\circ}$ and $\left(\frac{\Delta c_n}{\Delta \delta_a}\right)_{\alpha=0^\circ}$ and this effect is in qualitative agreement with low-speed two-dimensional and three-dimensional tests

(references 4, 7, and 8). A lower value of $\left(\frac{\Delta c_n}{\Delta \alpha}\right)_\delta$ would be advantageous in roll since the damping-moment coefficient is a function of this parameter.

Aileron.- In addition to relieving hinge moments, thickening the aileron trailing edge reduced section aileron loads appreciably at constant airfoil section normal-force coefficient (figs. 7 and 10), as is to be expected from the action of the bevel on the air flow (fig. 16). The aileron load for the beveled-trailing-edge aileron was affected quite irregularly by changes in angle of attack, aileron deflection, and Mach number.

Section Pitching Moment

The variation of section pitching-moment coefficient c_m with Mach number and aileron deflection is seen to be more regular for the airfoil with the true-contour aileron than for the airfoil with the beveled-trailing-edge aileron (figs. 6 and 9). Thickening the trailing edge, however, reduced pitching-moment coefficients.

The pitching-moment coefficient of the airfoil with the beveled-trailing-edge aileron was approximately the same magnitude for deflections of 12° and 18° at several of the airfoil section normal-force coefficients (figs. 9(b), 9(c), 9(d), and 9(e)). For these conditions, the flow followed the contour of the airfoil at a deflection of 12°; whereas at a deflection of 18°, there was appreciable separation. The effect of separation was to change the section pitching-moment coefficient in a positive direction. For the conditions represented in figure 9(f), appreciable separation had occurred also at a deflection of 12°, with a consequent spreading out of the section pitching-moment-coefficient curves for deflections of 12° and 18°.

The section pitching-moment coefficient of the airfoil with the true-contour aileron at a deflection of 18° decreased notably for some of the combinations of Mach number and airfoil section normal-force coefficient. This decrease in section pitching-moment coefficient was mainly due to the development of appreciable separation of the air flow off the upper surface of the airfoil, the separation occurring at lower Mach numbers as the airfoil section normal-force coefficient was increased (fig. 6).

The section parameter of the rate of change of airfoil section pitching-moment coefficient with deflection per unit value of aileron section effectiveness $\left(\frac{\Delta c_m}{\Delta \alpha}\right)_{c_n}$ is a measure of the tendency of an aileron to twist a wing (as a result of the pitching moments produced by the aileron) in terms of the section effectiveness developed by the aileron (fig. 14). It is seen that increasing the Mach number increased

the value of $\left(\frac{\Delta c_m}{\Delta \alpha}\right)_{c_n}$ for both configurations (fig. 14) and thereby made the wing-twist problem at high speeds worse. The increase of $\left(\frac{\Delta c_m}{\Delta \alpha}\right)_{c_n}$ with Mach number was mainly due to the decrease in section effectiveness $-\left(\frac{\Delta \alpha}{\Delta \delta_a}\right)_{c_n}$ with Mach number (fig. 12). The section pitching-moment parameter $\left(\frac{\Delta c_m}{\Delta \alpha}\right)_{c_n}$ was generally less, and the Mach number effects were not so pronounced, for the configuration with the beveled-trailing-edge aileron as for the configuration with the true-contour aileron (fig. 14). The reduction in the parameter $\left(\frac{\Delta c_m}{\Delta \alpha}\right)_{c_n}$ for the airfoil with the beveled-trailing-edge aileron resulted from smaller values of the section parameter $\left(\frac{\Delta c_m}{\Delta \delta_a}\right)_{c_n}$, which also decreased with Mach number instead of increasing as was the case for the airfoil with the true-contour aileron.

Section Critical Speed

The section critical Mach number of the airfoil with either aileron was 0.70 at an airfoil section normal-force coefficient of zero and with the aileron neutral (fig. 13). At positive aileron deflections the section critical Mach number was essentially the same for the airfoil with either aileron except at an airfoil section normal-force coefficient of 0.6, at which value the airfoil with the beveled-trailing-edge aileron had lower section critical-speed values. At negative deflections, the section critical Mach number of the airfoil with the beveled-trailing-edge aileron generally was lower than that of the airfoil with the true-contour aileron.

In the data of figure 13, the upper surface of the main portion of the airfoil was the critical surface, except at negative aileron deflections greater than -7.5° at an airfoil section normal-force coefficient of zero, at which conditions the lower surface of the main portion of the airfoil was the critical one. The pressures over the ailerons were more positive than the minimum pressure occurring on the main portion of the airfoil for all test conditions, so that the critical Mach number of the ailerons was greater than that of the main portion of the airfoil.

Figures 5 and 8 illustrate the characteristically flat chordwise pressure distributions of the 66-series airfoil section and the effect of Mach number on the pressures. The pressure diagrams over the main portion of the airfoil are seen to be very similar for both aileron configurations. The typical large changes in pressure distribution at supercritical Mach numbers for relatively small changes in Mach number are to be noted.

Wing Drag

The wing-drag data from force-test measurements (fig. 17) showed that, at constant airfoil section normal-force coefficient and with the aileron neutral, beveling the trailing edge of the aileron increased the drag of the airfoil. The increment in drag became greater at higher values of airfoil section normal-force coefficient. The variation of drag coefficient with Mach number was essentially the same for both configurations. The low-speed drag coefficient shown in figure 17 is appreciably higher than the low-speed profile-drag-coefficient value of 0.004 obtained in other tests (reference 11) for the NACA 66,1-115 airfoil section. The main reason for the discrepancy is the air leakage through the gap between the model and the tunnel walls, the effect of the leakage being to increase the force drag of the wing. The spanwise gaps on the upper and lower surfaces of the wing between the aileron and the aileron cover plates also probably increased the drag of the basic section somewhat.

CONCLUSIONS

An investigation was made in the Langley 8-foot high-speed tunnel of the section characteristics of a 24-inch-chord NACA 66,1-115 airfoil section equipped with unsealed 20-percent-chord plain ailerons of true-airfoil-contour profile and 30° beveled-trailing-edge profile. The airfoil was tested with aerodynamically smooth surfaces for Mach numbers up to 0.75, and for various airfoil angles of attack and aileron deflections. The test Reynolds number at the highest speed was 7.5×10^6. The following conclusions are indicated:

1. The aileron section effectiveness parameter $-\left(\frac{\Delta\alpha}{\Delta\delta_a}\right)_{c_n}$ for both of the aileron profiles investigated decreased between the Mach numbers 0.25 and 0.75 by about one-half the low-speed value, at the lower values of airfoil section normal-force coefficient.

2. The section pitching-moment parameter $\left(\frac{\Delta c_m}{\Delta\alpha}\right)_{c_n}$ for both aileron profiles increased with Mach number and thereby aggravated the wing-twist problem at high speeds.

3. Changing the aileron profile from the true-contour profile to the 30° beveled-trailing-edge profile caused

(a) a decrease in the aileron section effectiveness parameter $-\left(\frac{\Delta\alpha}{\Delta\delta_a}\right)_{c_n}$

(b) a reduction in hinge moments, but made the hinge-moment characteristics irregular with an overbalance of the section hinge-moment parameter $\left(\frac{\Delta c_h}{\Delta \delta_a}\right)_{\alpha=0^\circ}$ at moderate aileron deflections, the overbalance worsening with increase in Mach number

(c) a decrease in section normal-force-curve slopes $\left(\frac{\Delta c_n}{\Delta \alpha}\right)_{\delta_a=0^\circ}$ and $\left(\frac{\Delta c_n}{\Delta \delta_a}\right)_{\alpha=0^\circ}$

(d) a decrease in aileron section loads, at constant airfoil section normal-force coefficient

(e) a general decrease in the section pitching-moment parameter $\left(\frac{\Delta c_m}{\Delta \alpha}\right)_{c_n}$

(f) generally only small change in the section critical Mach number of the airfoil at positive aileron deflections and a decrease in section critical Mach number at the larger negative aileron deflections, at constant airfoil section normal-force coefficient

Langley Aeronautical Laboratory
National Advisory Committee for Aeronautics
Langley Field, Va., July 1, 1948

REFERENCES

1. Stevenson, David B., and Byrne, Robert W.: High-Speed Wind-Tunnel Tests of an NACA 16-009 Airfoil Having a 32.9-Percent-Chord Flap with an Overhang 20.7 Percent of the Flap Chord. NACA TN No. 1406, 1947.

2. Stevenson, David B., and Adler, Alfred A.: High-Speed Wind-Tunnel Tests of an NACA 0009-64 Airfoil Having a 33.4-Percent-Chord Flap with an Overhang 20.1 Percent of the Flap Chord. NACA TN No. 1417, 1947.

3. Lindsey, W. F.: Effect of Compressibility on the Pressures and Forces Acting on a Modified NACA 65,3-019 Airfoil Having a 0.20-Chord Flap. NACA ACR No. L5G31a, 1946.

4. Jones, Robert T., and Ames, Milton B., Jr.: Wind-Tunnel Investigation of Control-Surface Characteristics. V - The Use of a Beveled Trailing Edge to Reduce the Hinge Moment of a Control Surface. NACA ARR, March 1942.

5. Allen, H. Julian, and Vincenti, Walter G.: The Wall Interference in a Two-Dimensional-Flow Wind Tunnel with Consideration of the Effect of Compressibility. NACA Rep. No. 782, 1944.

6. Vincenti, Walter G., and Graham, Donald J.: The Effect of Wall Interference upon the Aerodynamic Characteristics of an Airfoil Spanning a Closed-Throat Circular Wind Tunnel. NACA ACR No. 5D21, 1945.

7. Underwood, William J., Braslow, Albert L., and Cahill, Jones F.: Two-Dimensional Wind-Tunnel Investigation of 0.20-Airfoil-Chord Plain Ailerons of Different Contour on an NACA 65_1-210 Airfoil Section. NACA ACR No. L5F27, 1945.

8. Rogallo, F. M., and Purser, Paul E.: Wind-Tunnel Investigation of a Plain Aileron with Various Trailing-Edge Modifications on a Tapered Wing. II - Ailerons with Thickened and Beveled Trailing Edges. NACA ARR, Oct. 1942.

9. Purser, Paul E., and McKee, John W.: Wind-Tunnel Investigation of a Plain Aileron with Thickened and Beveled Trailing Edges on a Tapered Low-Drag Wing. NACA ACR, Jan. 1943.

10. Rogallo, F. M., and Crandall, Stewart M.: Wind-Tunnel Investigation of Trimming Tabs on a Thickened and Beveled Aileron on a Tapered Low-Drag Wing. NACA ACR, March 1943.

11. Robinson, Harold L.: High-Speed Investigation of Skin Wrinkles on Two NACA Airfoils. NACA TN No. 1121, 1946.

TABLE I

AIRFOIL ORDINATES FOR NACA 66,1-115 AIRFOIL

[Station and ordinates in percent of wing chord]

Upper surface		Lower surface	
Station	Ordinates	Station	Ordinates
1.188	1.851	1.312	-1.744
2.429	2.532	2.571	-2.346
4.922	3.501	5.078	-3.185
7.419	4.239	7.581	-3.815
9.920	4.843	10.080	-4.325
14.925	5.803	15.075	-5.131
19.932	6.535	20.068	-5.739
24.942	7.095	25.058	-6.200
29.953	7.505	30.047	-6.533
39.976	7.984	40.024	-6.912
44.988	8.049	45.012	-6.951
50.000	7.988	50.000	-6.884
60.022	7.434	59.978	-6.362
70.038	6.058	69.962	-5.086
80.040	4.029	79.960	-3.233
90.026	1.763	89.974	-1.245
95.014	.740	94.986	-.424
100.000	0	100.000	0
Slope of radius through L.E.: 0.062 L.E. radius: 0.0161c			

NACA

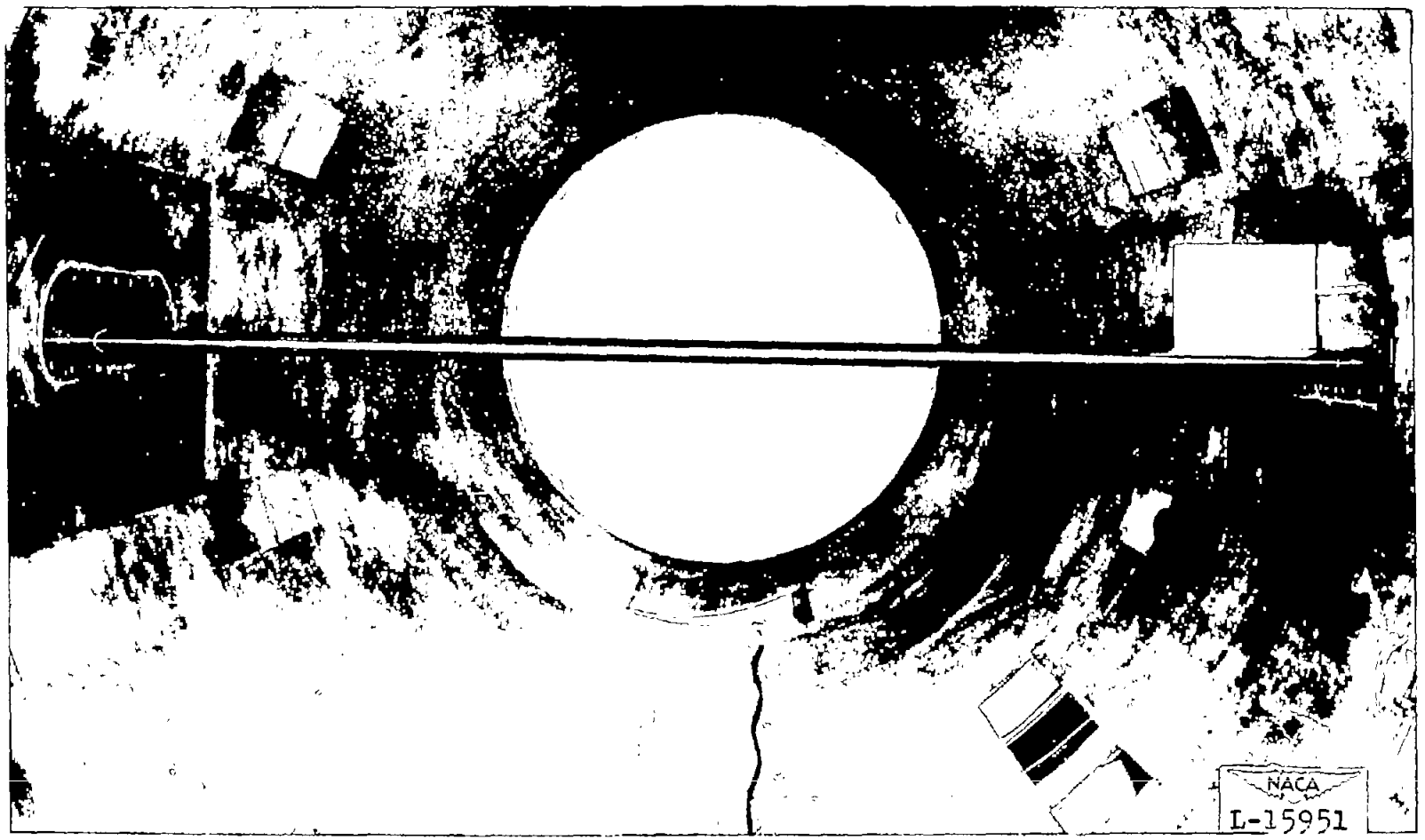

Figure 1.- Method of model installation in Langley 8-foot high-speed tunnel for present tests.

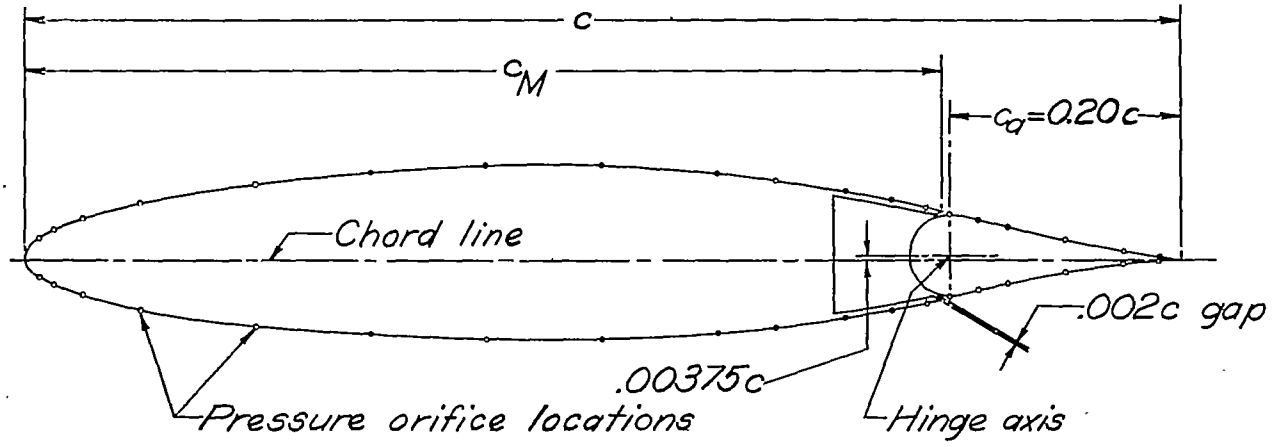

(a) Wing section with true-contour aileron.

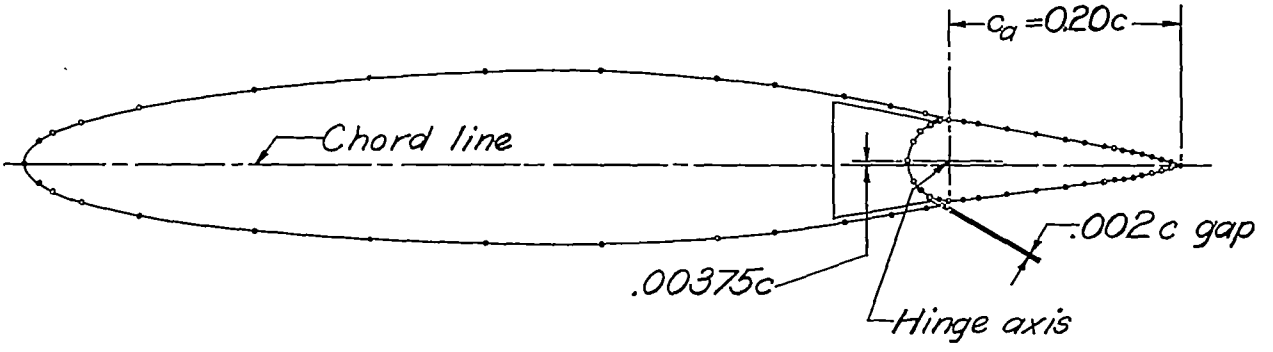

(b) Wing section with beveled-trailing-edge aileron.

Figure 2.- NACA 66,1-115 airfoil section equipped with unsealed 0.20c plain ailerons of true-airfoil-contour profile and beveled-trailing-edge profile. Chordwise static-pressure orifice locations are shown. c=24 inches.

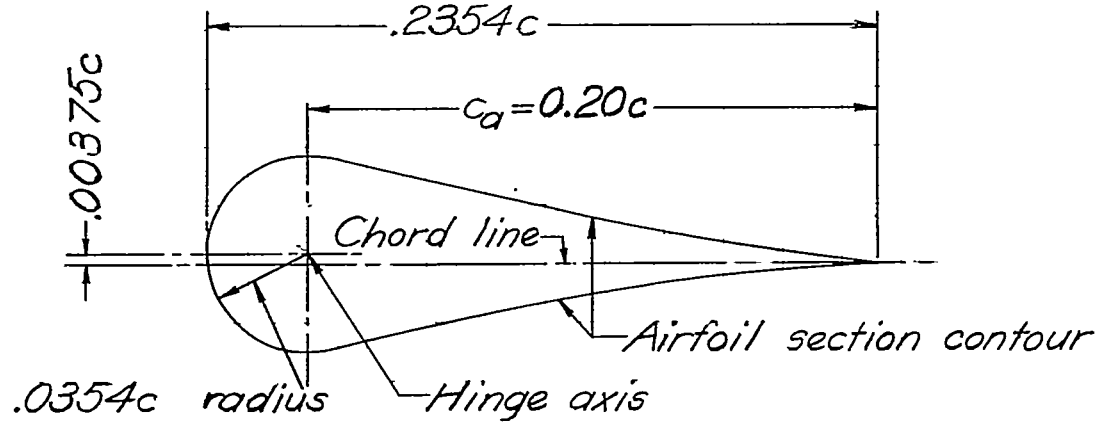

(a) True-contour aileron.

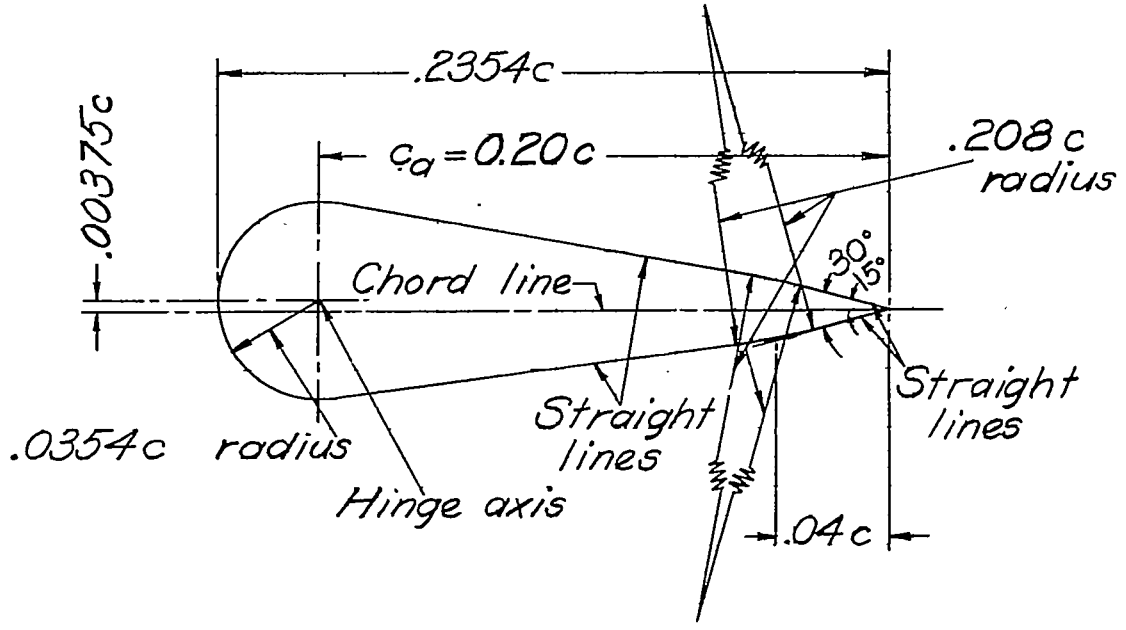

(b) Beveled-trailing-edge aileron.

Figure 3.- Dimensions of 0.20c plain ailerons used on NACA 66,1-115 airfoil section. c=24 inches.

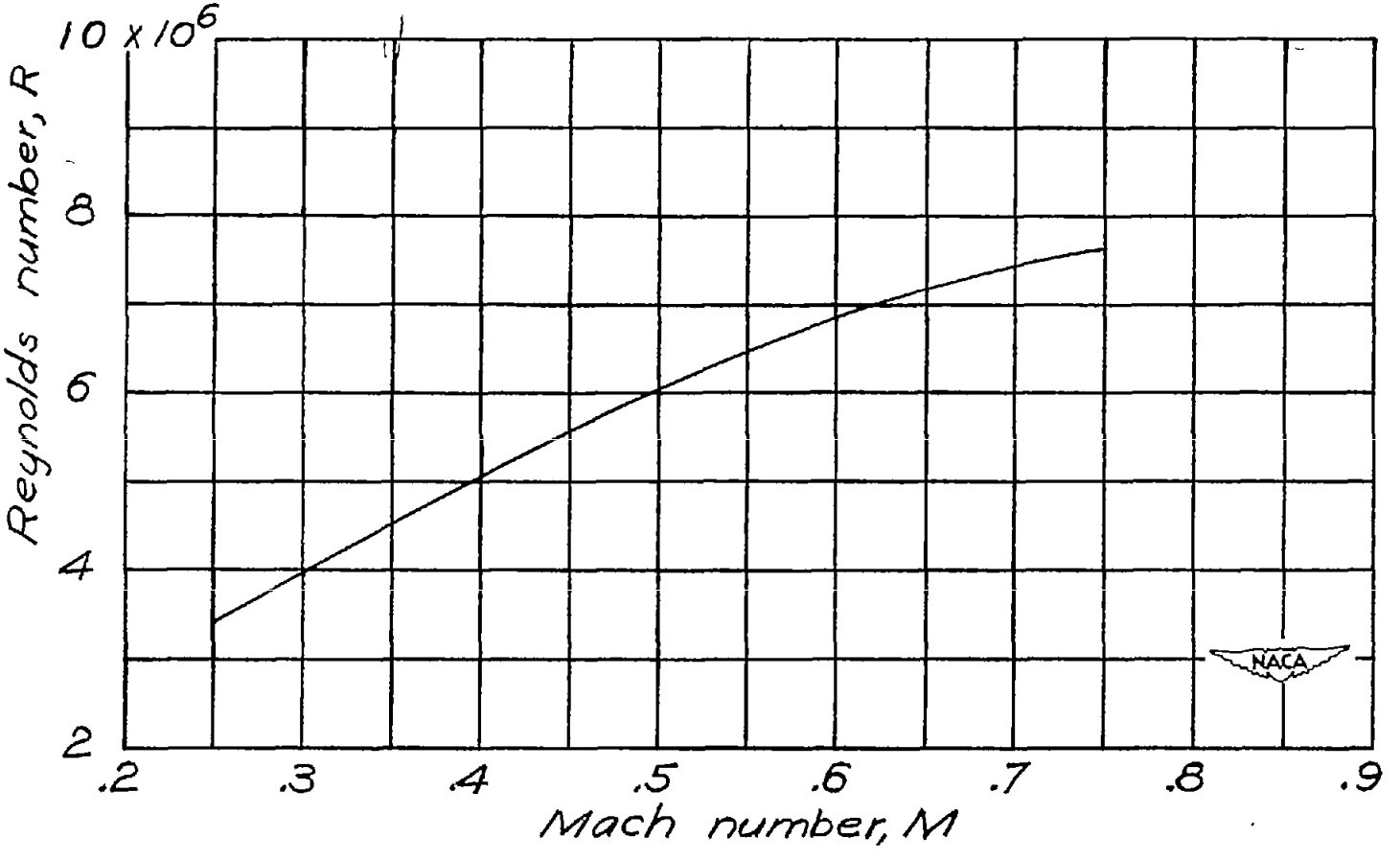

Figure 4.- Variation of Reynolds number with Mach number in the wind-tunnel tests of an NACA 66,1-115 airfoil section equipped with 0.20c plain ailerons.

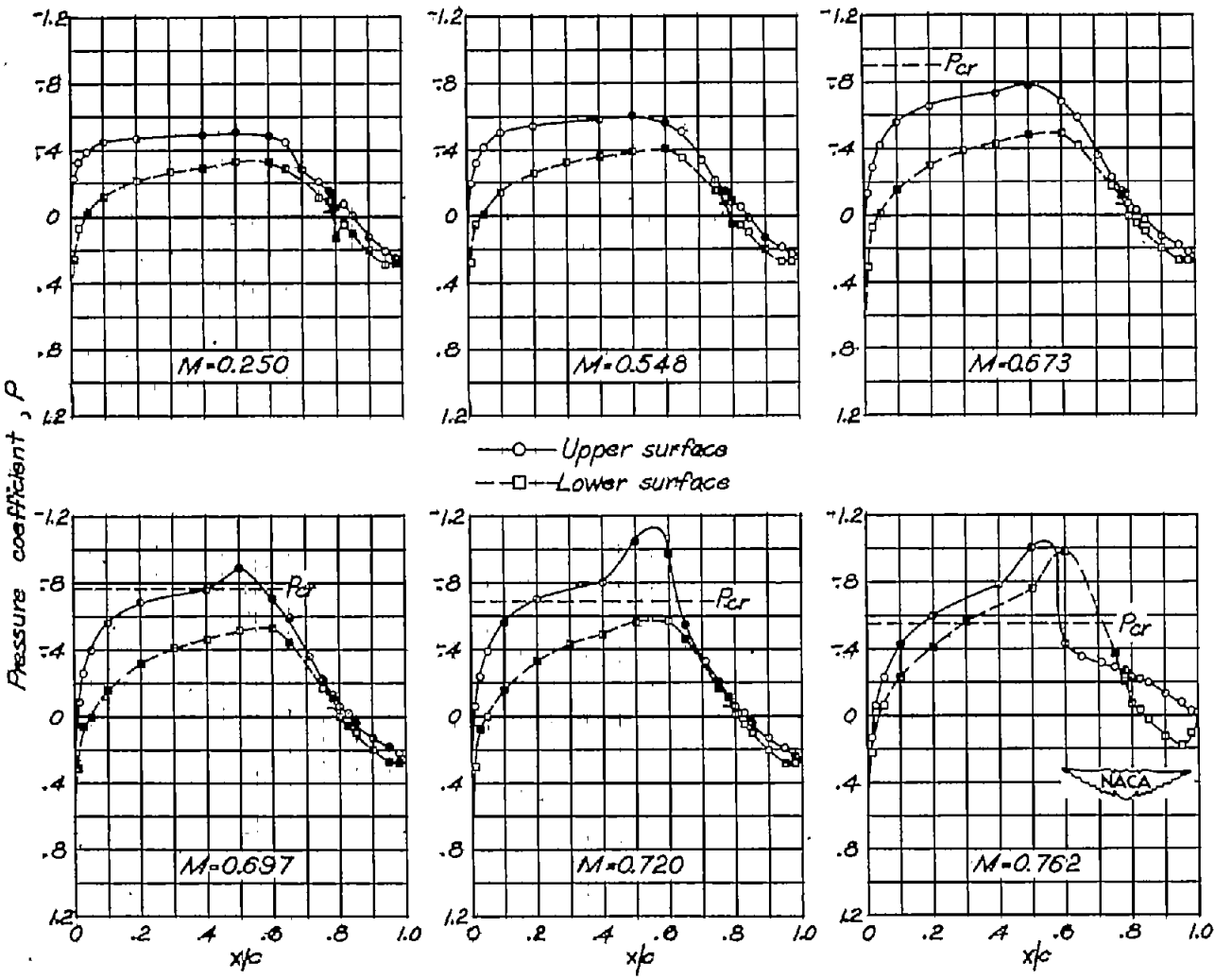

Figure 5.— Pressure distribution about an NACA 66,1-115 airfoil section equipped with an unsealed 0.20c plain aileron of true-airfoil-contour profile. $\delta_a = 0°$; $\alpha = 1°$.

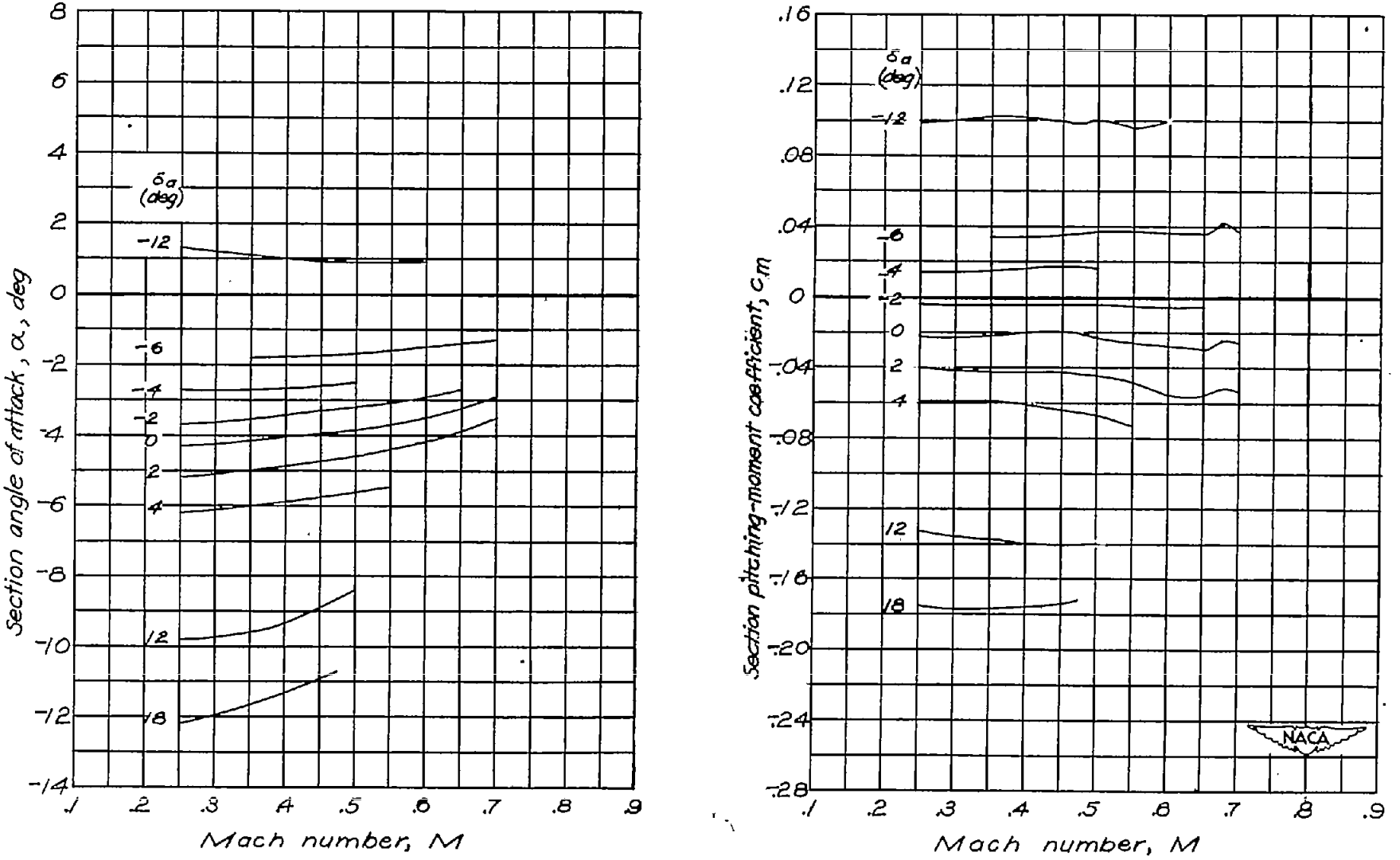

(a) $c_n = -0.4$.

Figure 6.– Variation of angle of attack and pitching-moment coefficient with Mach number for an NACA 66,1-115 airfoil section equipped with an unsealed 0.20c plain aileron of true-airfoil-contour profile.

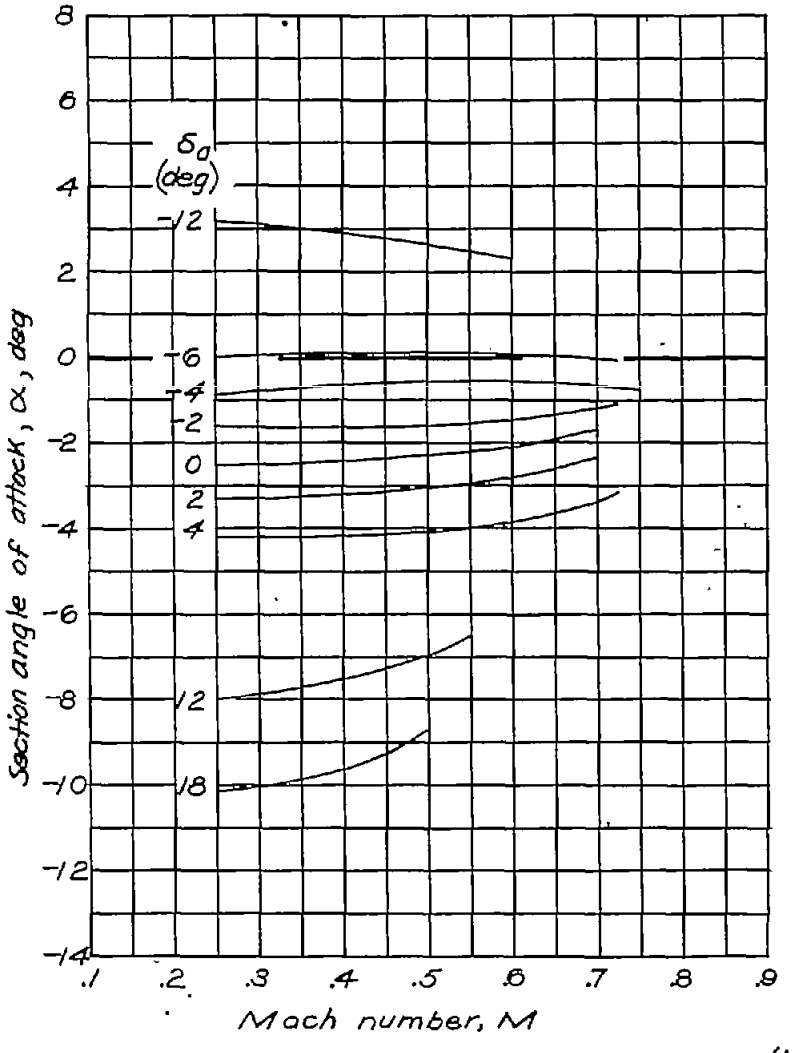

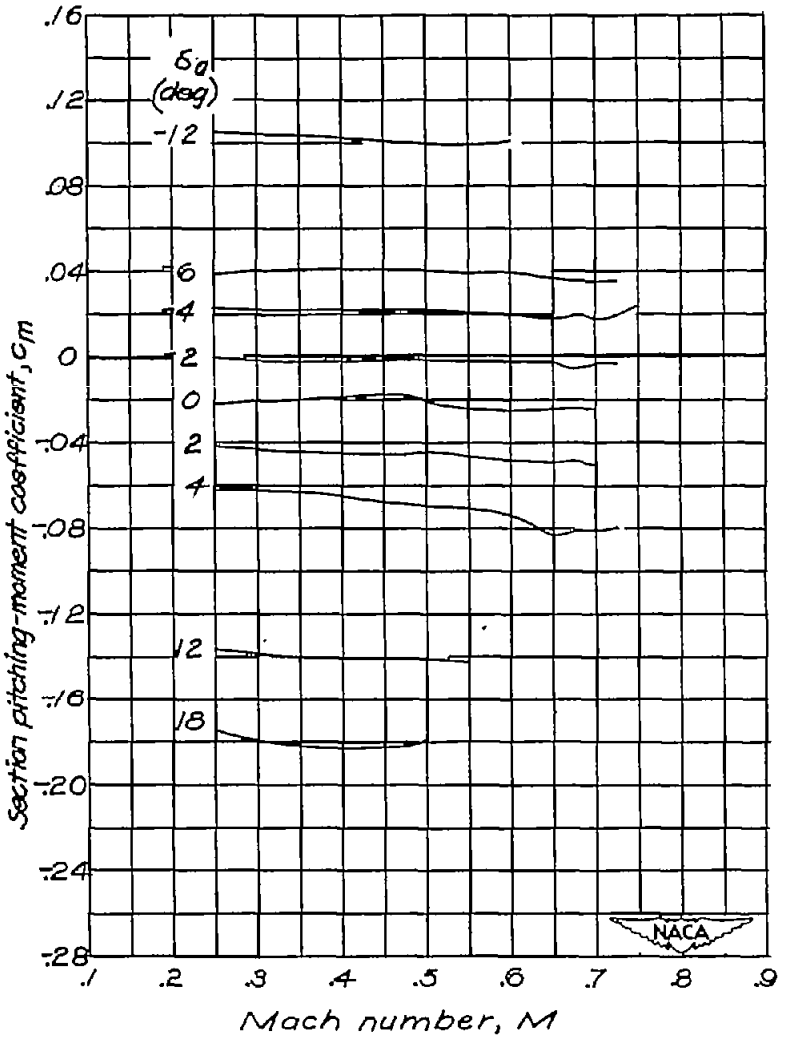

(b) $c_n = -0.2$.

Figure 6 .- Continued.

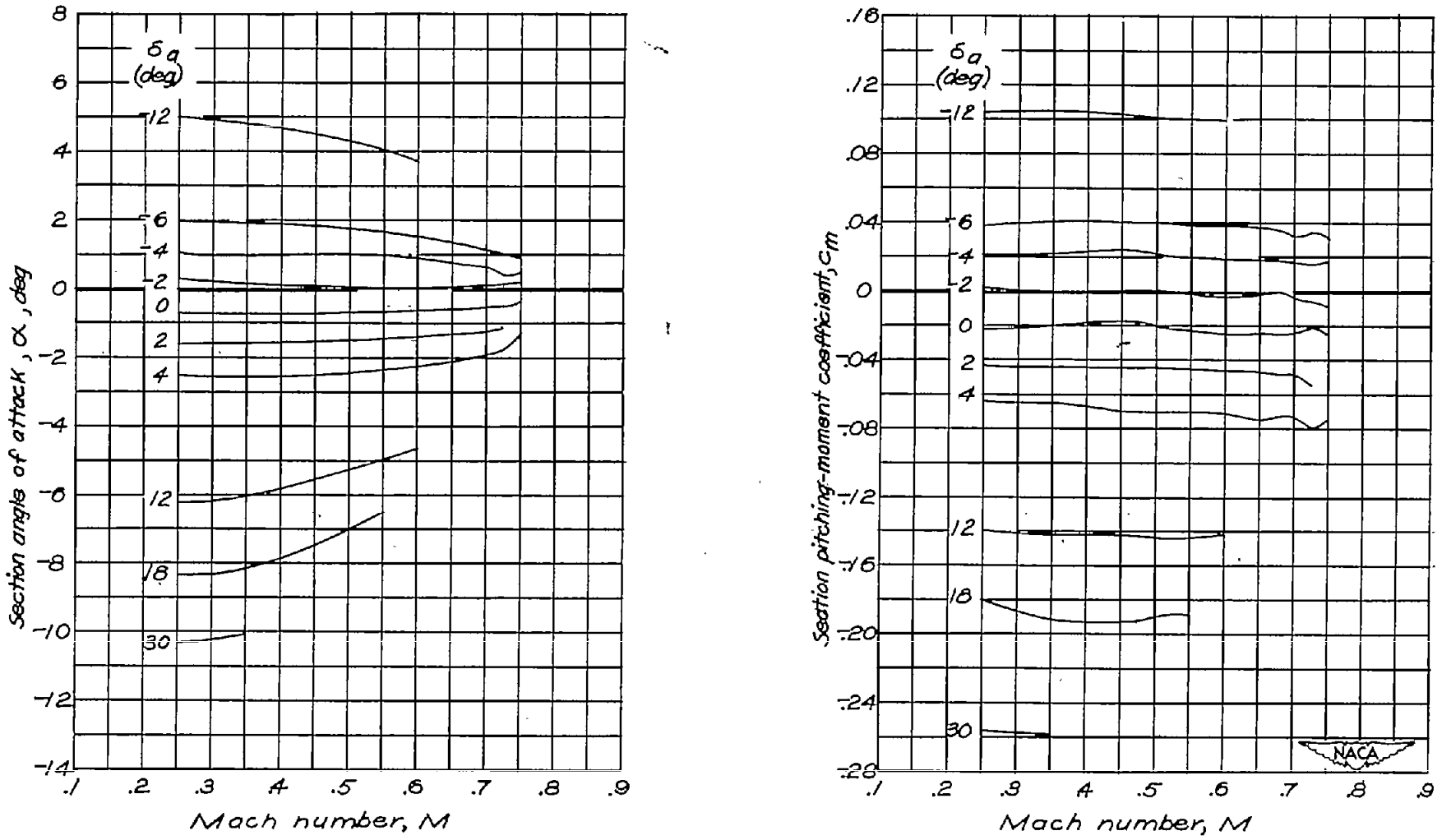

(c) $c_n = 0$.

Figure 6 .—Continued.

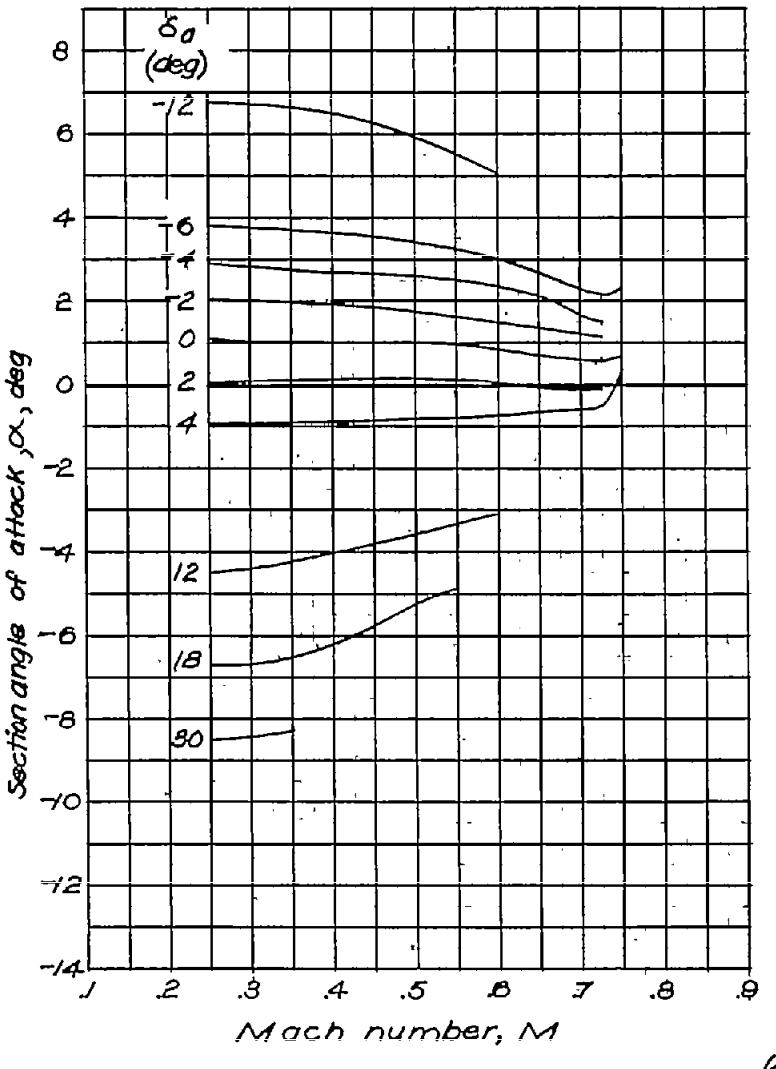

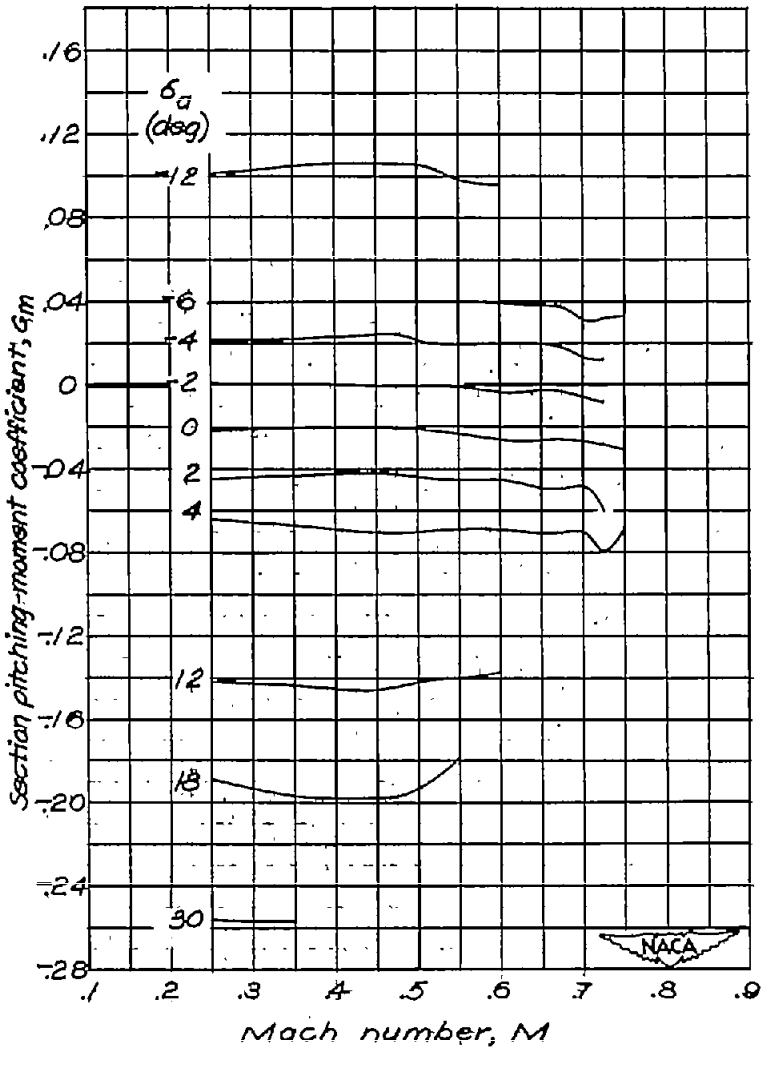

(d) $c_n = 0.2$.

Figure 6 .- Continued.

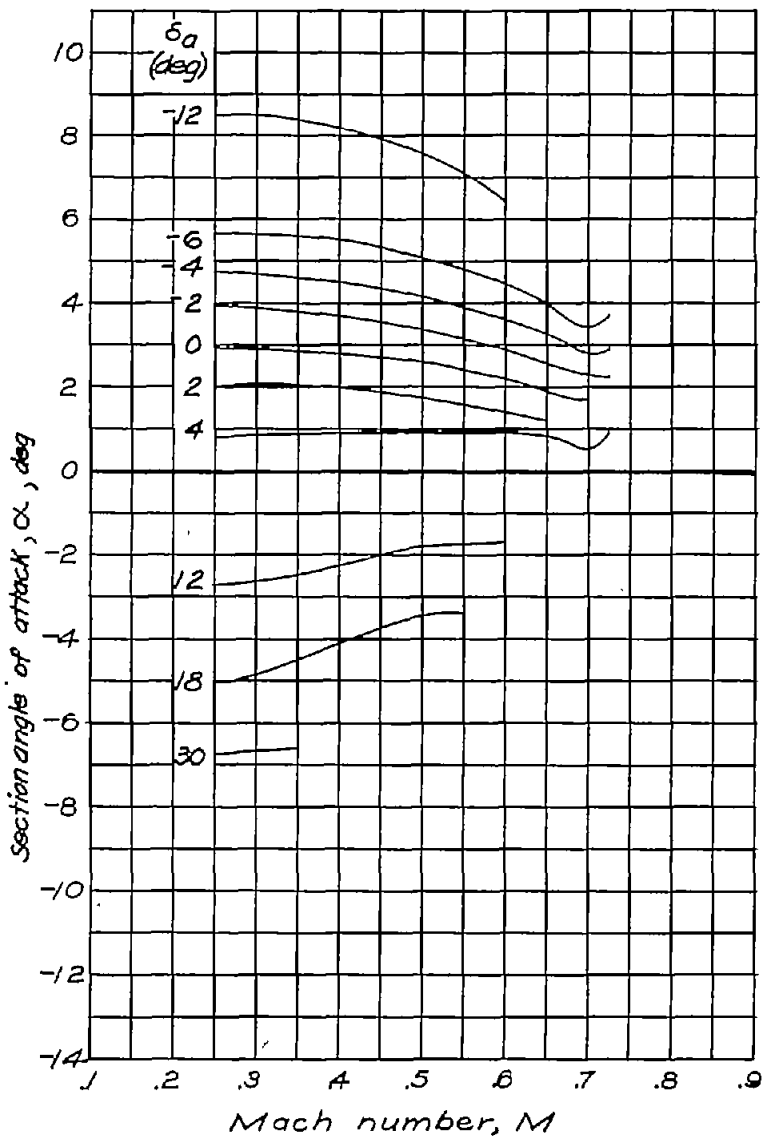

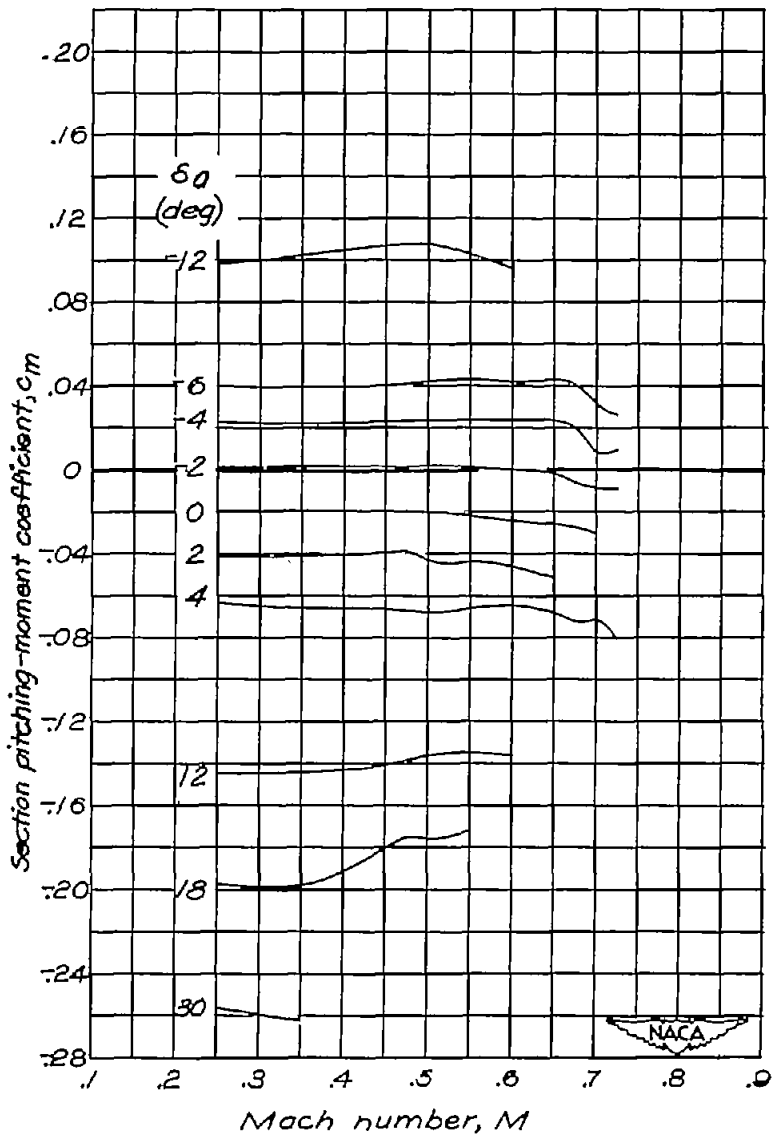

(e) c_n=0.4.

Figure 6 .- Continued.

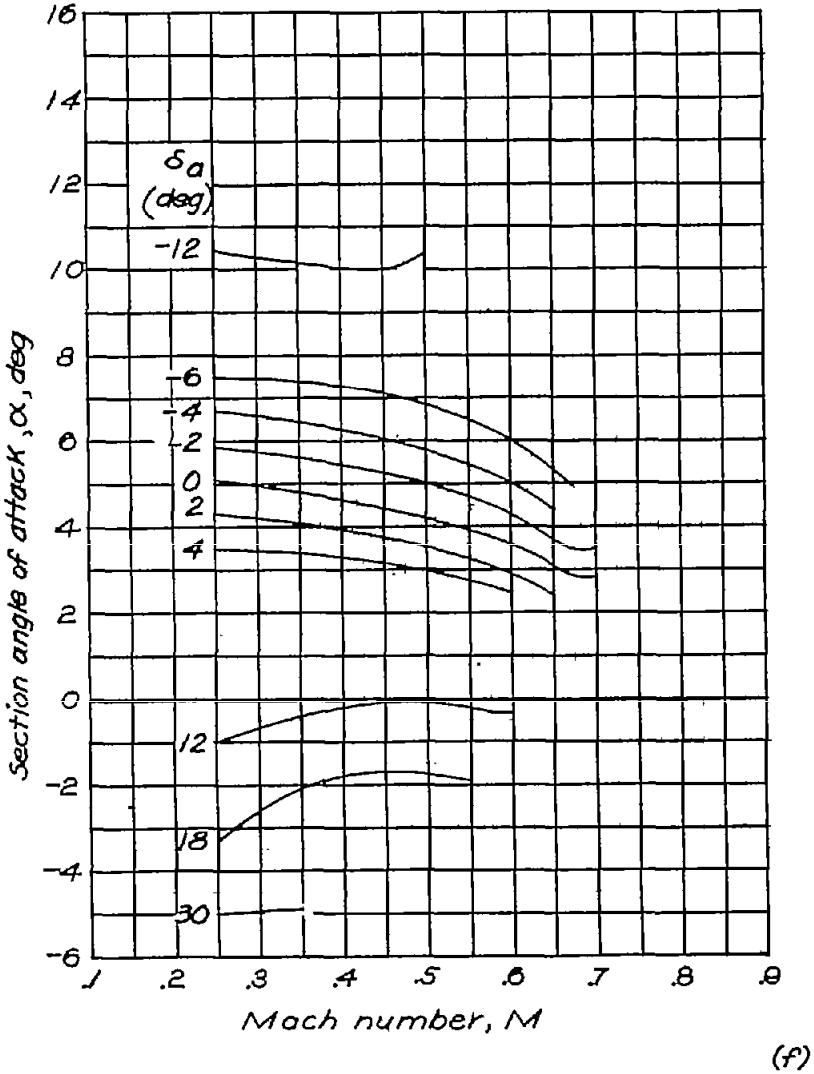

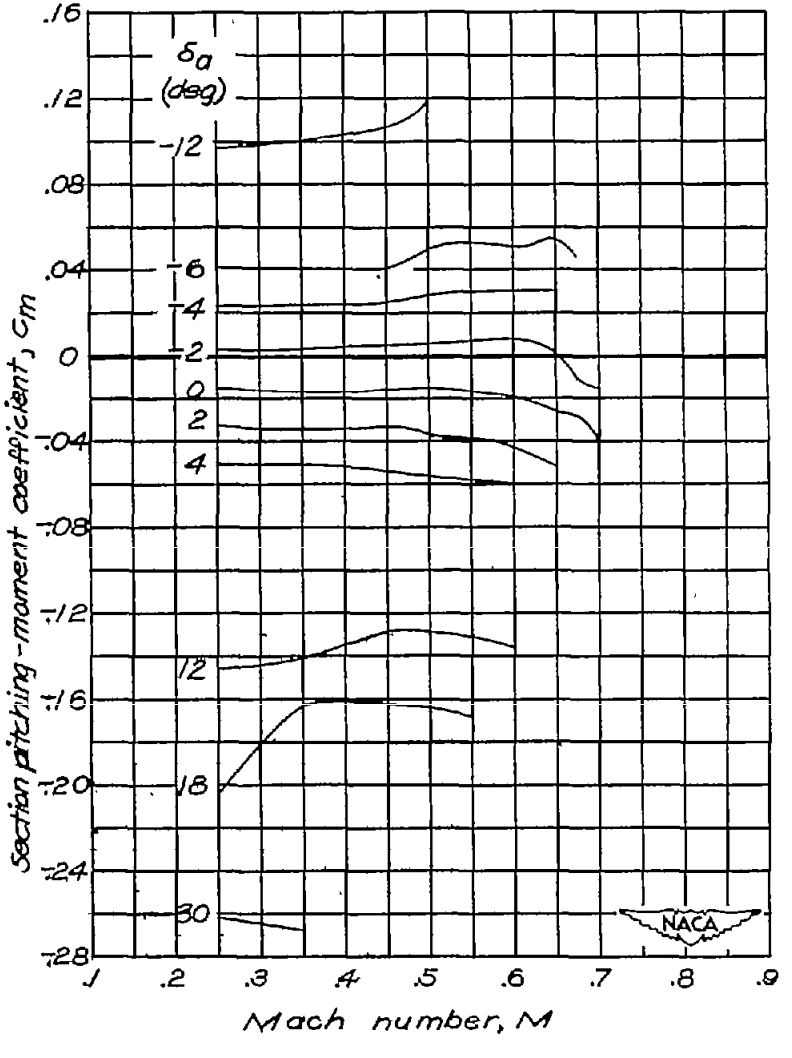

(f) $c_n = 0.6$.

Figure 6 .- Continued.

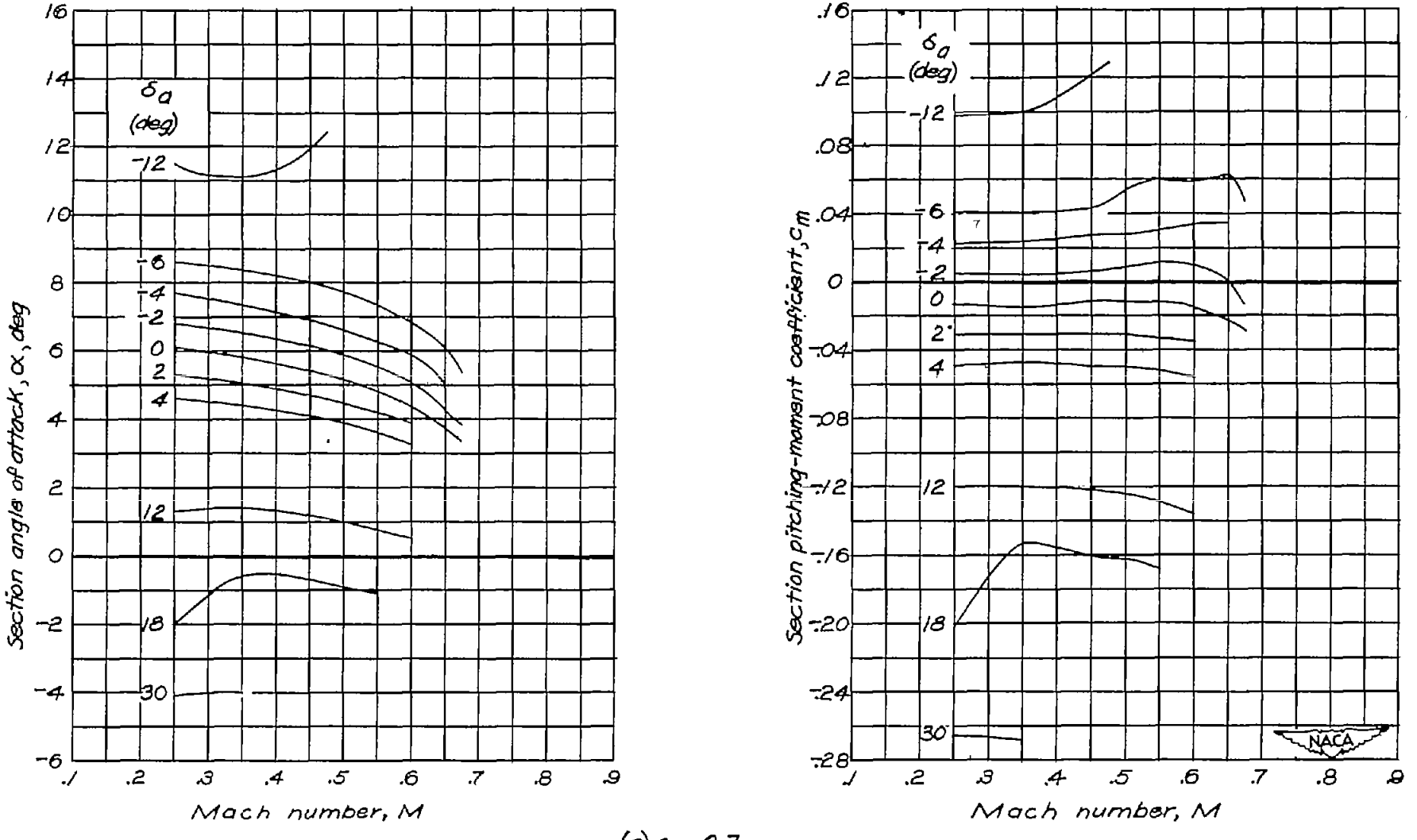

(g) $c_n = 0.7$.

Figure 6 .- Continued.

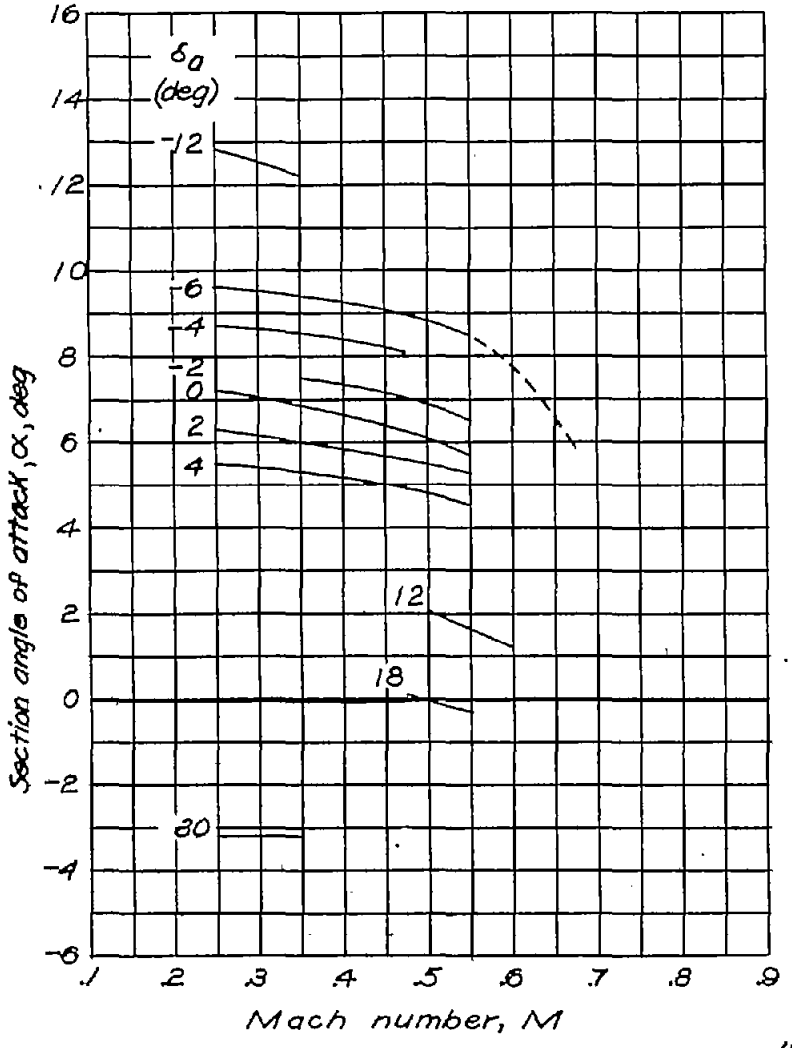

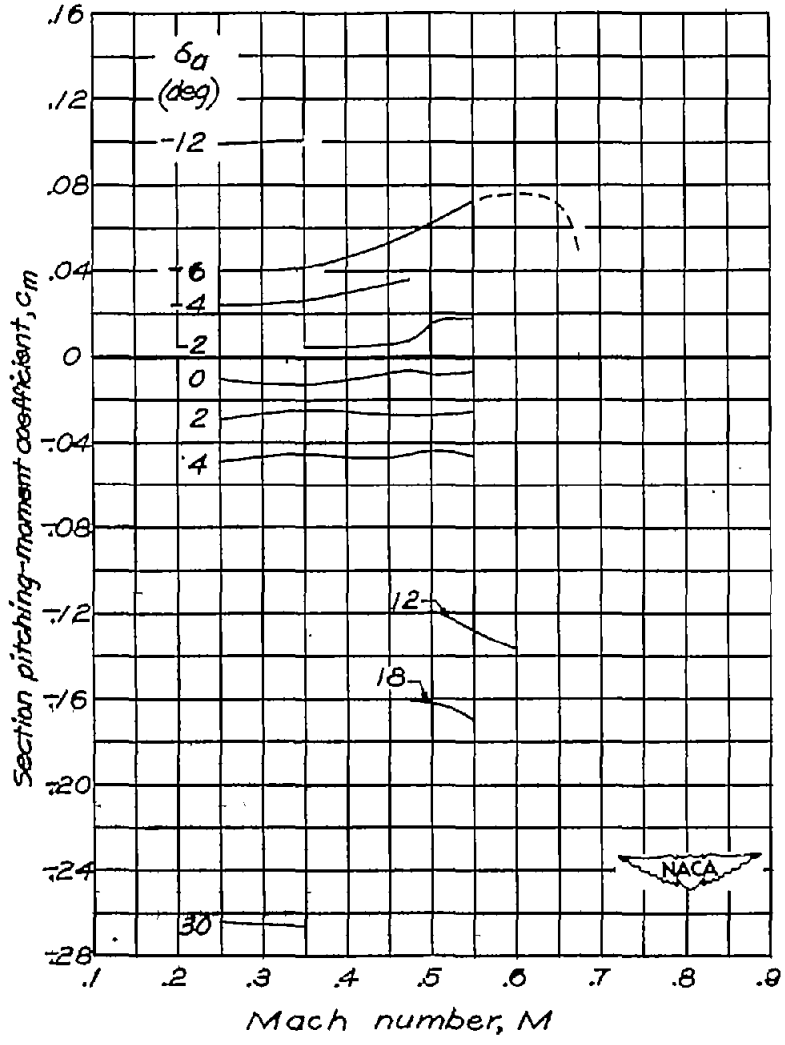

(h) $c_n = 0.8$.

Figure 6.- Concluded.

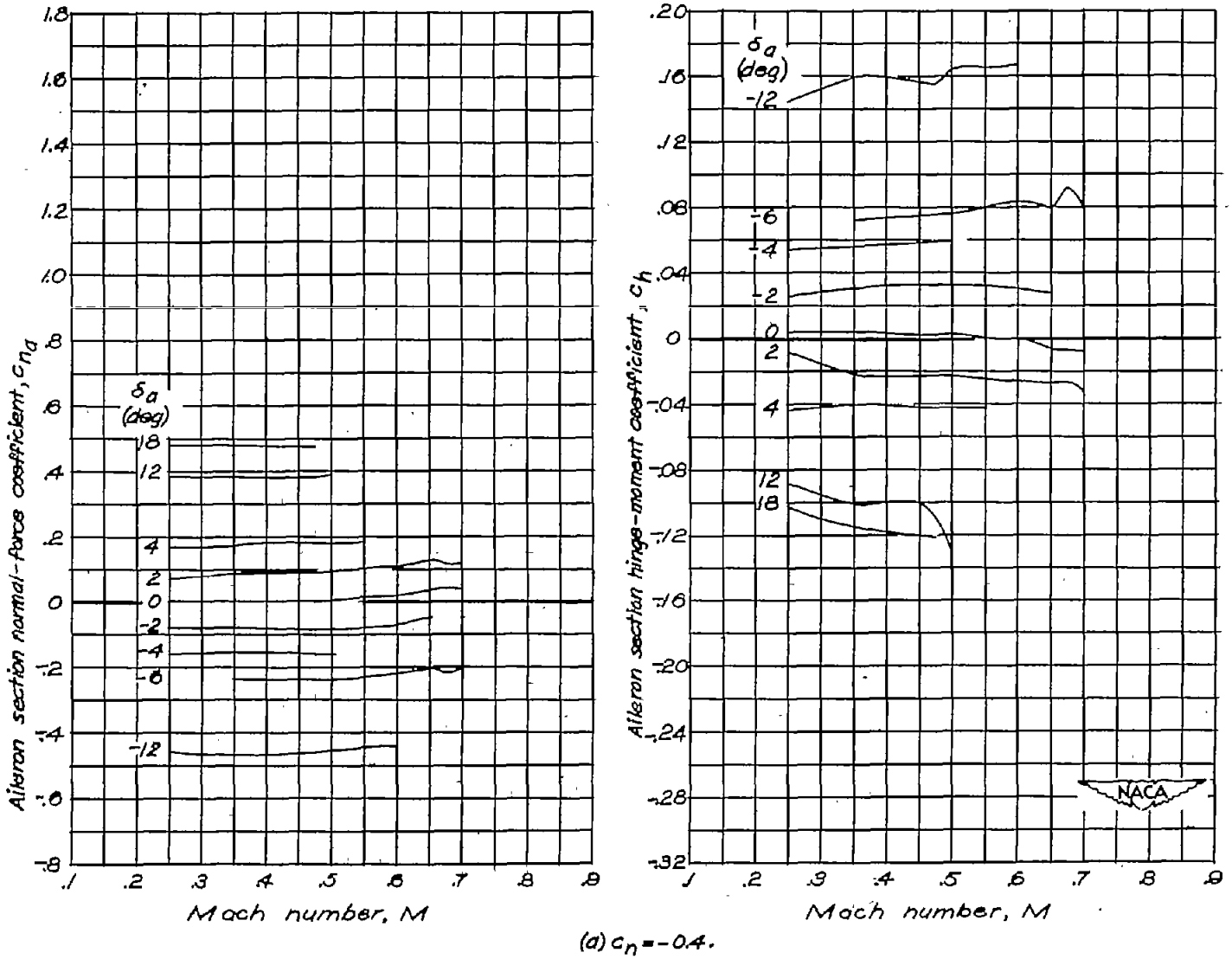

(a) $c_n = -0.4$.

Figure 7.- Variation of aileron normal-force and hinge-moment coefficients with Mach number for an unsealed 0.20c plain aileron of true-airfoil-contour profile mounted on an NACA 66,1-115 airfoil section.

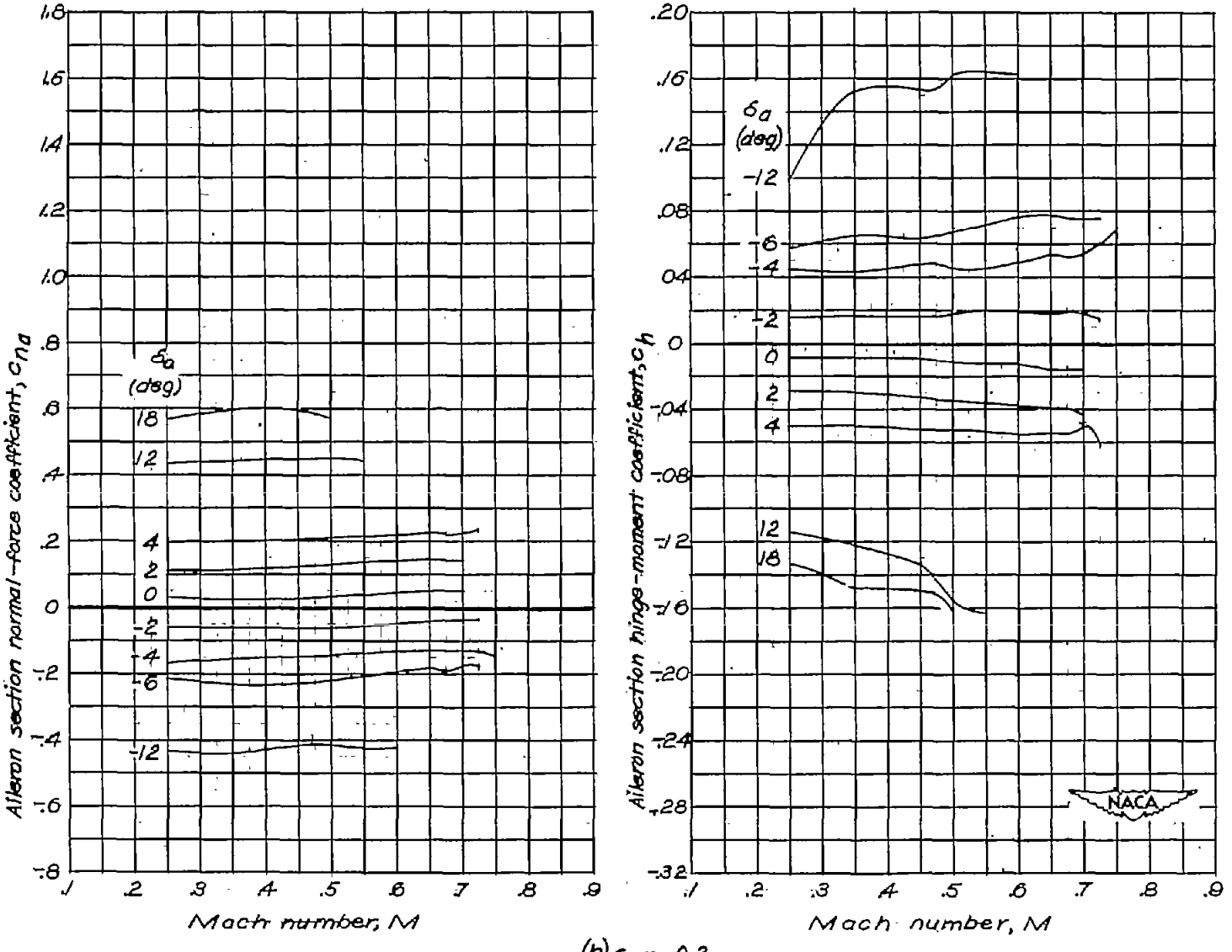

(b) $c_n = -0.2$.

Figure 7 .- Continued.

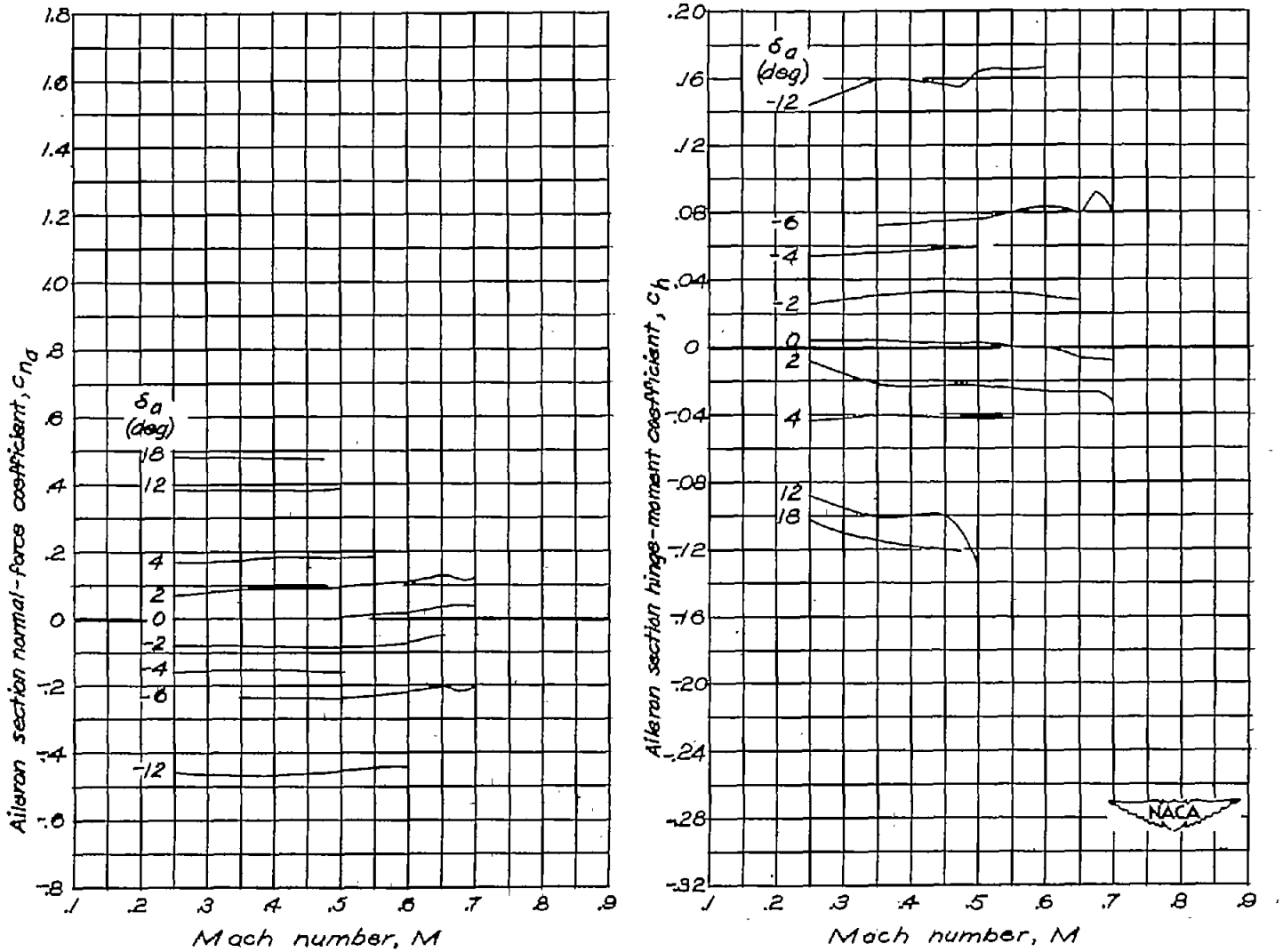

(a) $c_n = -0.4$.

Figure 7.- Variation of aileron normal-force and hinge-moment coefficients with Mach number for an unsealed 0.20c plain aileron of true-airfoil-contour profile mounted on an NACA 66,1-115 airfoil section.

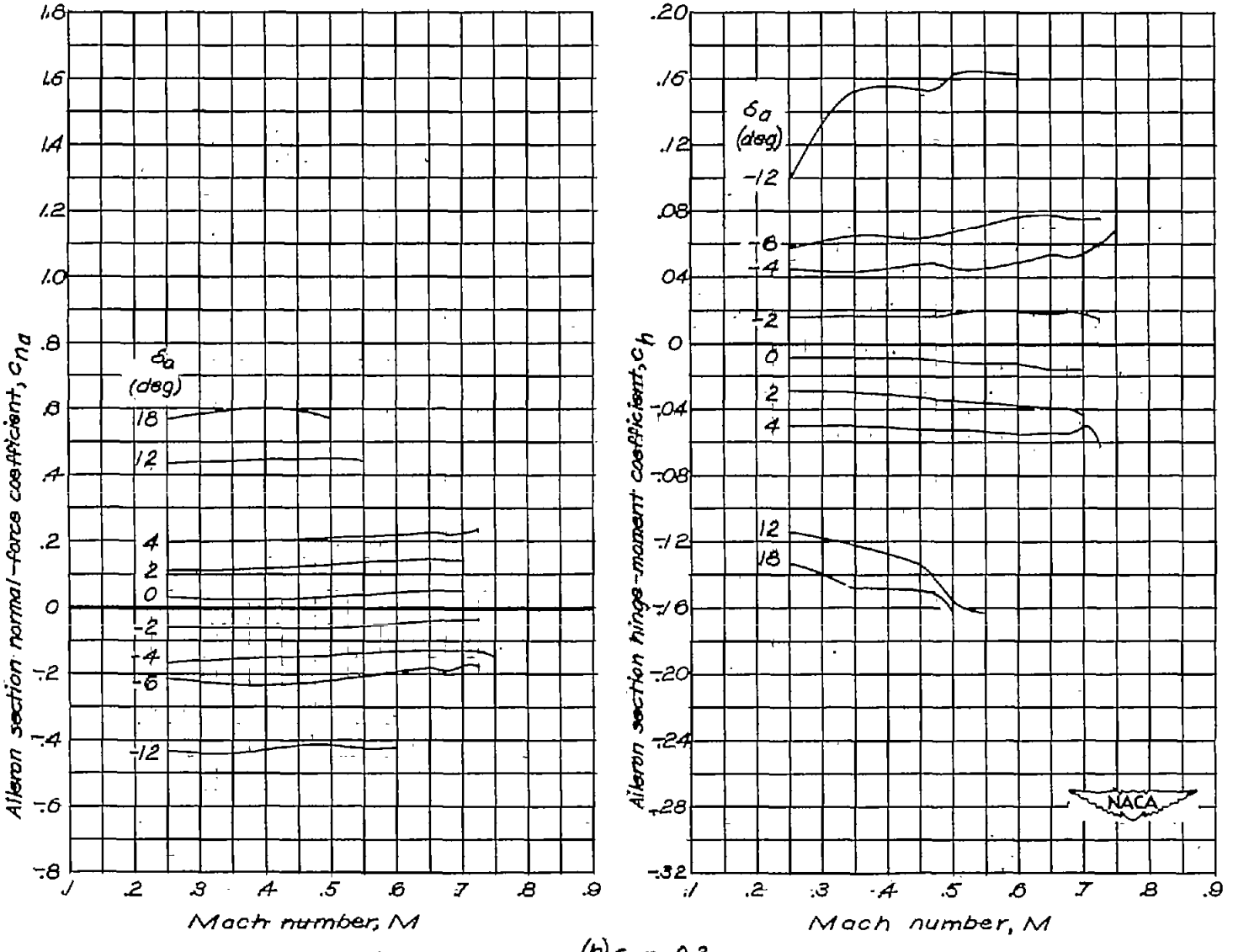

(b) $c_n = -0.2$.

Figure 7 .- Continued.

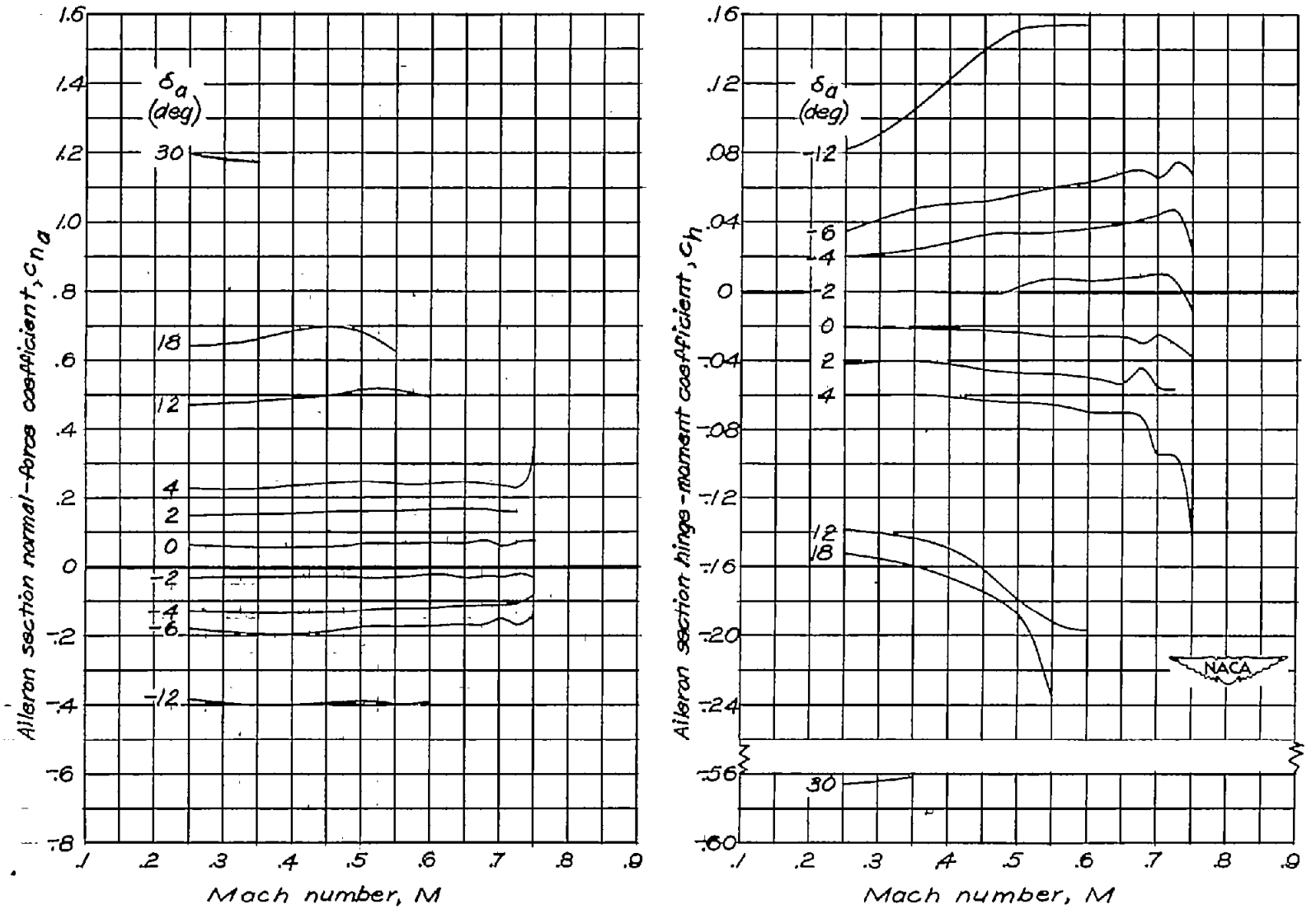

(c) $c_n = 0$.

Figure 7 .- Continued.

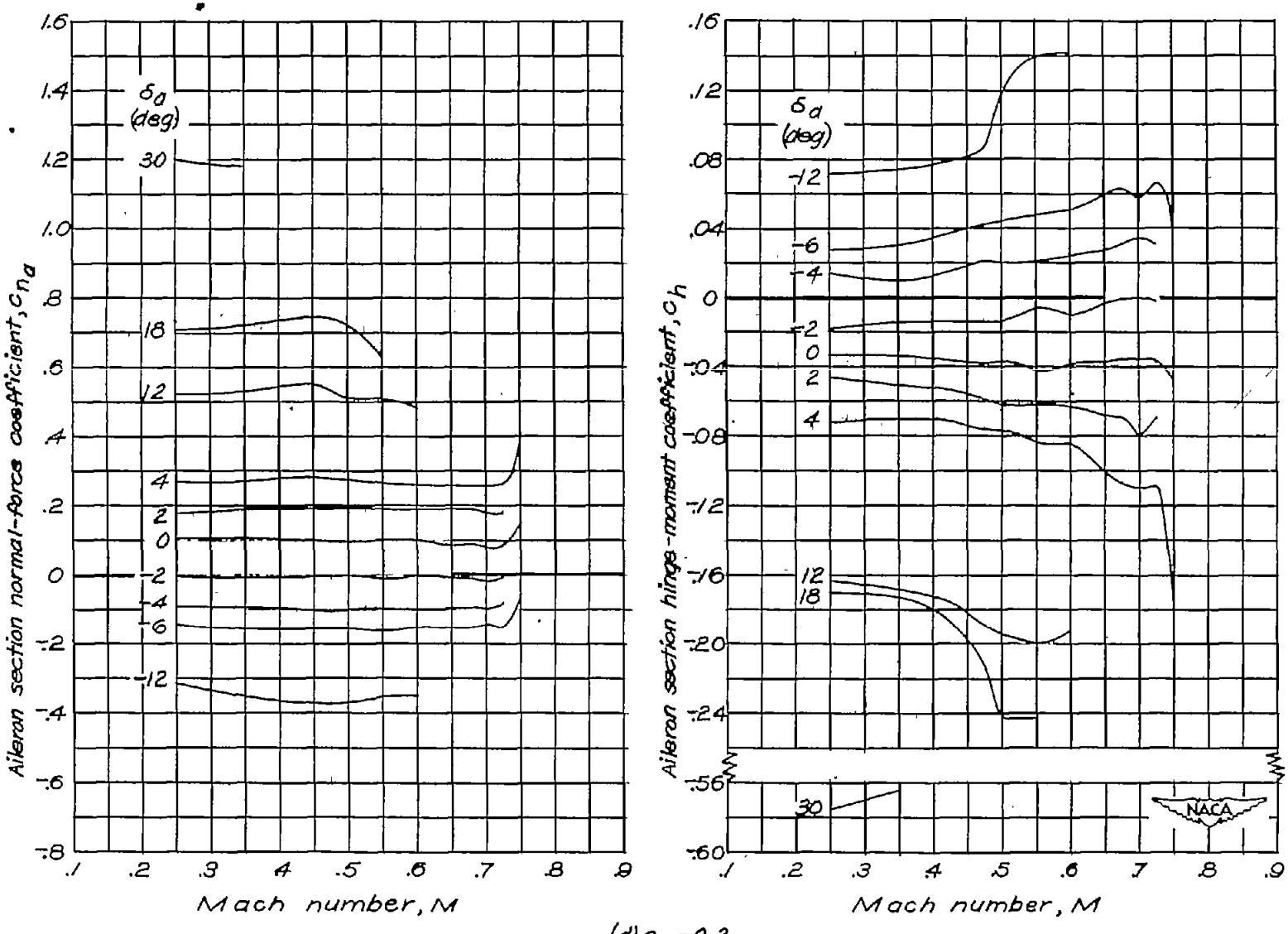

(d) $c_n = 0.2$.

Figure 7 .—Continued.

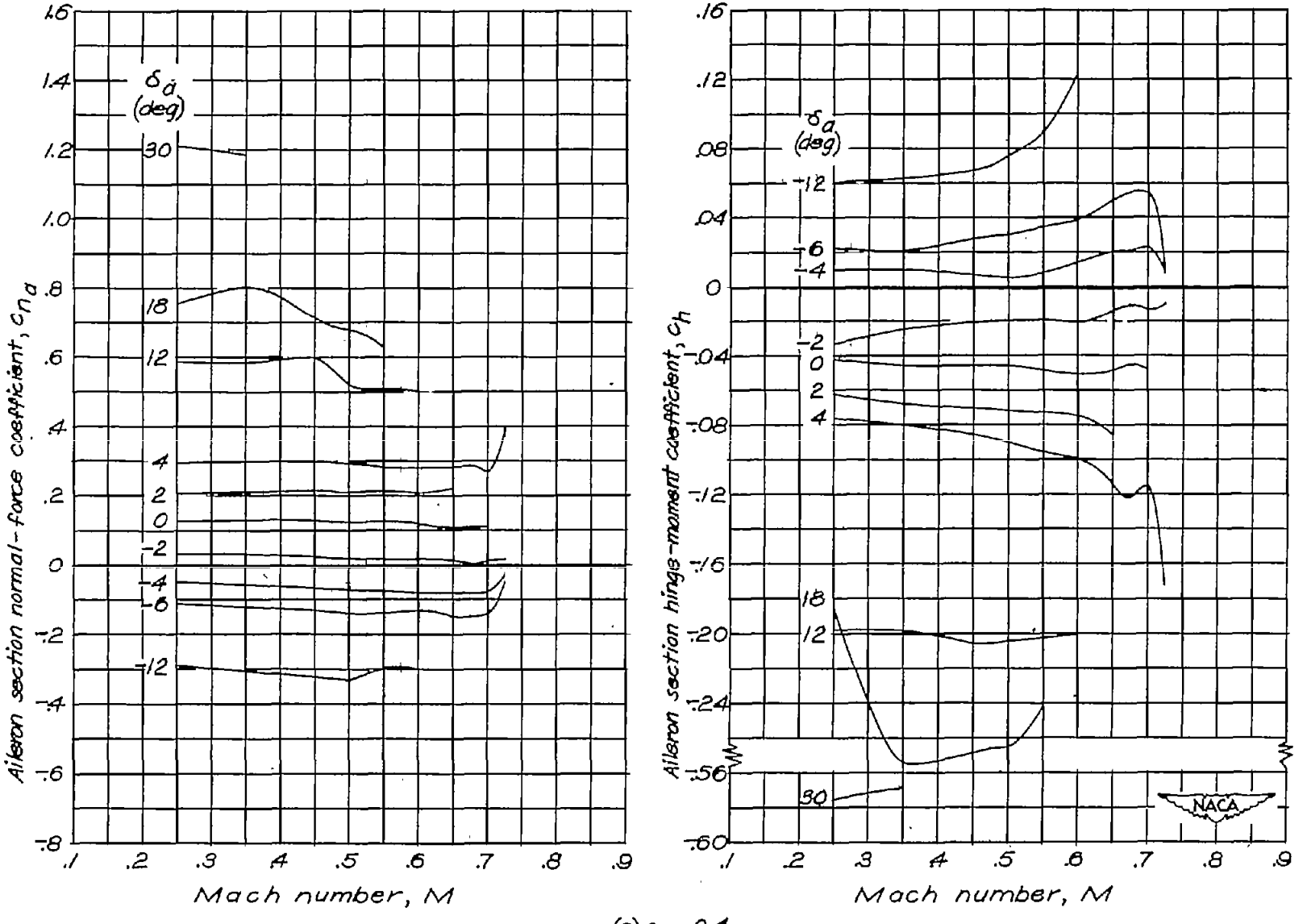

(a) $c_n = 0.4$.

Figure 7 .- Continued.

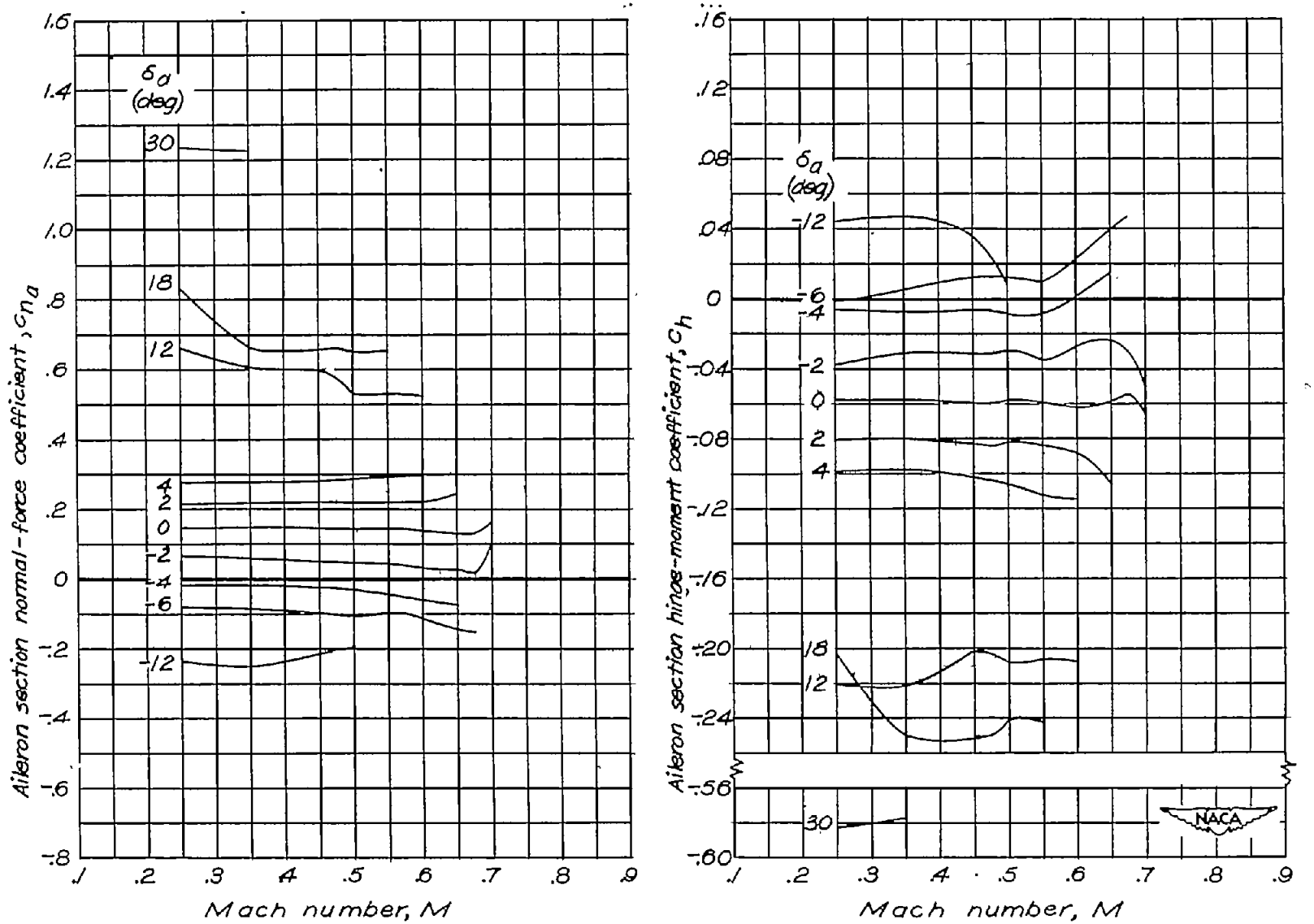

Mach number, M

(f) $c_n = 0.6$.

Figure 7 .- Continued.

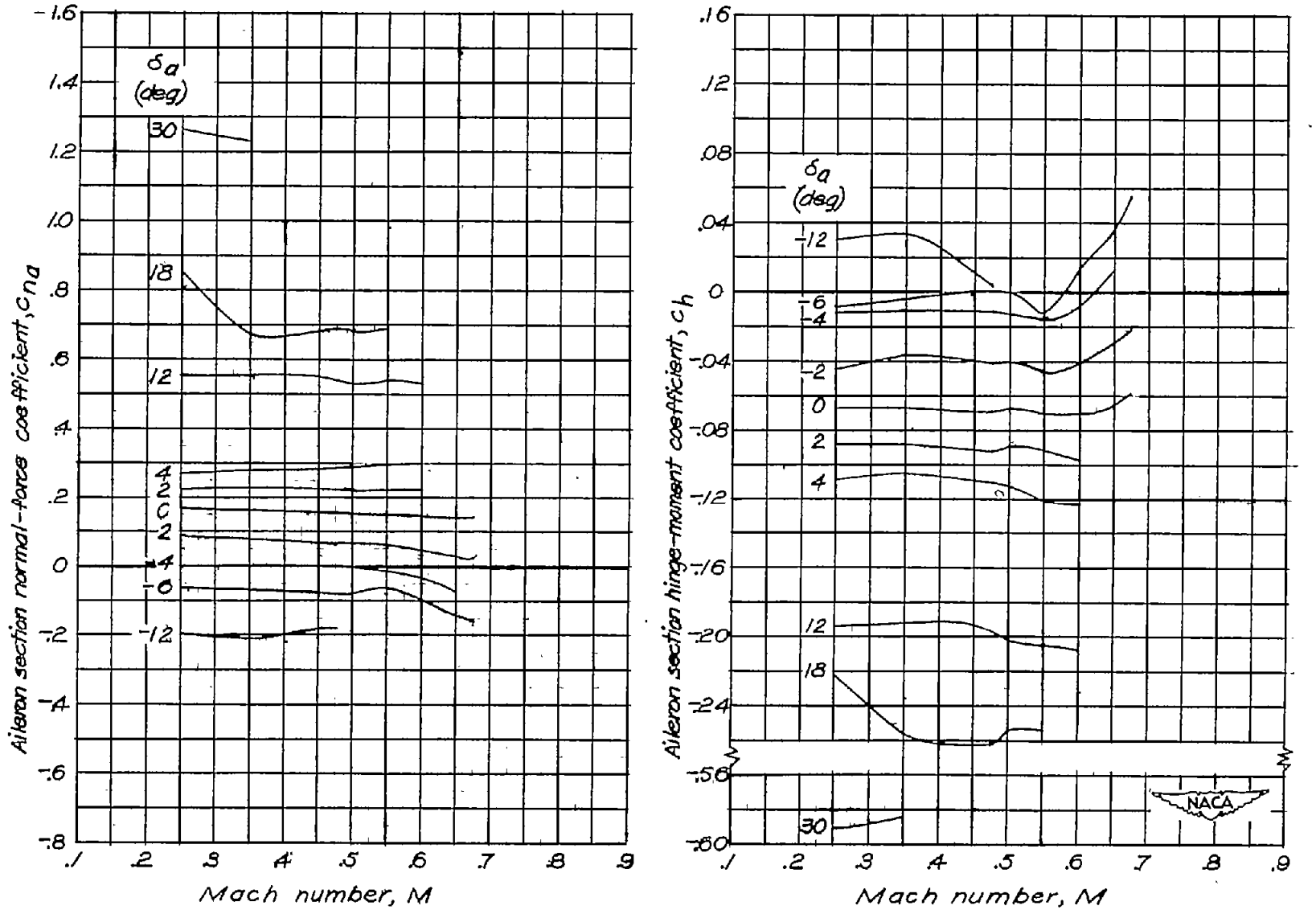

(g) $c_n = 0.7$.

Figure 7.—Continued.

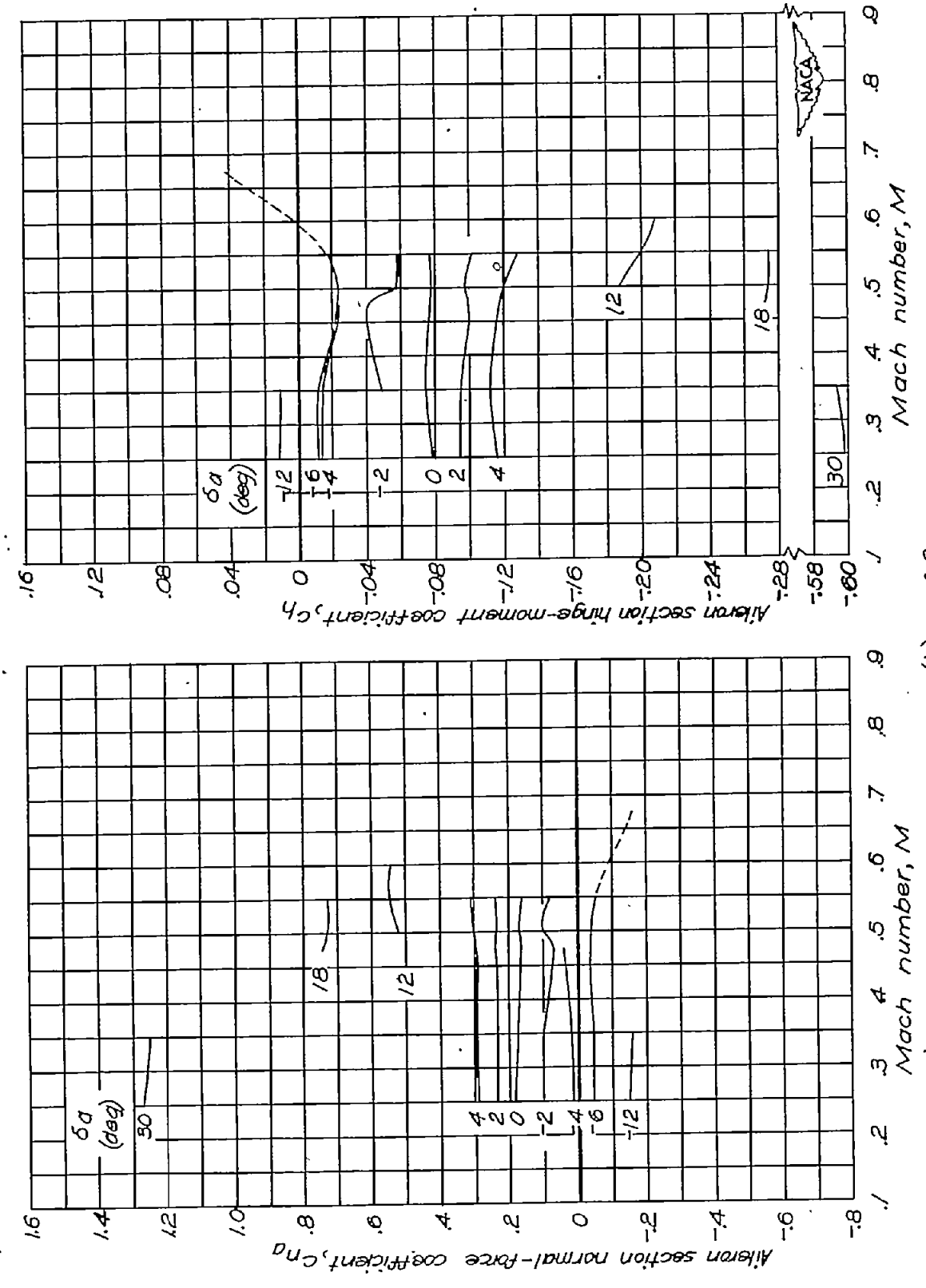

(h) c_n=0.8.

Figure 7 - Concluded.

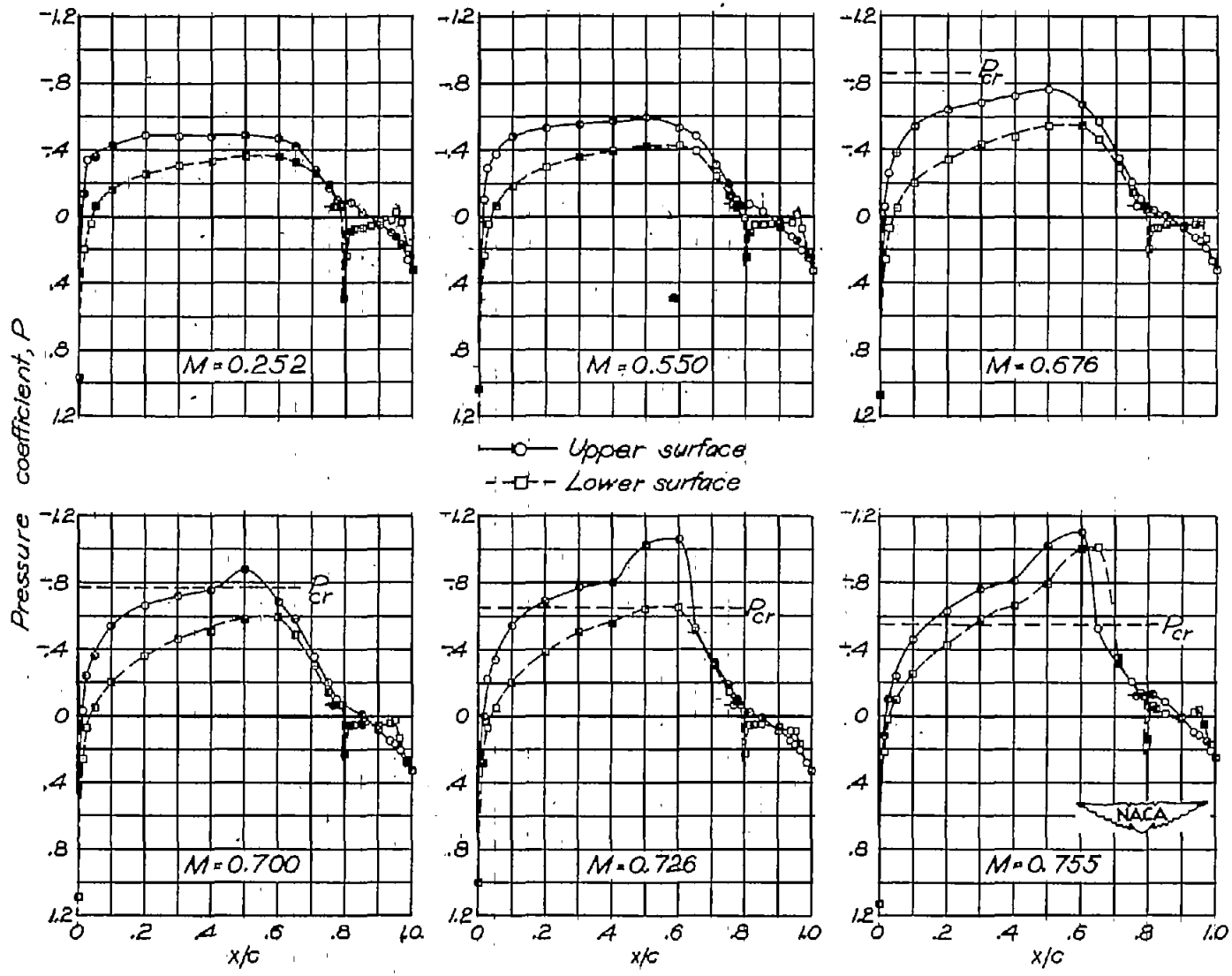

Figure 8.– Pressure distribution about an NACA 66,1-115 airfoil section equipped with an unsealed 0.20c plain aileron of beveled-trailing-edge profile. $\delta_a = 0°$, $\alpha = 1°$.

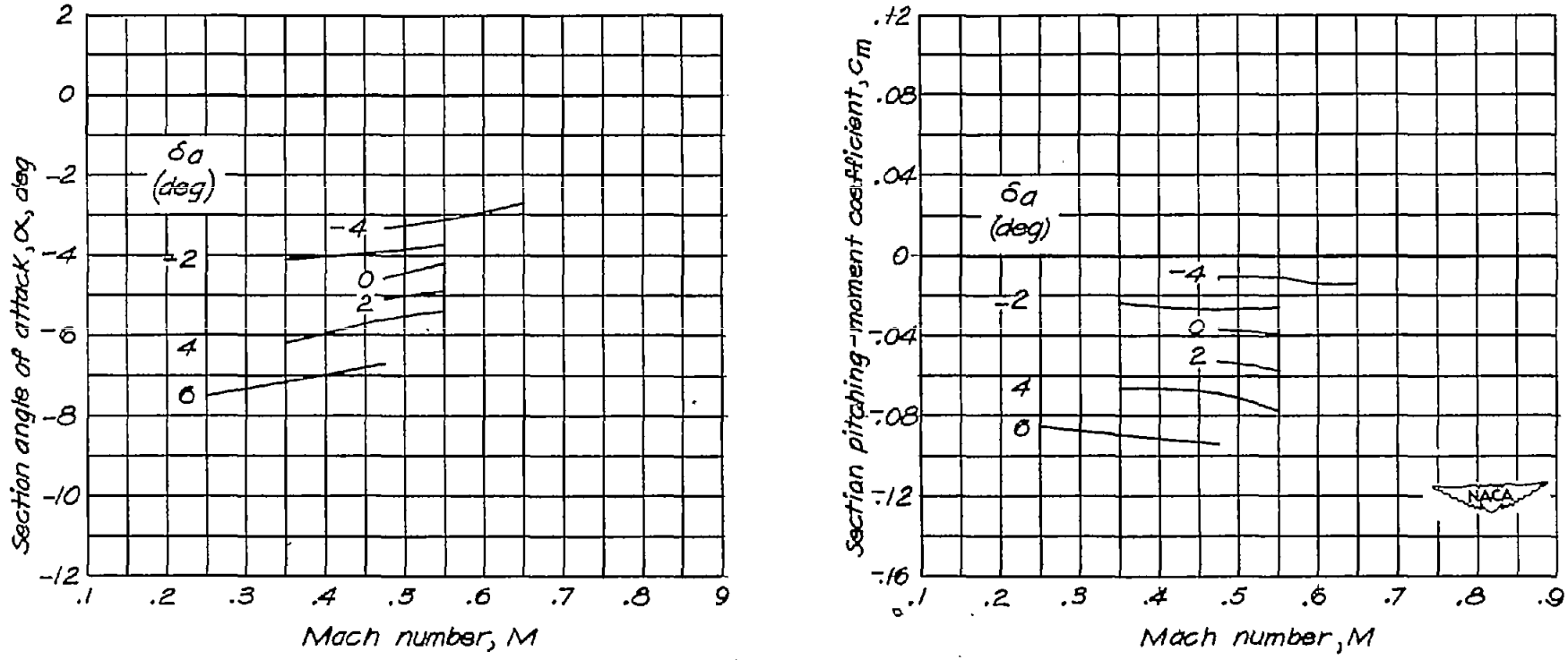

(a) c_n=-0.4.

Figure 9.- Variation of angle of attack and pitching-moment coefficient with Mach number for an NACA 66,1-115 airfoil section equipped with an unsealed 0.20c plain aileron of beveled-trailing-edge profile.

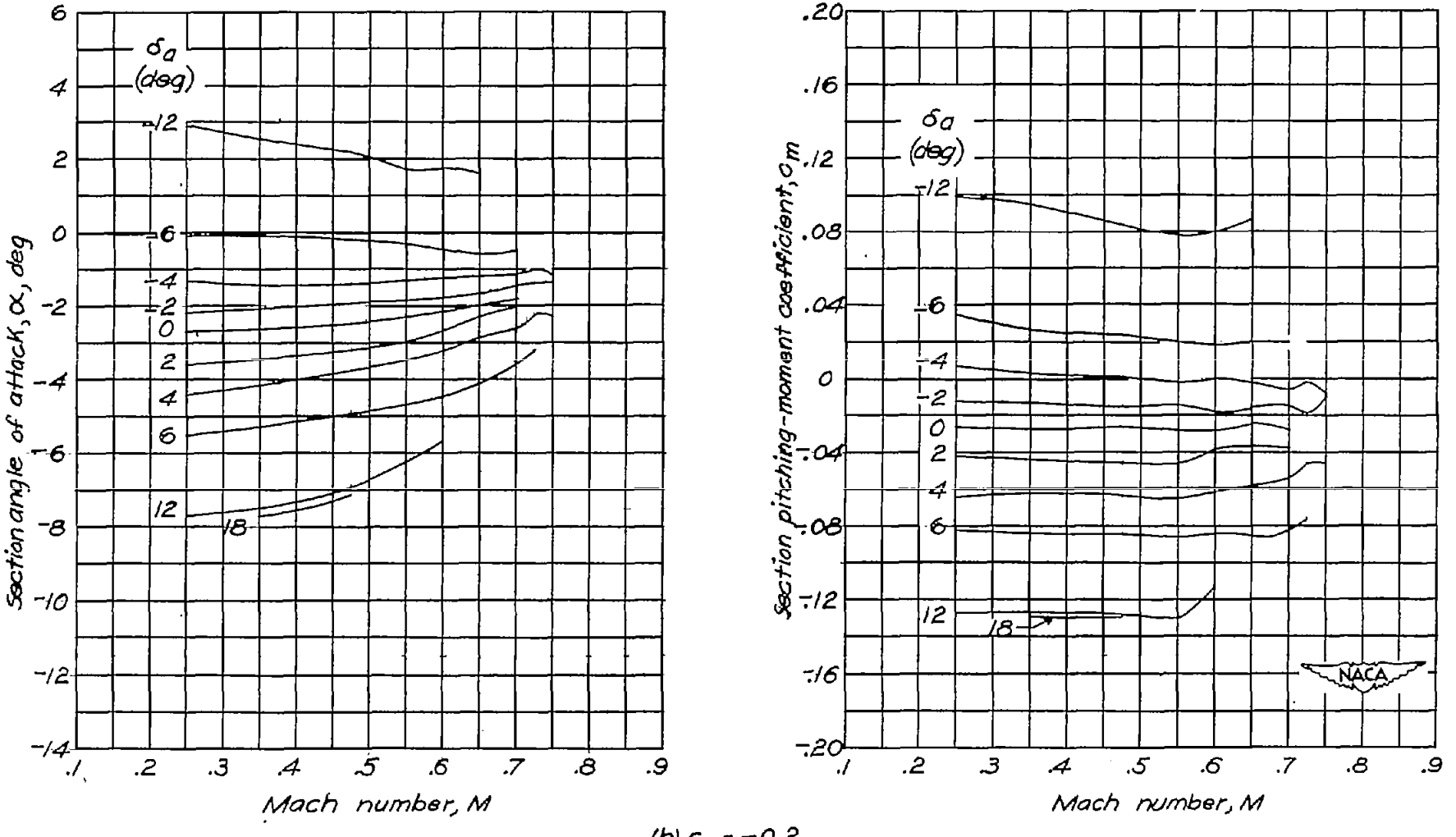

(b) $c_n = -0.2$.

Figure 9.—Continued.

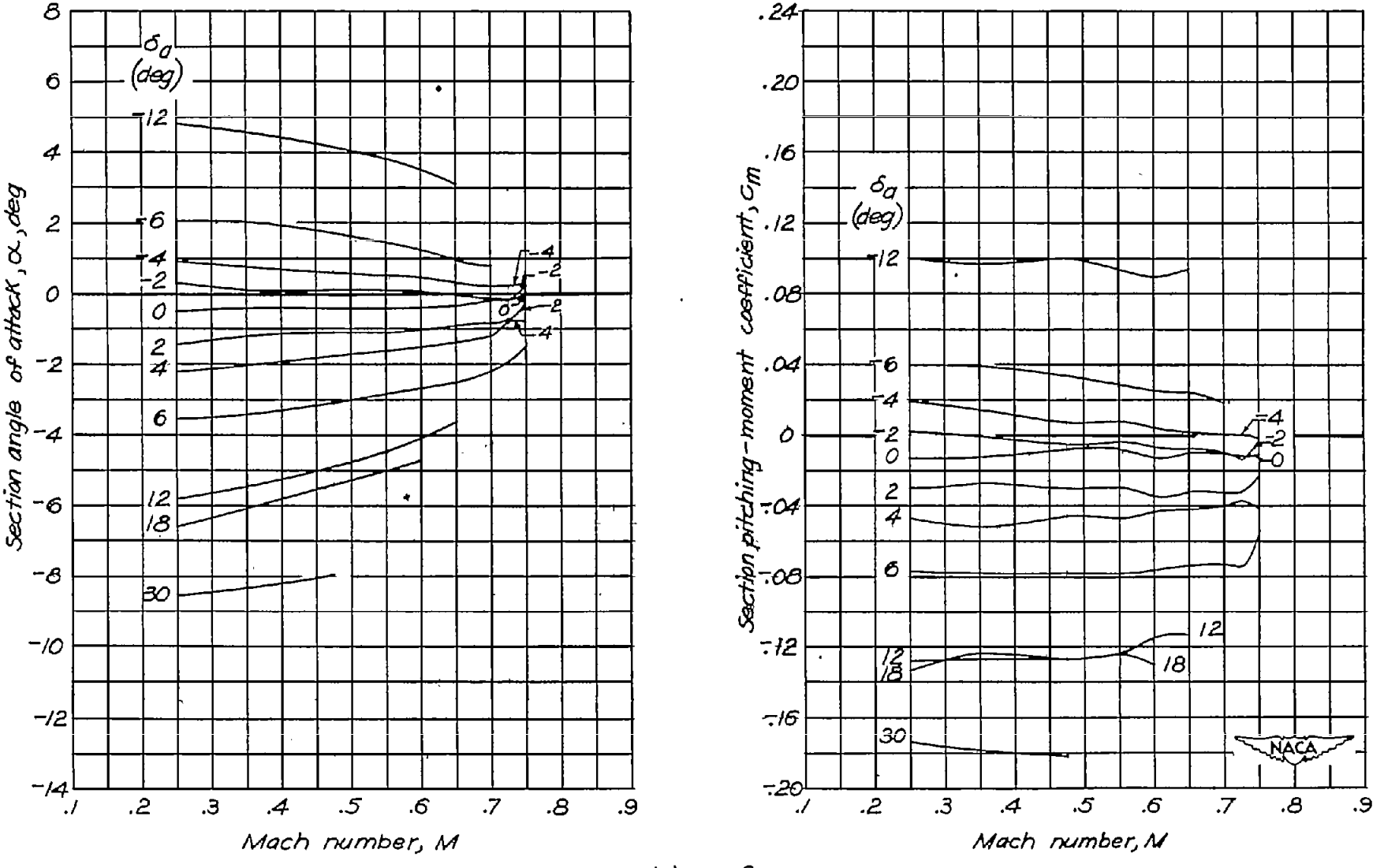

(c) $c_n = 0$.

Figure 9.- Continued.

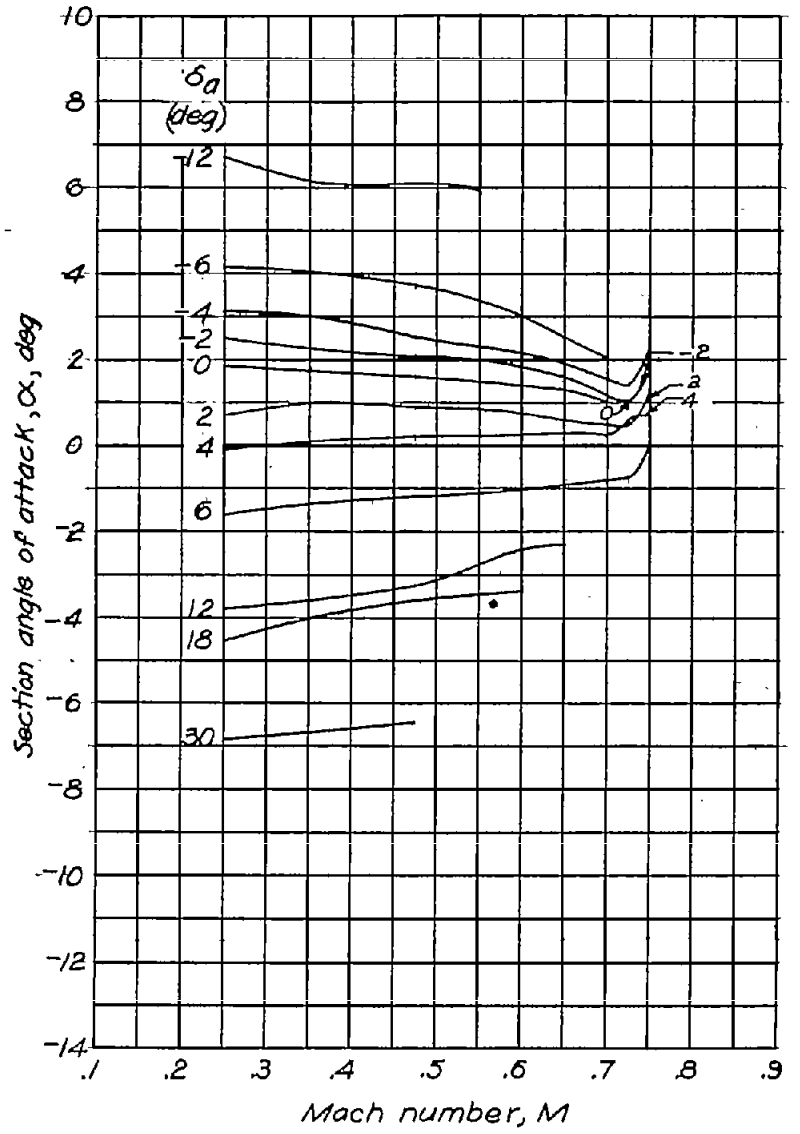

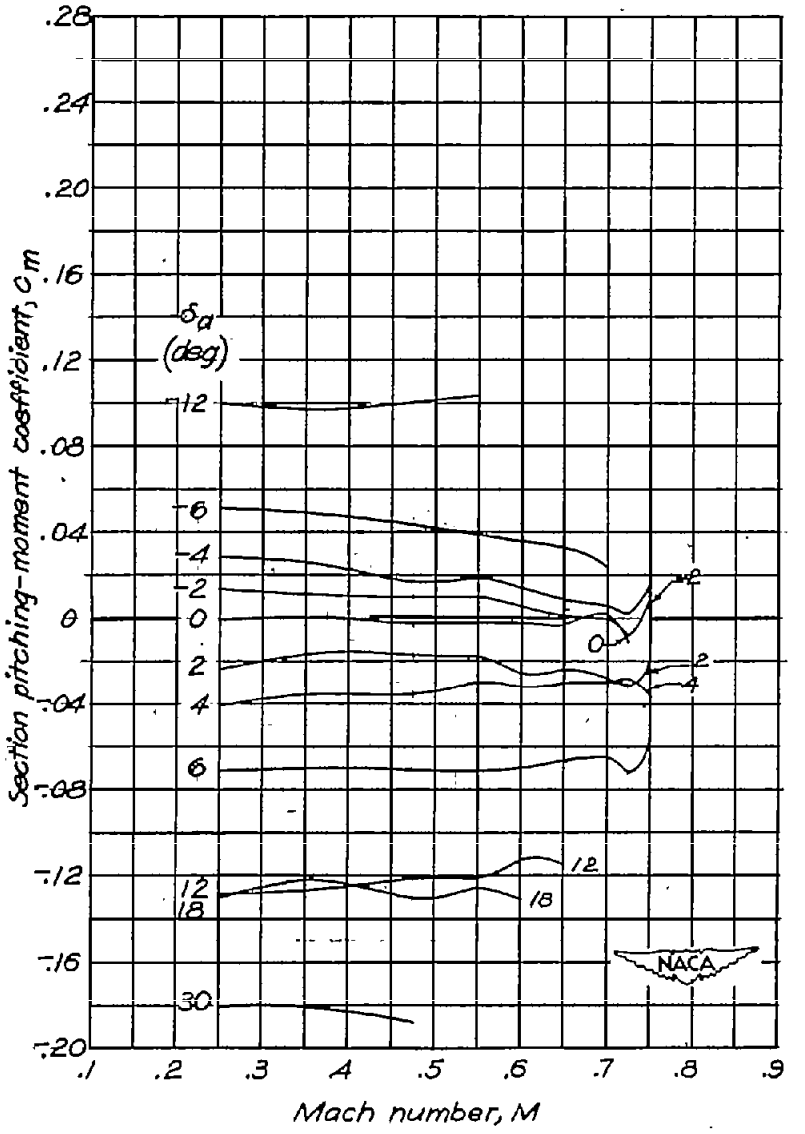

(d) $c_n = 0.2$.

Figure 9.- Continued.

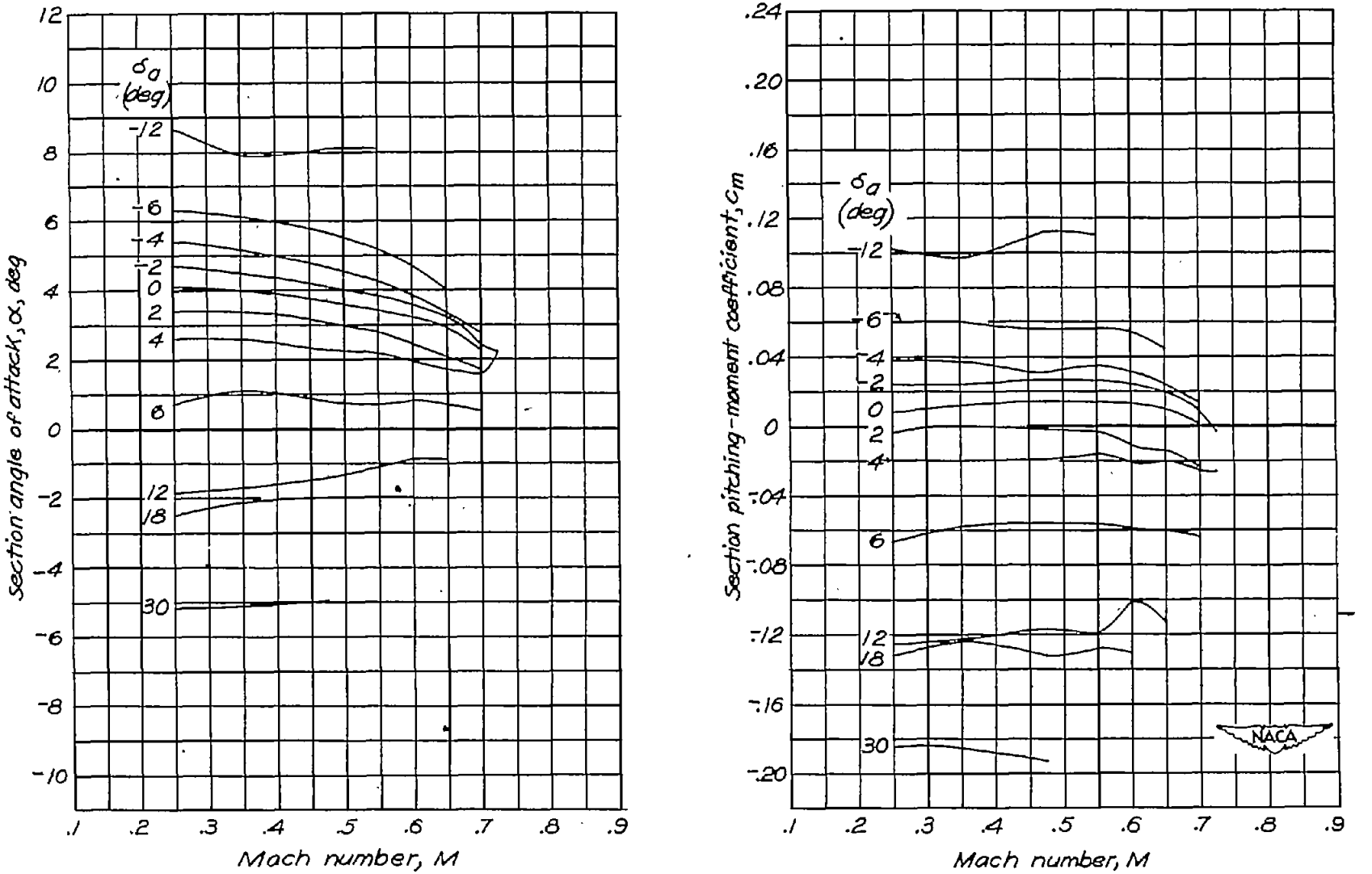

(e) $c_n = 0.4$.

Figure 9.—Continued.

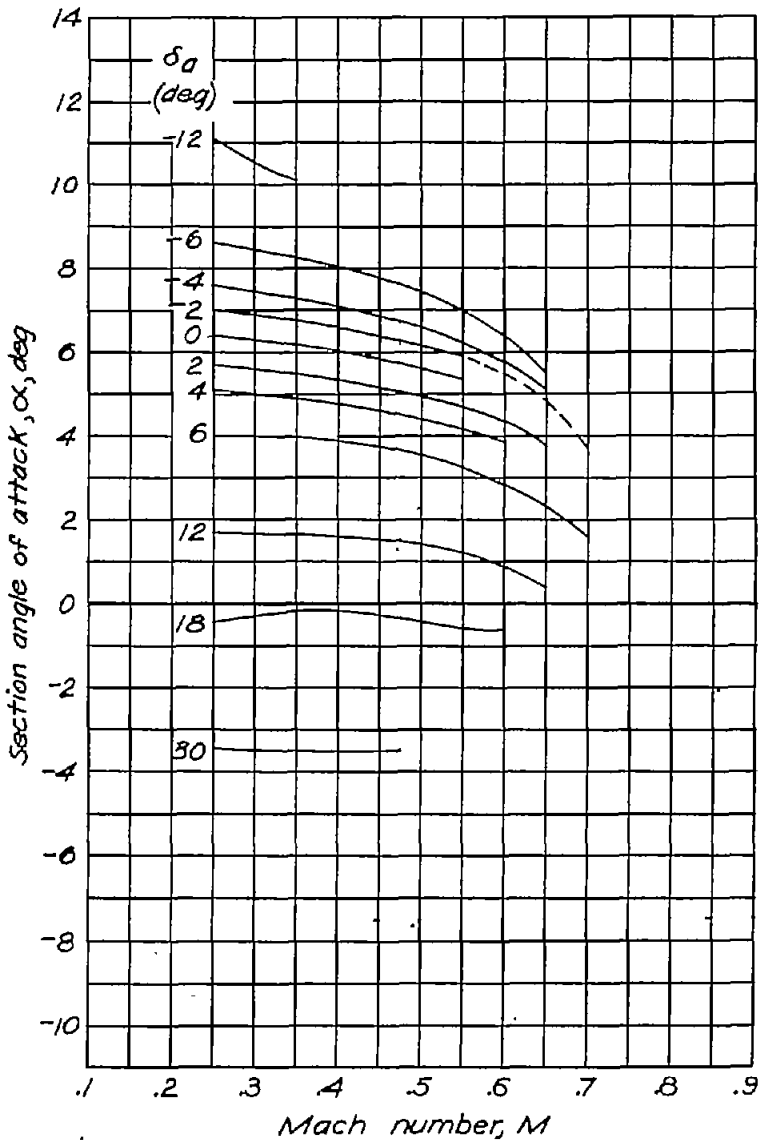

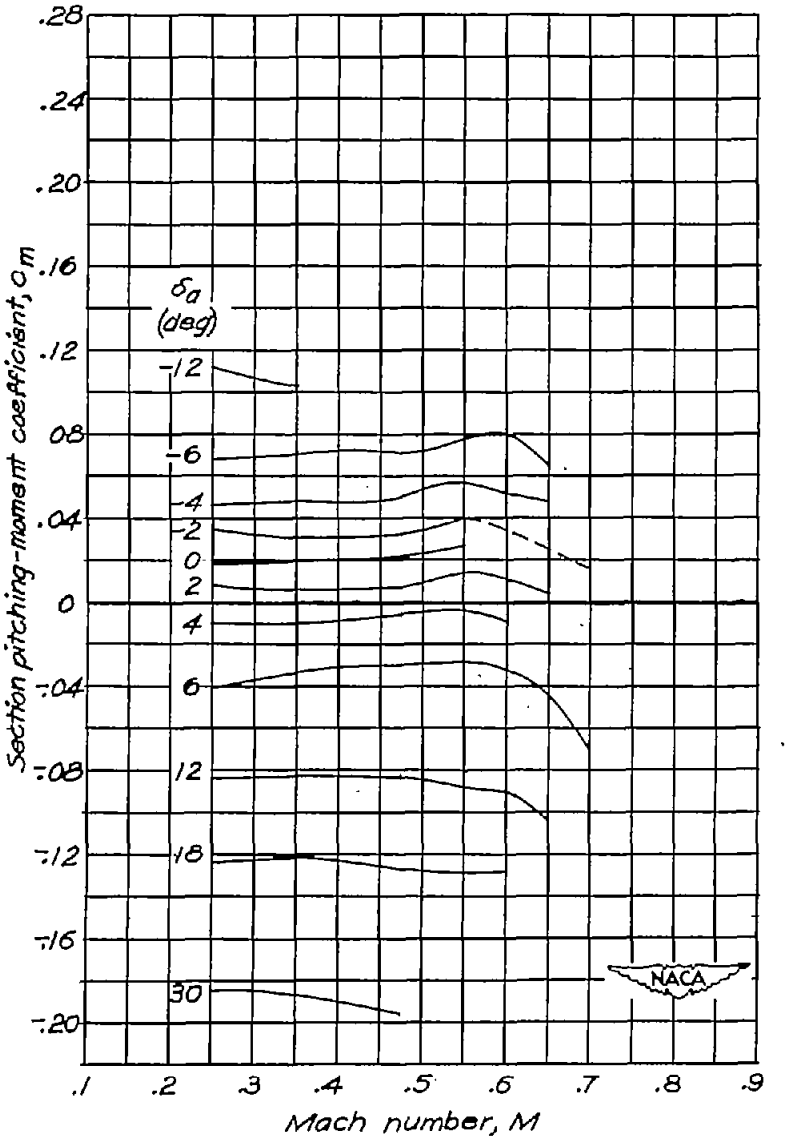

(f) $c_n = 0.6$.

Figure 9 .– Continued.

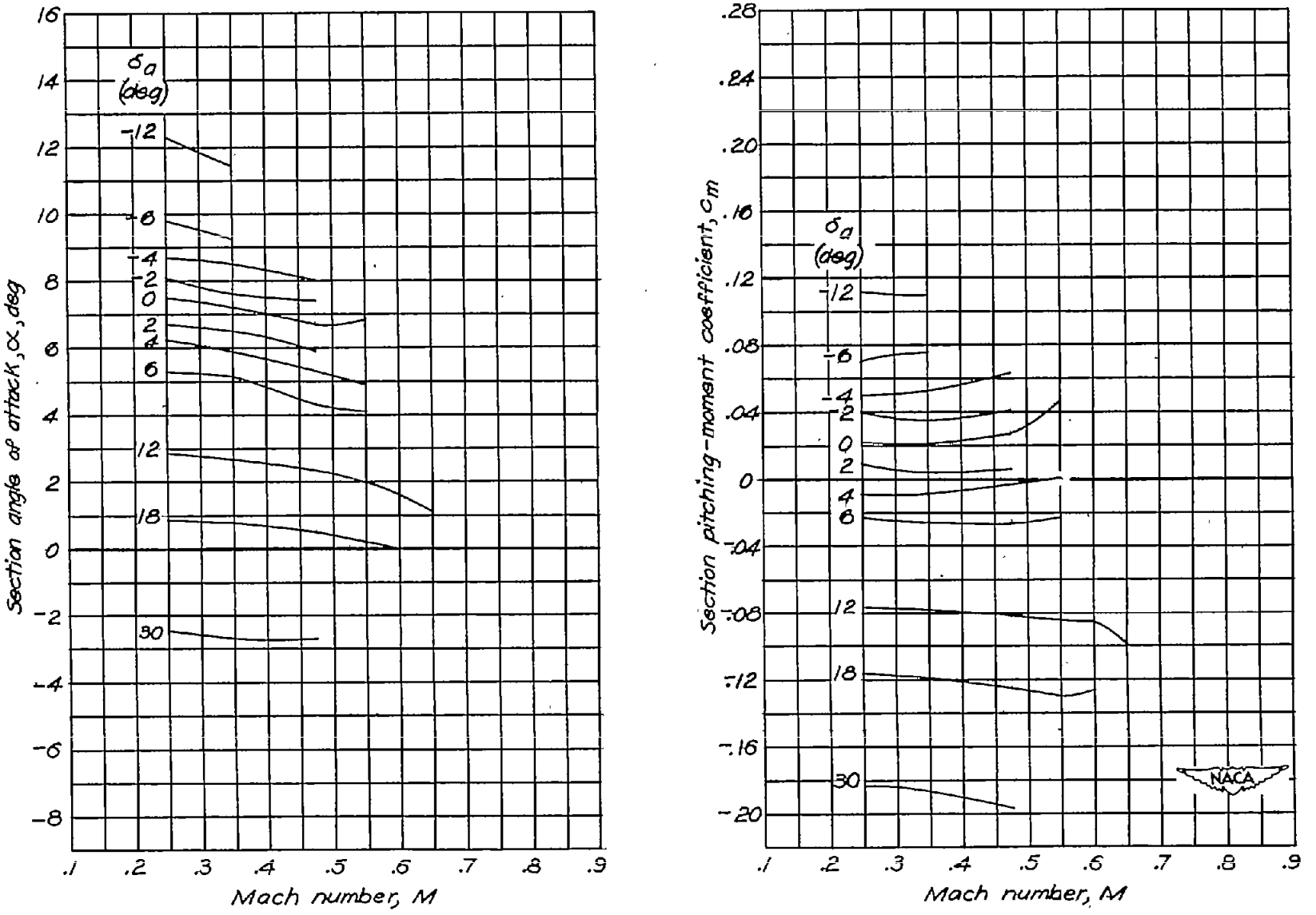

(g) $c_n = 0.7$.

Figure 9.- Continued.

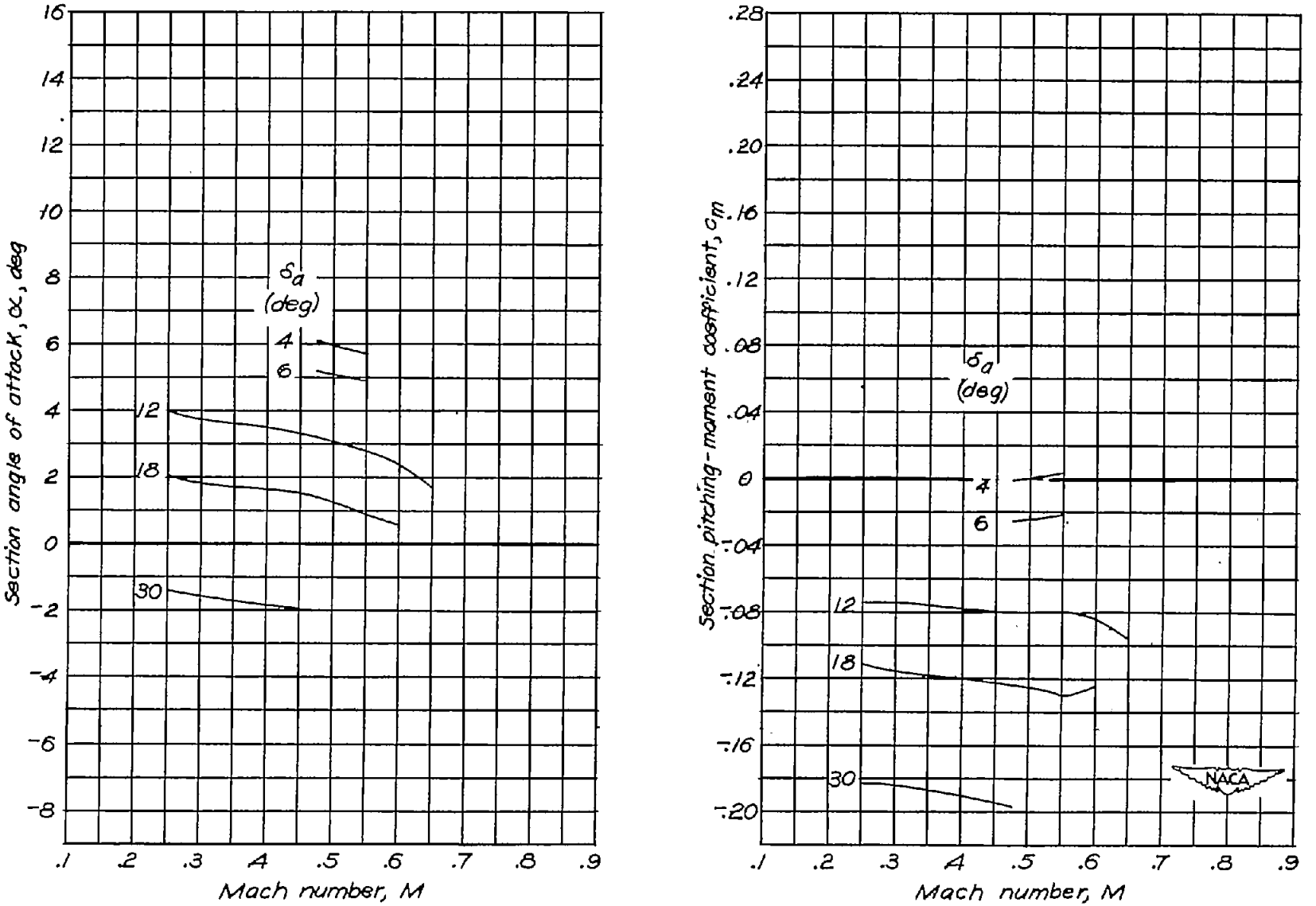

(h) $c_n = 0.8$.

Figure 9.—Concluded.

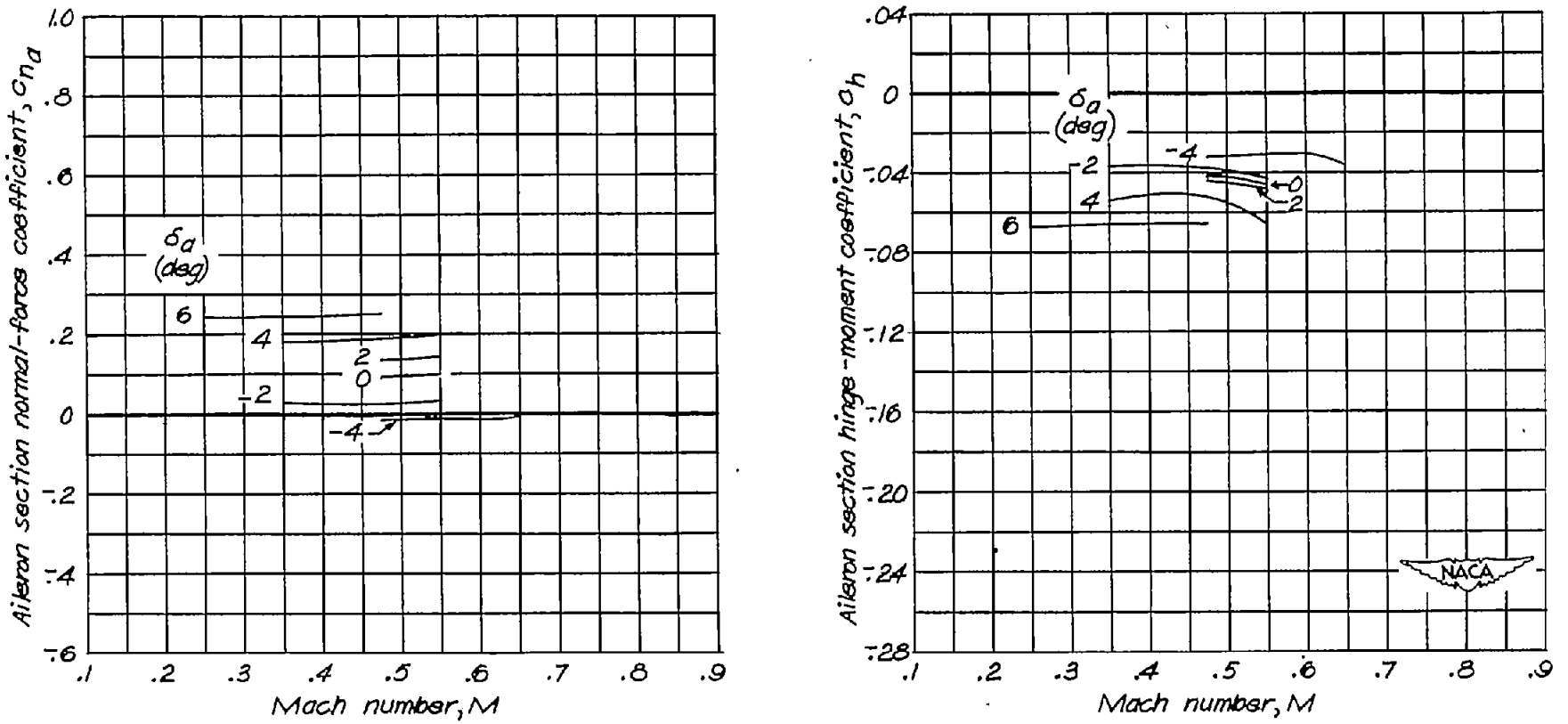

(a) $c_n = -0.4$.

Figure 10.- Variation of aileron normal-force and hinge-moment coefficients with Mach number for an unsealed 0.20c plain aileron of beveled-trailing-edge profile mounted on an NACA 66,1-115 airfoil section.

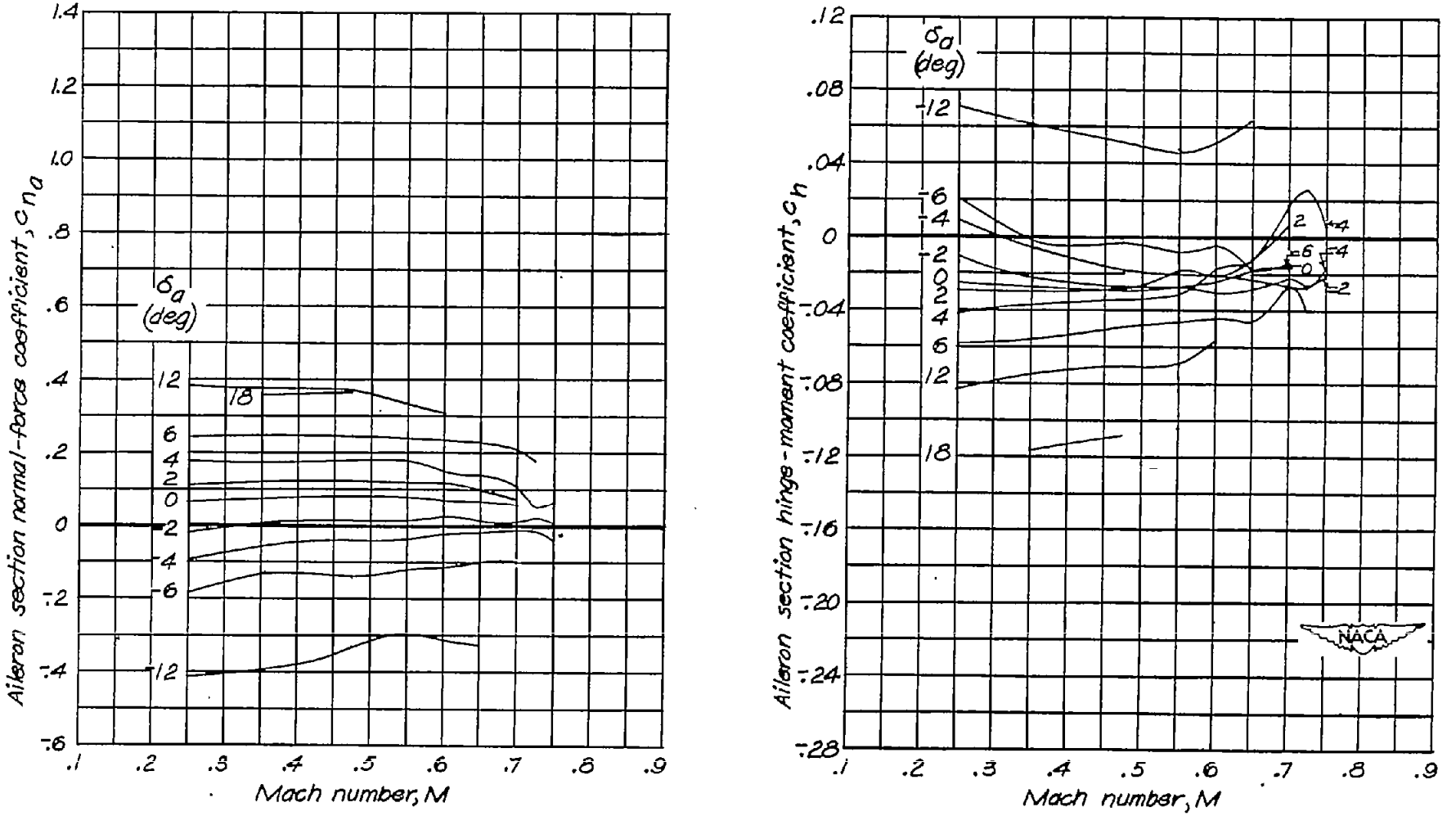

(b) $c_n = -0.2$.

Figure 10.-Continued.

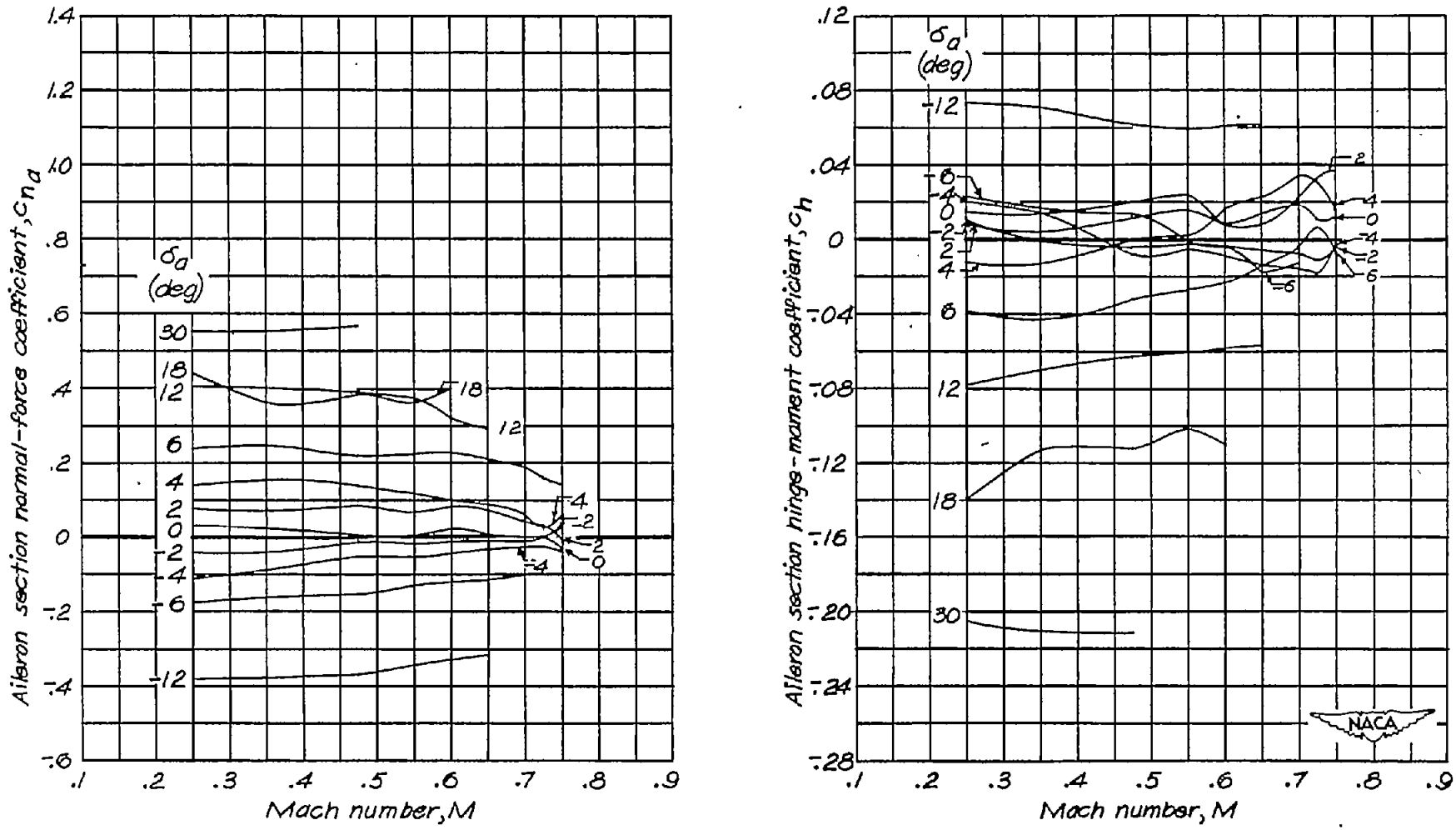

(c) $c_n = 0$.

Figure 10.- Continued.

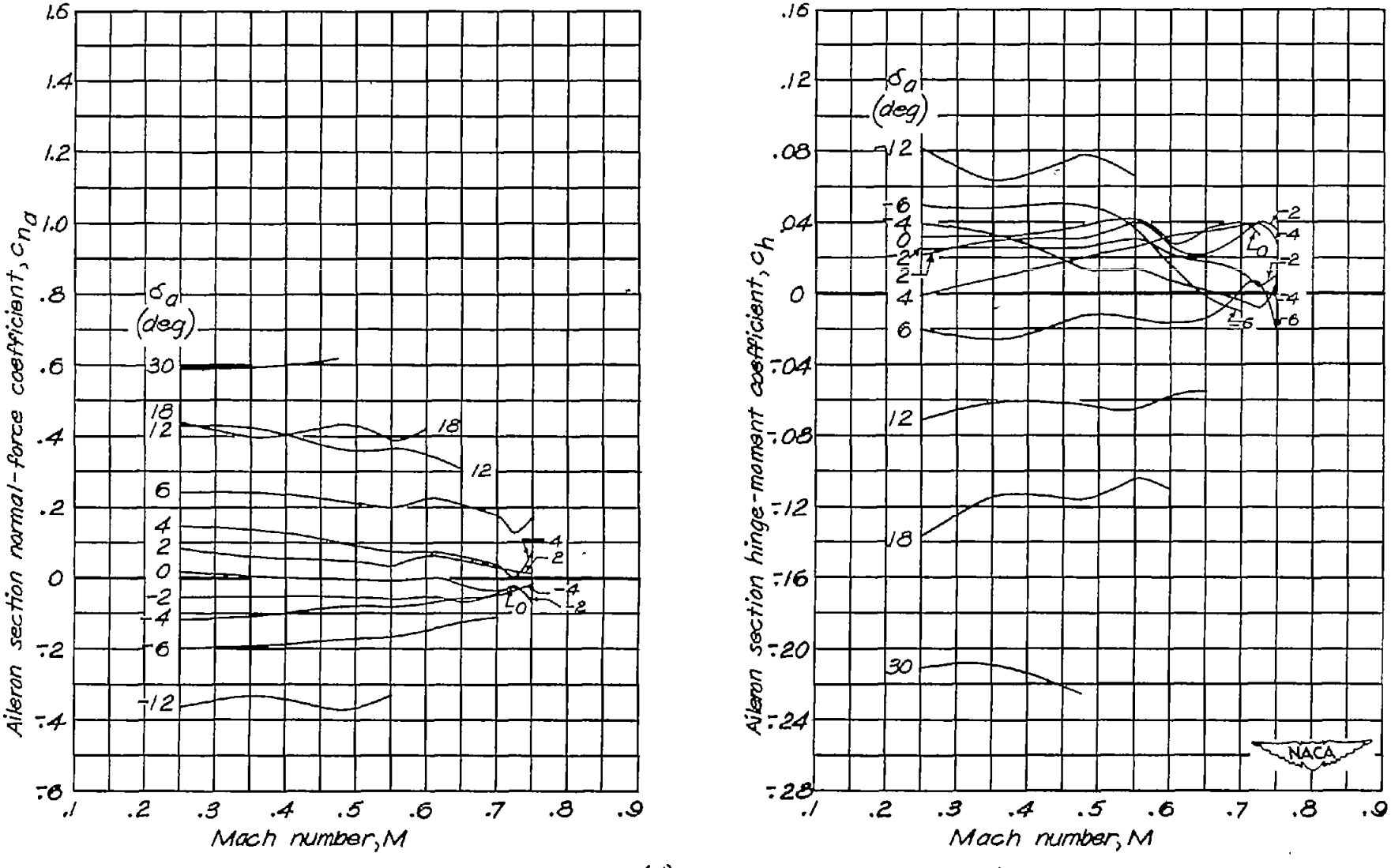

(d) c_n=0.2.

Figure 10.- Continued.

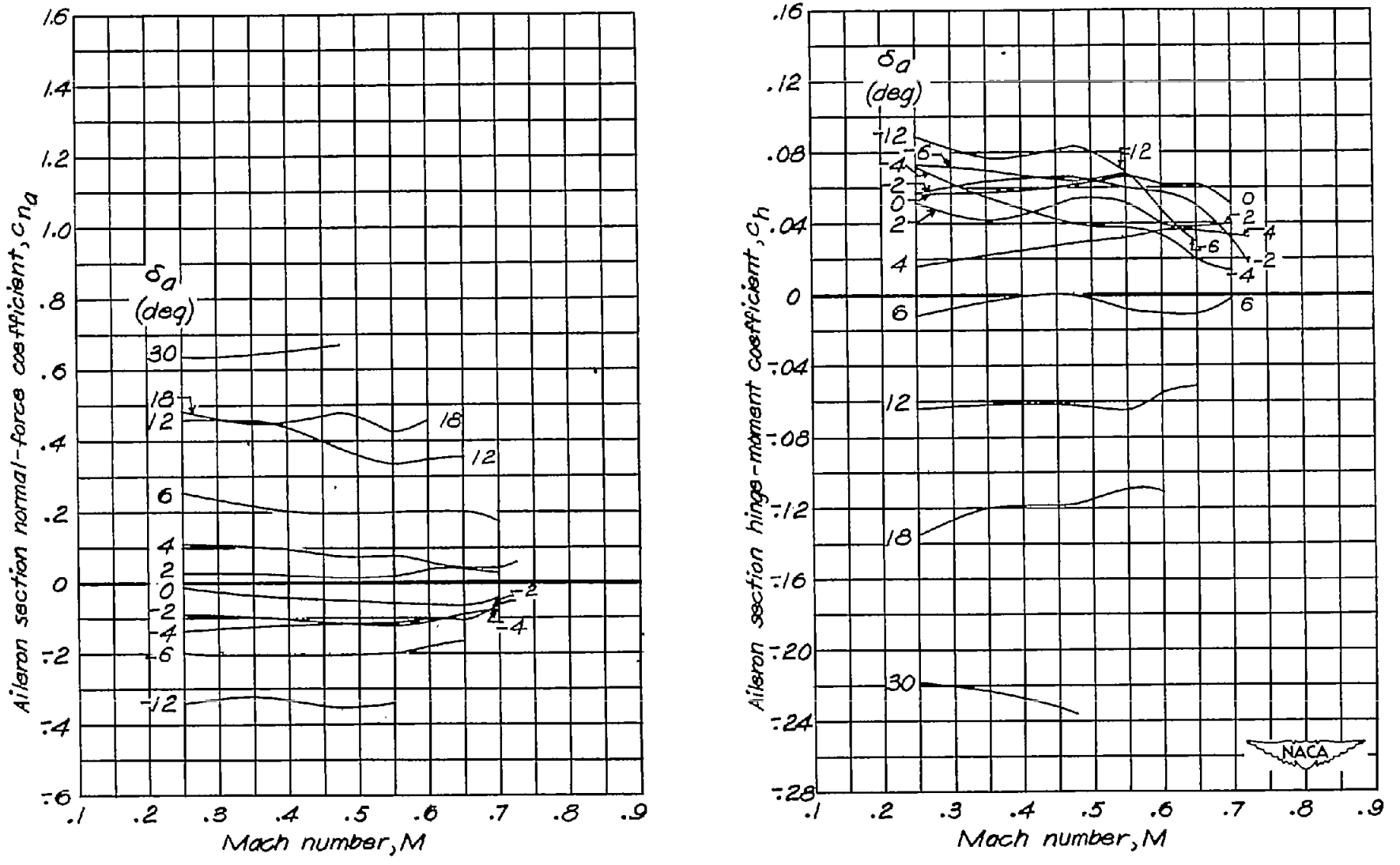

(e) $c_n = 0.4$.

Figure 10.- Continued.

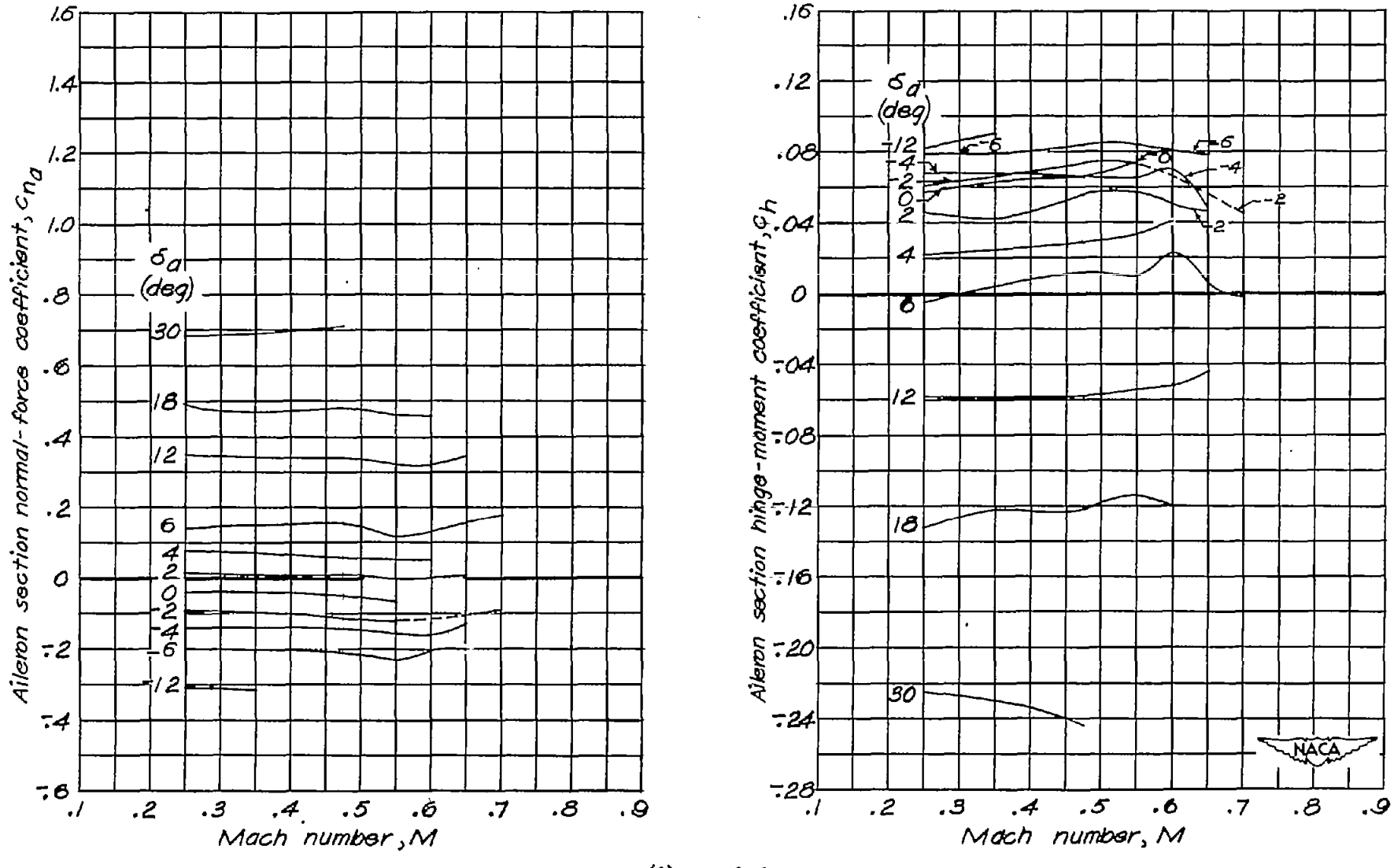

(f) $c_n = 0.6$.

Figure 10.-Continued.

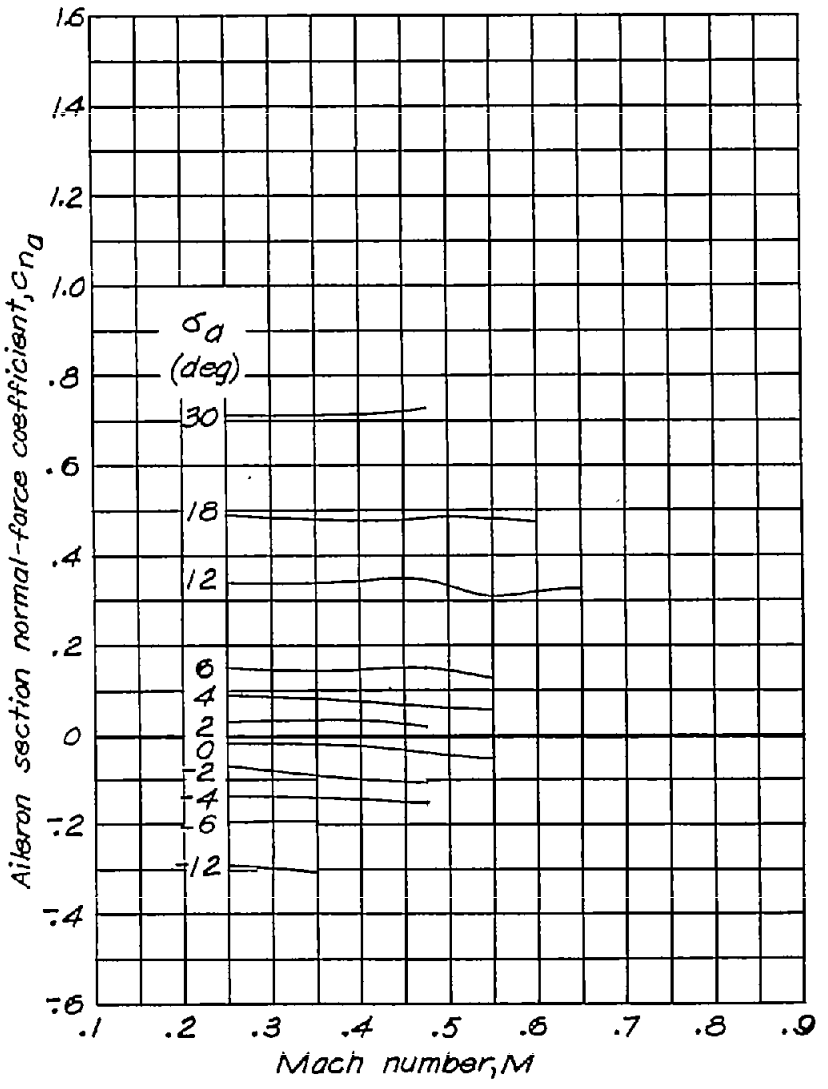

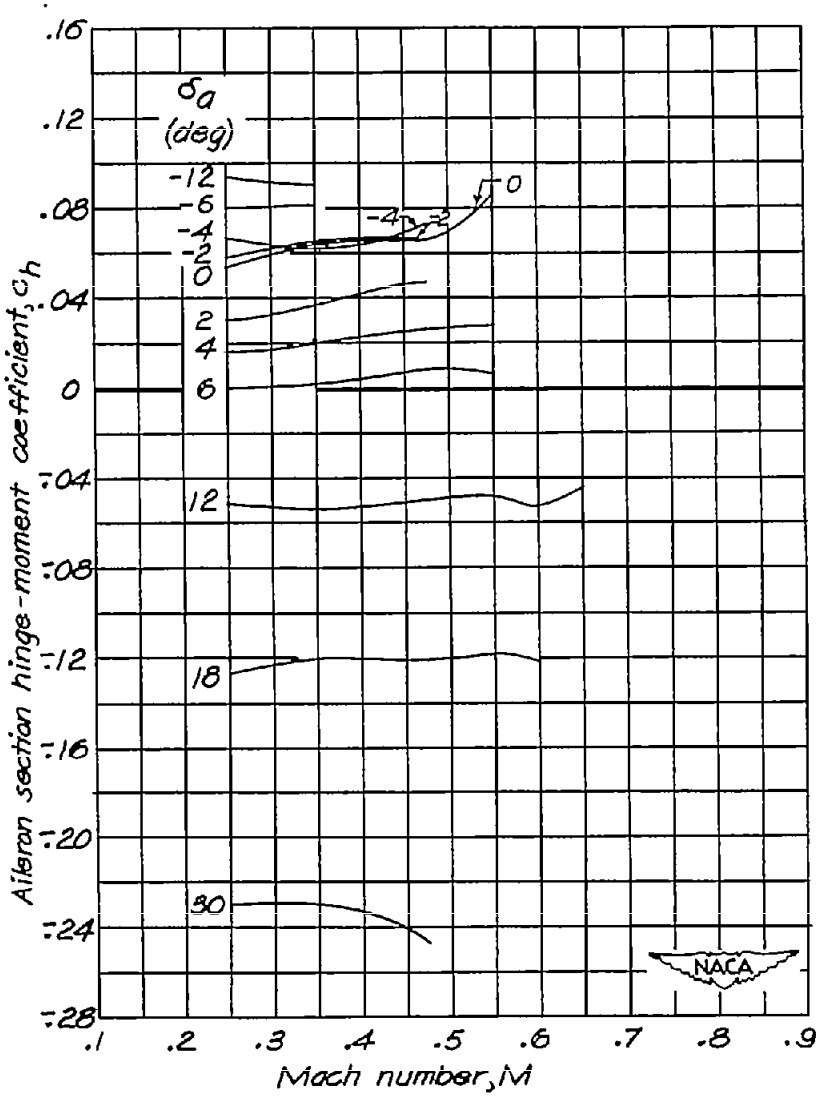

(g) $c_n = 0.7$.

Figure 10 .- Continued.

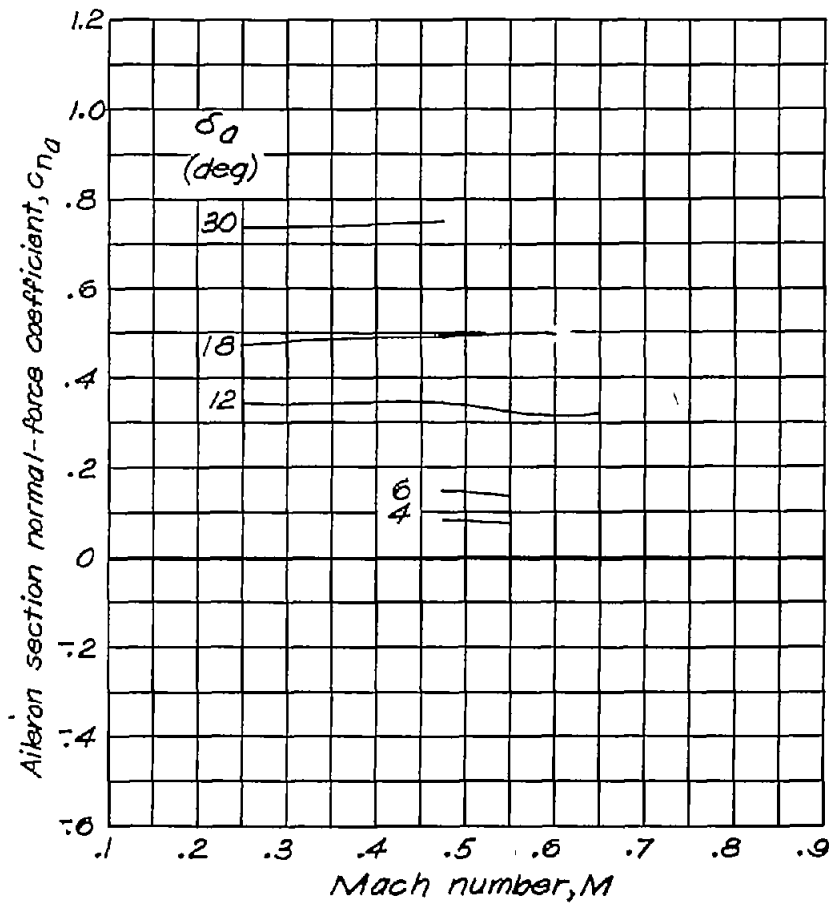

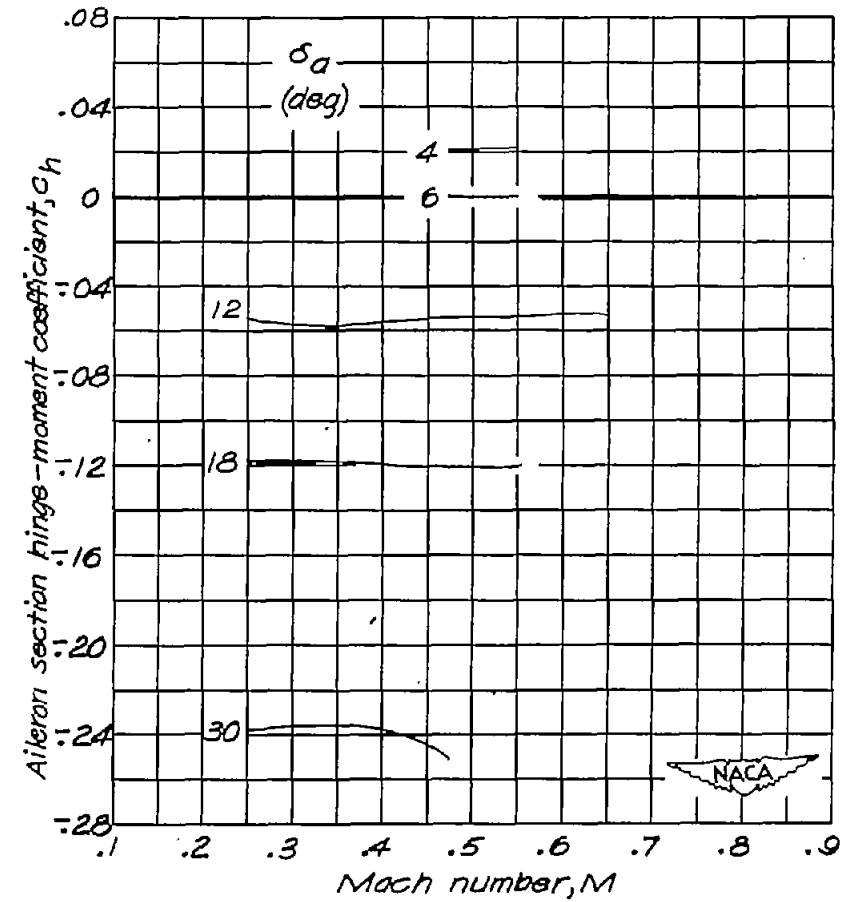

(h) $c_n = 0.8$.

Figure 10.- Concluded.

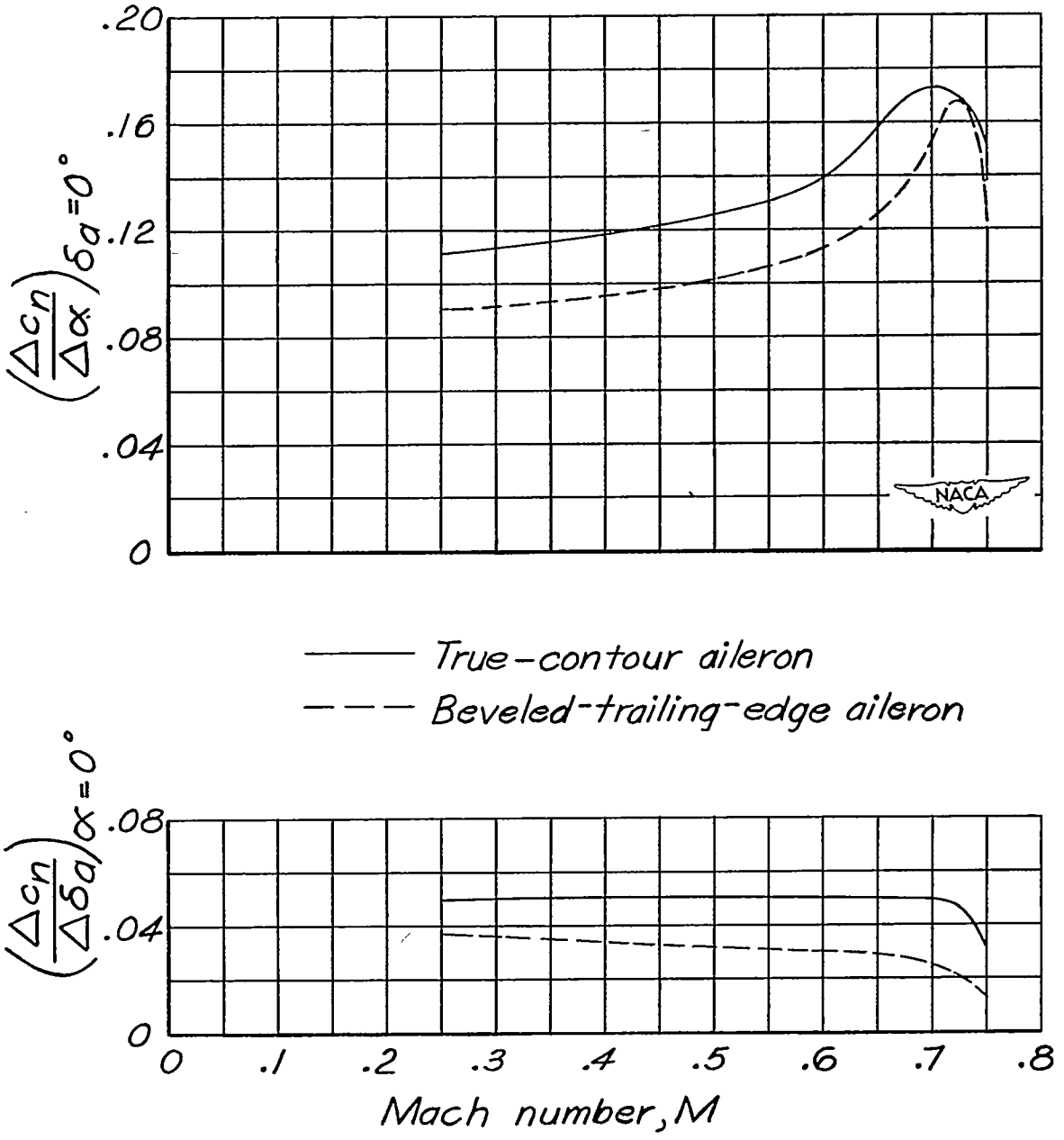

Figure 11.- Variation of normal-force-coefficient-curve slopes with Mach number for an NACA 66,1-115 airfoil section equipped with unsealed 0.20c plain ailerons.

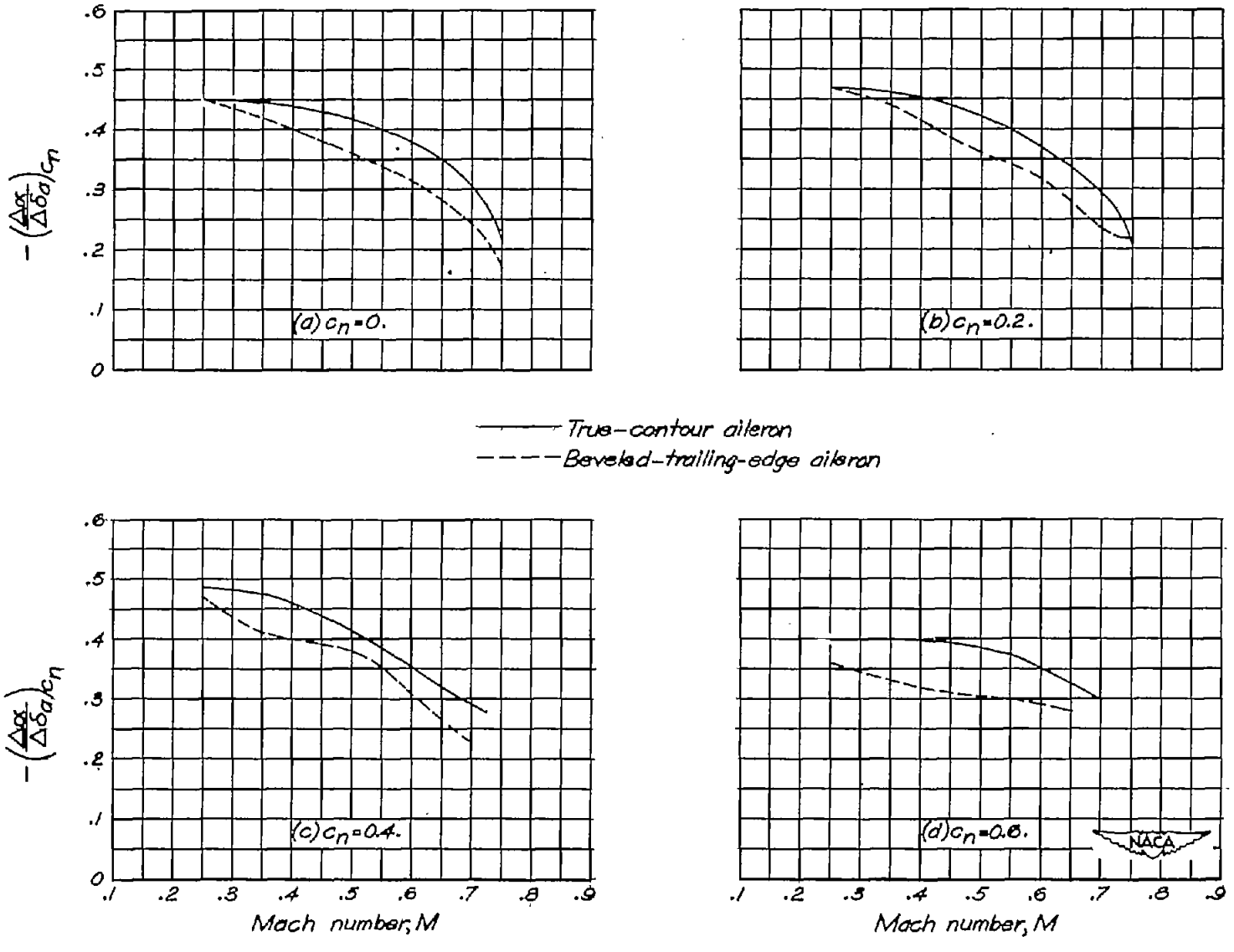

Figure 12.– Variation of aileron effectiveness $\left(\frac{\Delta\alpha}{\Delta\delta_a}\right)_{c_n}$ with Mach number for an NACA 66,1-115 airfoil section equipped with unsealed 0.20c plain ailerons.

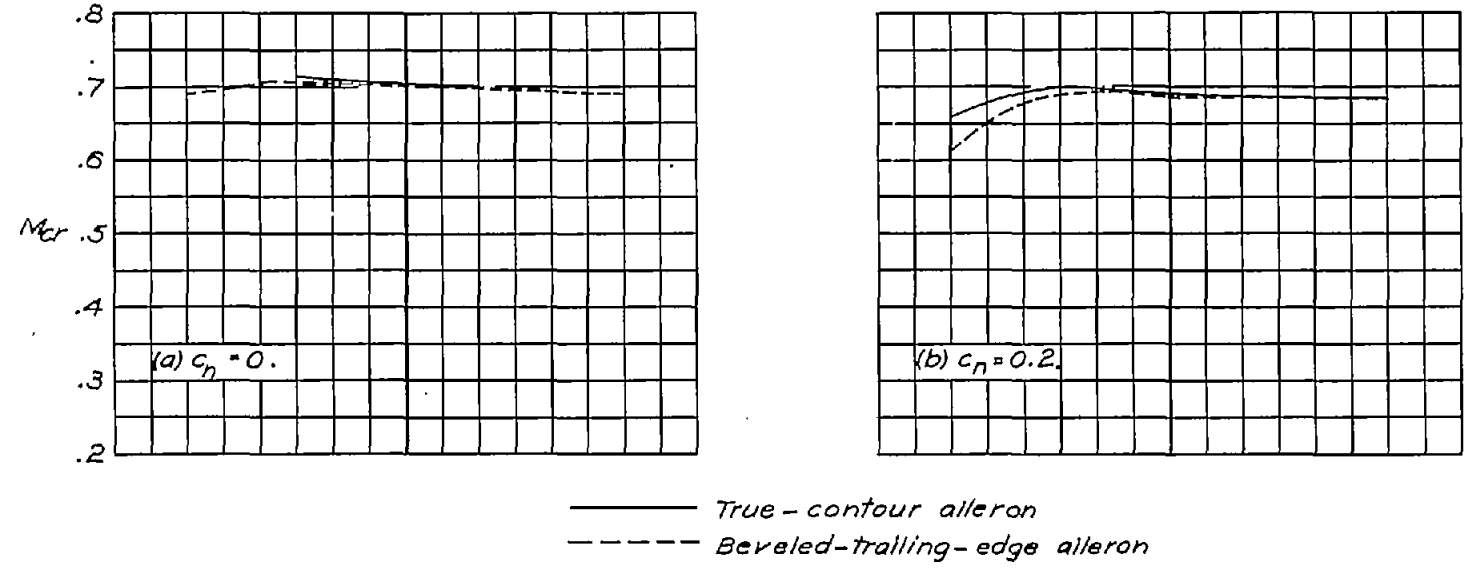

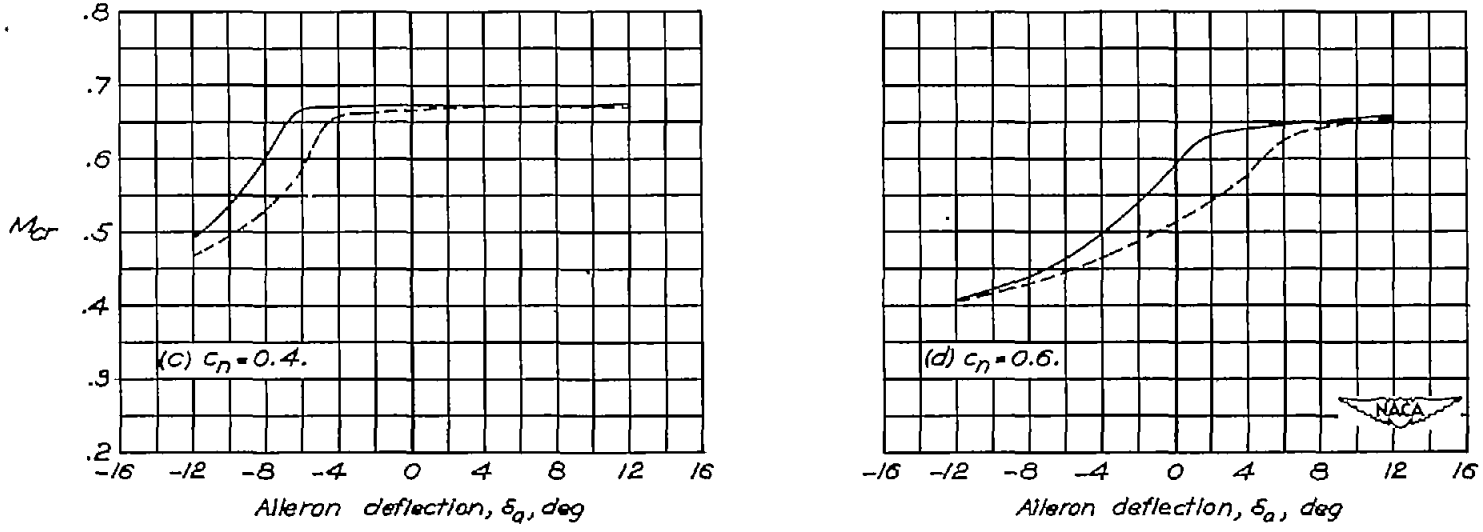

Figure 19.- Variation of critical Mach number with aileron deflection for an NACA 66,1-115 airfoil section equipped with unsealed 0.20c plain ailerons.

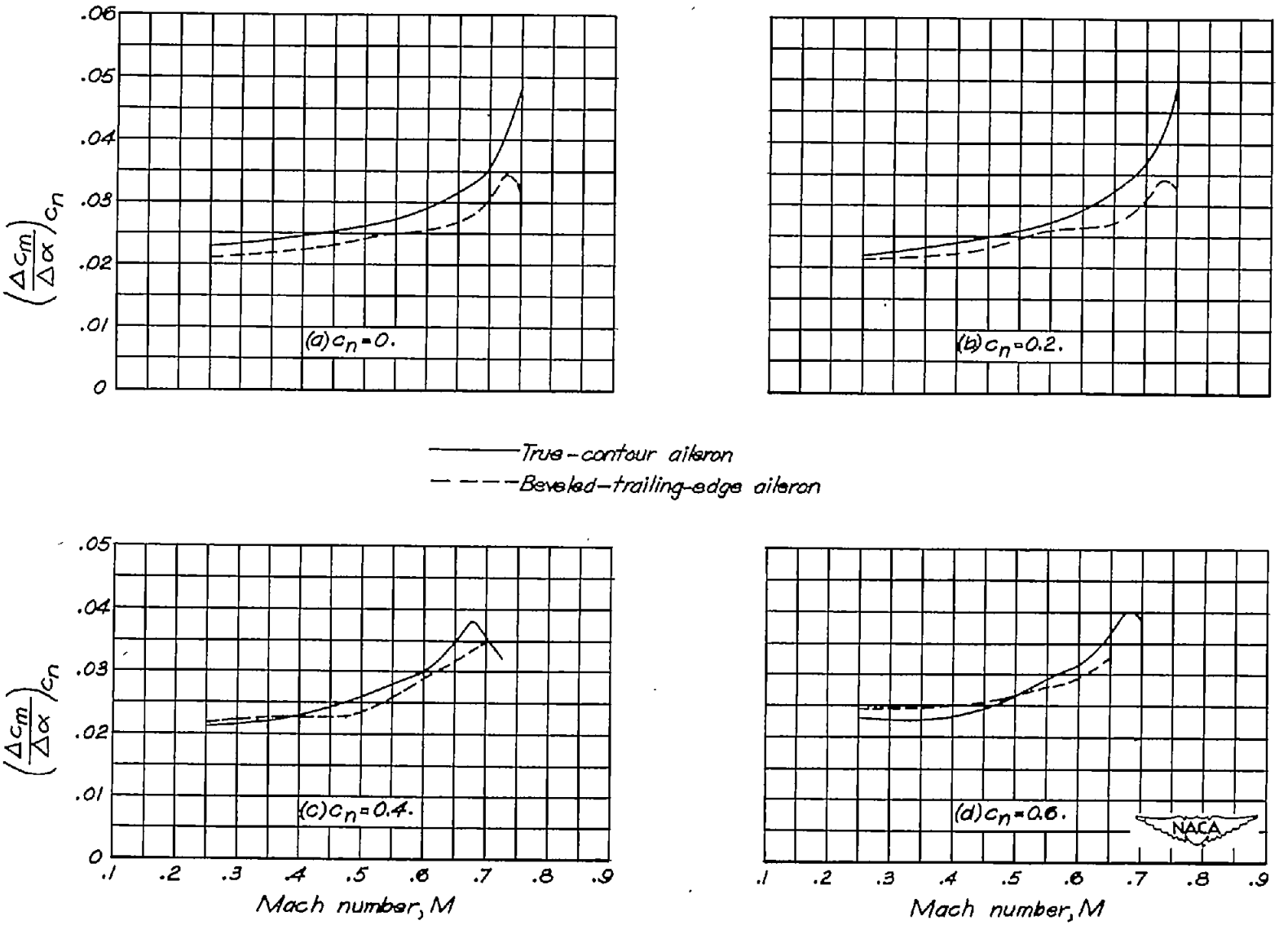

Figure 14.- Variation of $\left(\frac{\Delta c_m}{\Delta \alpha}\right)_{c_n}$ with Mach number for an NACA 66,1-115 airfoil section equipped with unsealed 0.20c plain ailerons.

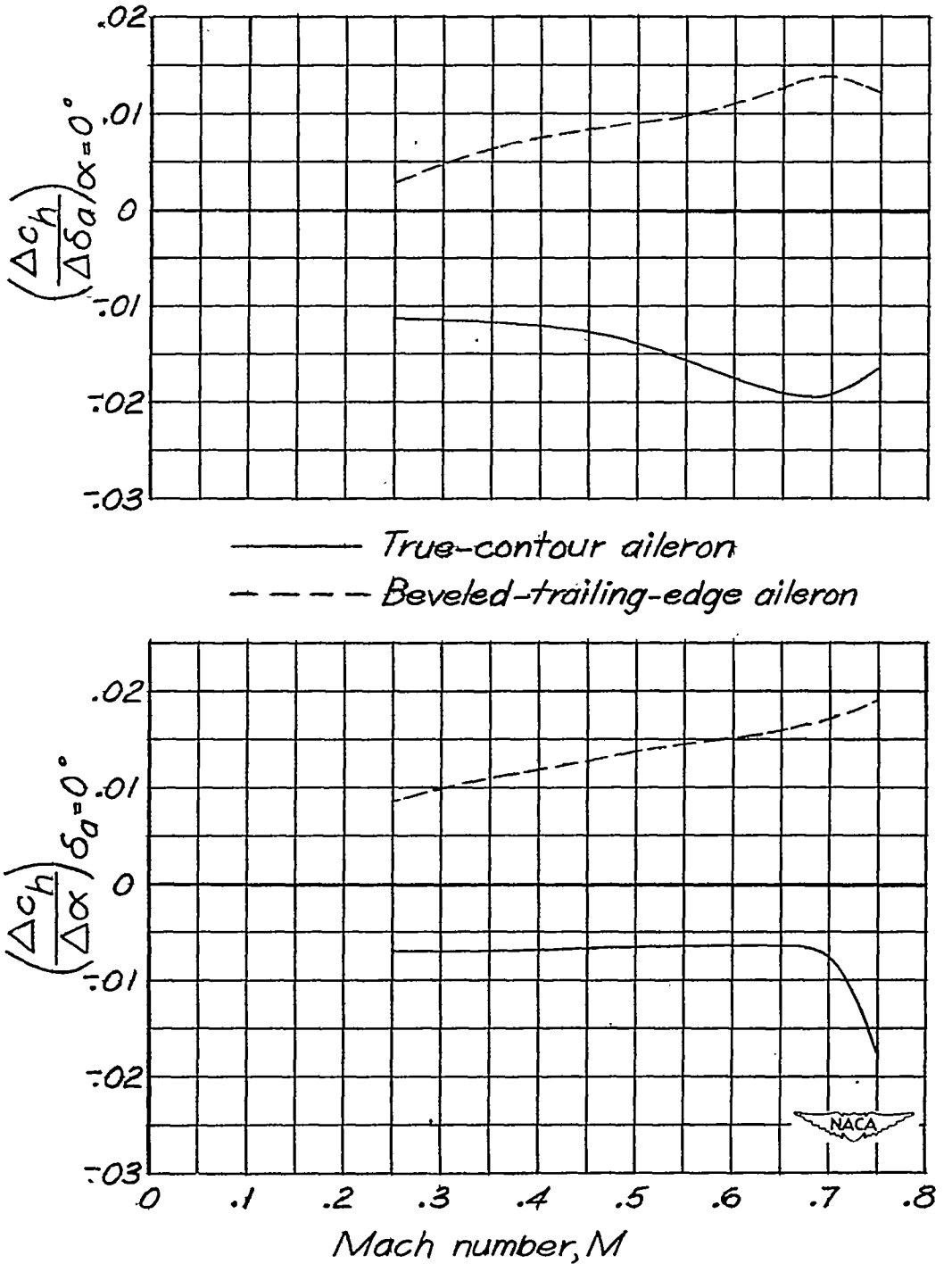

Figure 15.- Variation of aileron hinge-moment-coefficient-curve slopes with Mach number for an NACA 66,1-115 airfoil section equipped with unsealed 0.20c plain ailerons.

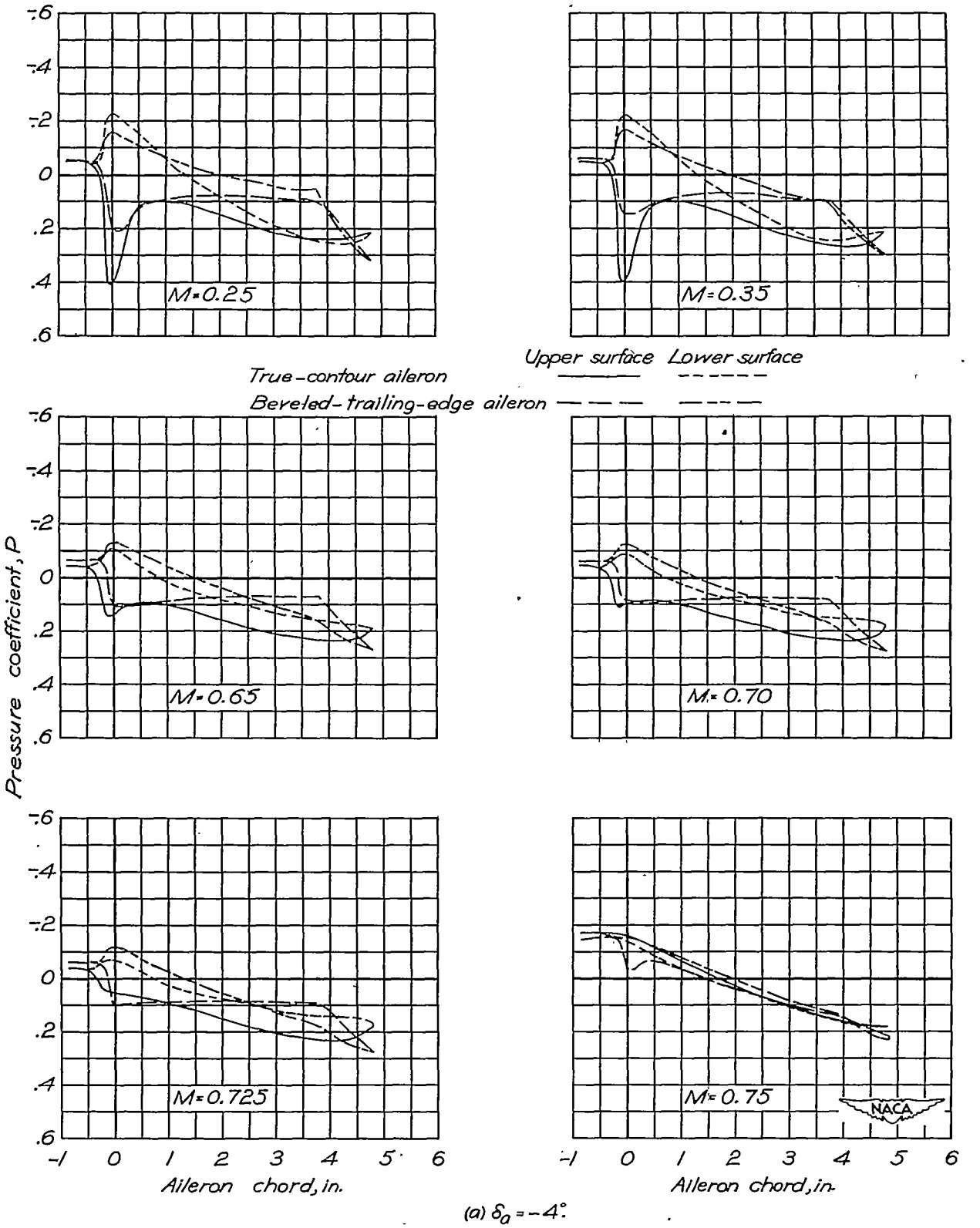

(a) $\delta_a = -4°$.

Figure 16.— Aileron pressure distribution for an NACA 66,1-115 airfoil section equipped with unsealed 0.20c plain ailerons. $\alpha = 1°$.

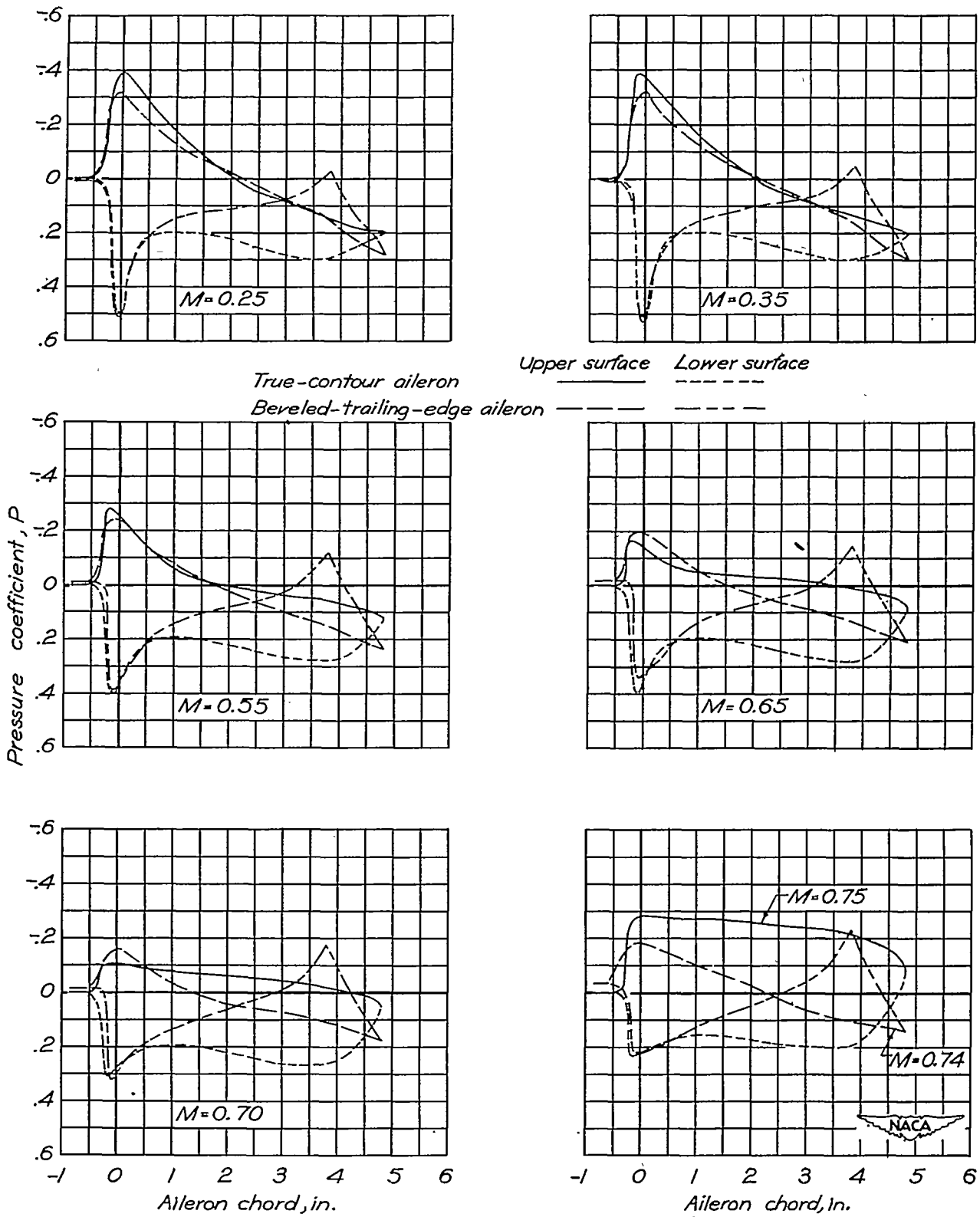

(b) $\delta_a = 4°$.

Figure 16.—Concluded.

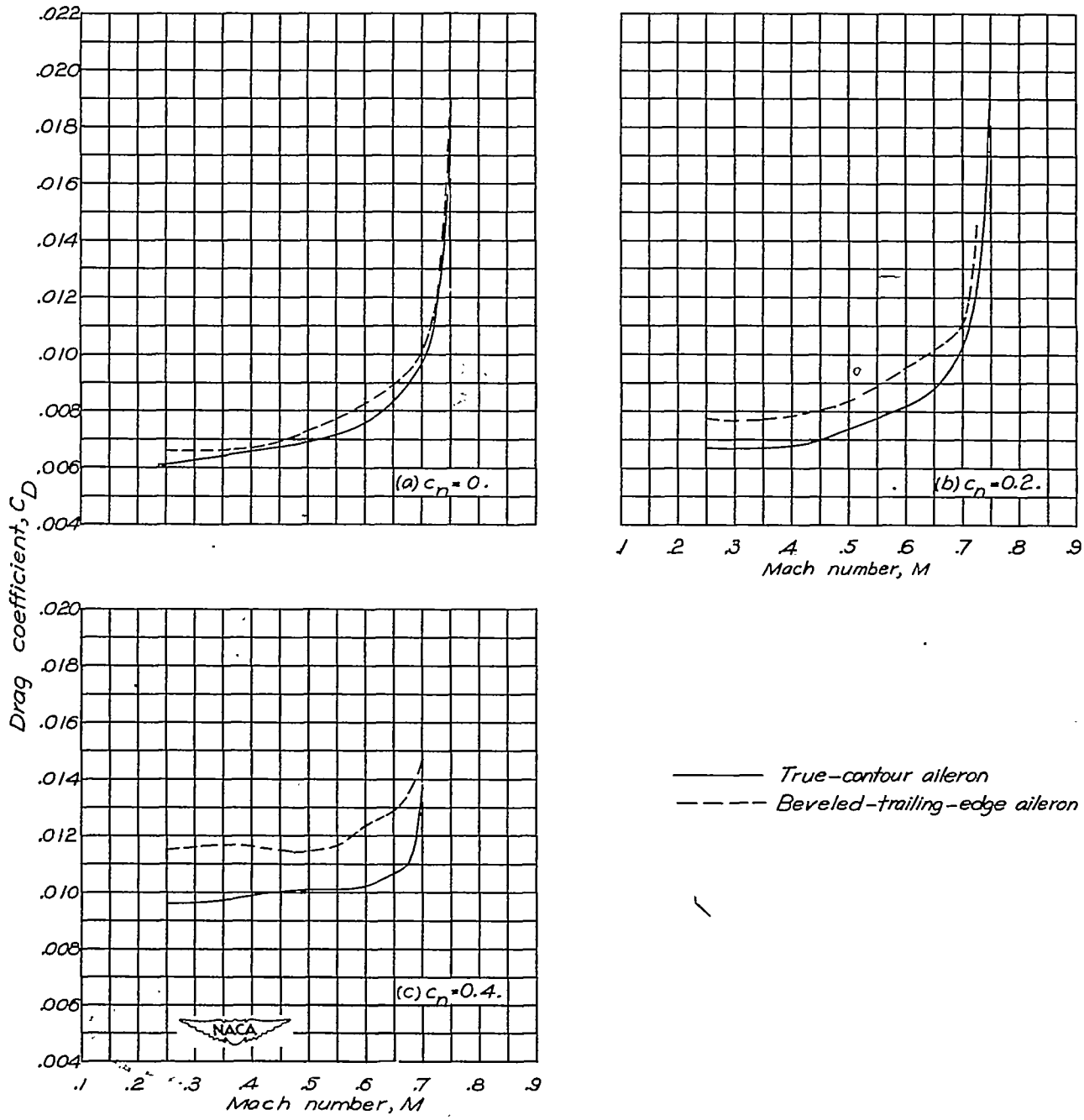

Figure 17.– Variation of wing drag coefficient with Mach number for an NACA 66,1-115 airfoil section equipped with unsealed 0.20c plain ailerons. $\delta_a = 0°$. Drag data from force-test measurements.